Journal of Medicinal Chemistry

Article

Tetrahydroisoquinoline-derived urea and 2,5-diketopiperazine derivatives as selective antagonists of the transient receptor potential melastatin 8 (TRPM8) channel receptor and anti-prostate cancer agents

Luciano De Petrocellis, Francisco José Arroyo, Pierangelo Orlando, Aniello Schiano Moriello, Rosa Maria Vitale, Pietro Amodeo, Aránzazu Sánchez, Cesáreo Roncero, Giulia Bianchini, M. Antonia Martín, Pilar López-Alvarado, and J. Carlos Menéndez

J. Med. Chem., **Just Accepted Manuscript** • DOI: 10.1021/acs.jmedchem.5b01448 • Publication Date (Web): 27 May 2016

Just Accepted

ACS Publications

Journal of Medicinal Chemistry is published by the American Chemical Society. 1155 Sixteenth Street N.W., Washington, DC 20036

Tetrahydroisoquinoline-derived urea and 2,5-diketopiperazine derivatives as selective antagonists of the transient receptor potential melastatin 8 (TRPM8) channel receptor and anti-prostate cancer agents

Luciano De Petrocellis[a,*], Francisco J. Arroyo,[b] Pierangelo Orlando,[c] Aniello Schiano Moriello,[a] Rosa Maria Vitale,[a] Pietro Amodeo,[a] Aránzazu Sánchez,[d] Cesáreo Roncero,[d] Giulia Bianchini,[b] M. Antonia Martín,[e] Pilar López-Alvarado[b], J. Carlos Menéndez[b,*]

[a]Endocannabinoid Research Group, Institute of Biomolecular Chemistry, National Research Council, Via Campi Flegrei 34, Comprensorio Olivetti, 80078 Pozzuoli, Naples, Italy. [b]Departamento de Química Orgánica y Farmacéutica, Facultad de Farmacia, Universidad Complutense, 28040 Madrid, Spain. [c]Endocannabinoid Research Group, Institute of Protein Biochemistry, National Research Council, Via P. Castellino 111, 80131 Naples, Italy. [d]Departamento de Bioquímica y Biología Molecular II, Facultad de Farmacia, Universidad Complutense, 28040 Madrid, Spain.

[e]S.D. Química Analítica, Facultad de Farmacia, Universidad Complutense, 28040 Madrid, Spain.

KEYWORDS Tetrahydroisoquinolines, ureas, diketopiperazines, TRPM8 channels, apoptosis, anti-prostate cancer activity.

ABSTRACT. Tetrahydroisoquinoline derivatives containing embedded urea functions were identified as selective TRPM8 channel receptor antagonists. Structure activity relationships were investigated, with the following conclusions: (a) The urea function and the tetrahydroisoquinoline system are necessary for activity. (b) Bis(1-aryl-6,7dimethoxy-1,2,3,4-tetrahydroisoquinolyl)ureas are more active than compounds containing one tetrahydroisoquinoline ring and than an open phenetylamine ureide. (c) *Trans* compounds are more active than their *cis* isomers. (d) Aryl substituents are better than alkyls at the isoquinoline C-1 position. (e) Electron-withdrawing substituents lead to higher activities. The most potent compound is the 4-F derivative, with IC_{50} in the 10^{-8} M range and selectivities around 1000:1 for most other TRP receptors. Selected compounds were found to be active in reducing the growth of LNCaP prostate cancer cells. TRPM8 inhibition reduces proliferation in the tumor cells tested, but not in non-tumor prostate cells, suggesting that the activity against prostate cancer is linked to TRPM8 inhibition.

Introduction

Transient receptor potential melastatin 8 (TRPM8) is a member of the transient receptor potential (TRP) superfamily, a class of non-selective cation channels that are activated by a variety of physical and chemical stimuli.[1] Owing to the fact that menthol and other agents that elicit the sensation of coolness, such as icilin and eucalyptol,[2-4] act as TRPM8 agonists, the TRPM8 ion channel was initially known as the cold menthol receptor-1 (CMR-1).[2] A number of TRP channels are thermo-responsive, become activated at different ranges of temperature and seem to act as thermo-sensors *in vivo*.[5] Thus, TRPV1 is required for hot temperature sensing[6] and TRPV3[7] and TRPV4[8] for warm temperature sensing; TRPA1 is activated by noxious cold (<10 °C) *in vitro*[9,10] and *in vivo*[11]. Similarly, TRPM8 is activated *in vitro* by temperatures ranging from innocuous cold (23–15 °C) to noxious cold (< 15 °C)[1,2] and is required as a neuronal sensor of mildly cold temperatures, as shown by knockout mouse studies.[12-17] As with TRPV1, TRPM8 is involved in thermoregulation: menthol and icilin cause a transient rise in basal temperature[18-21] at least for the former TRPM8 mediated;[22] on the other hand, TRPM8 antagonists induce a decrease in body temperature[13,23,24] although the hypothermic response was less than 1 °C unlike the febrile response toTRPV1 antagonists.

The TRPM8 gene encodes for a 1104-residue transmembrane protein, whose quaternary structure is a homotetramer channel.[25] The transmembrane portion is formed by six helices, out of which the protonated residues at S4 and the S4-S5 linker have an important role in the receptor activation and S2 and S3 include the binding sites for menthol and icilin, although they do not fully overlap since menthol recognition is mostly associated with S2, with tyrosine 745 (Y745) being critical for the interaction, while icilin interacts mainly with residues

located at S3[26,27] The last two helices constitute the permeable pore module, the sixth one being responsible for the ion selectivity of TRPM8.[28,29]

Correlating with the cold sensing function, TRPM8 has been localized in a subpopulation of primary small diameter sensory neurons (on nociceptive Aδ and C fiber neurons) of the dorsal root and trigeminal ganglia.[1,2,30-33] TRPM8-positive neurons being different from those expressing TRPV1 and/or TRPA1.[34] In addition, TRPM8 is expressed in a range of tissues, mainly in the prostate and liver and, in lesser amounts, in the brain, lung, bladder, gastrointestinal tract, blood vessels, and immune cells.[35]

Under some pathological conditions, TRPM8 expression is up-regulated on nociceptive afferent neurons, resulting in cold allodynia[36,37] whose mechanism after chronic constriction injury (CCI) has been studied.[38-40]. TRPM8 can have analgesic effects by diminishing neuropathic and visceral pain[36,41,42] or by attenuating cold hypersensitivity in inflammatory and nerve-injury pain models,[26,43] cold hyperalgesia and cold allodynia, which are commonly associated with certain types of neuropathic and inflammatory pain.[44-46]

The role of TRPM8 is not confined to the perception of cold: in prostatic tumour tissue the expression level of TRPM8 correlates with malignancy,[47] although the activation of TRPM8 by menthol suppresses cellular viability of human melanoma cells.[48] Subsequent experimentation has shown that modulators of TRPM8 may be useful in the treatment of prostate cancer[49,50] as well as in colorectal cancer.[51].

TRPM8 activation has been reported to be involved in overactive bladder and painful bladder syndrome, playing a role in the symptomatology and pathophysiology of human urinary bladder disorders.[52] Preclinically, an antagonist of TRPM8 has been shown to decrease the frequency of volume-induced bladder contractions, without reducing the amplitude of

contraction in rats,[53] suggesting a role for TRPM8 antagonists in chronic pain conditions as well as in painful bladder syndromes.[45]

With regard to agonists, at least eighteen natural and synthetic compounds have been found to activate the channel, including menthol, icilin, eucalyptol[1,2] and the potent synthetic menthane-derived amide **1** (WS-12).[54] However, menthol is not selective for TRPM8, since its responses were reduced, but not abolished, in TRPM8 null mice.[24] Studies on genetically modified mice demonstrated that the effects of icilin were mediated by TRPM8 and not TRPA1, while menthol-induced cold hypersensitivity was dependent on expression of TRPA1 and not TRPM8.[55]

Most of the antagonists reported in the literature[56] lack selectivity for TRPM8, since they also act on TRPV1 and TRPA1.[57] Capsazepine, a well-known TRPV1 antagonist, inhibits TRPM8,[3] but it also has non-specific activity on voltage-gated calcium channels and nicotinic acetylcholine receptors.[58-60] Similarly, **2** (BCTC) inhibits TRPM8-mediated Ca^{2+} influx,[3] but it also functions as a TRPA1 agonist.[61] The antimycotics clotrimazole[62] and the even more potent econazole[63] have TRPM8 antagonistic activity, but they also strongly activate TRPV1 and TRPA1 actions. Compound **4** (SKF96365), a non-specific blocker of several types of calcium channels, receptor-operated channels, and inwardly rectifying potassium channels[64,65] also inhibits TRPM8 *in vitro*.[66] Anandamide and N-arachidonoyldopamine were previously found to inhibit menthol- and icilin-induced response in TRPM8-HEK-293 cells,[67] and the same response was obtained from some plant-derived cannabinoids.[68,69] Recently, some compounds endowed with improved TRPM8 selectivity have been described, such as the 2-pyridyl-benzensulfonamide **5** (RQ-00203078).[70] Some additional potent, small-molecule TRPM8 antagonists have been reported in the literature as potential therapeutics, although

these compounds have off-target effects. They include menthylamides,[71] tryptamine derivatives, which are also ligands for 5-benzyloxytryptamine receptors,[72] benzyloxybenzamides,[73] cinnamamides as open-chain analogs of icilin,[74] benzimidazoles[75,76] benzothiophene phosphonates,[77,78] fused piperidines,[79,80] oxazole and thiazole derivatives,[81] arylglycine-based analogs,[82] spiro[chromene-2,4'-piperidines] **6**,[83] urea derivatives (*e.g.* compound **7**),[80] 2-pyridyl-benzensulfonamides[70] and indole alkaloids.[84]

The structurally related compounds **8** and **9** (Figure 1) have been studied for their antinocioceptive activity.[43,46] A survey of recent patents reveals reports of several structural classes containing examples of compounds having potent TRPM8 blockade activity by many companies such as Amgen, Bayer Health, Glenmark Pharmaceuticals, GW Pharma, Janssen Pharmaceuticals and Raqualia Pharma (for recent reviews, see references 85-87). Most attention is being devoted to the use of TRPM8 antagonists as analgesics, and their potential against prostate cancer remains almost unexplored.

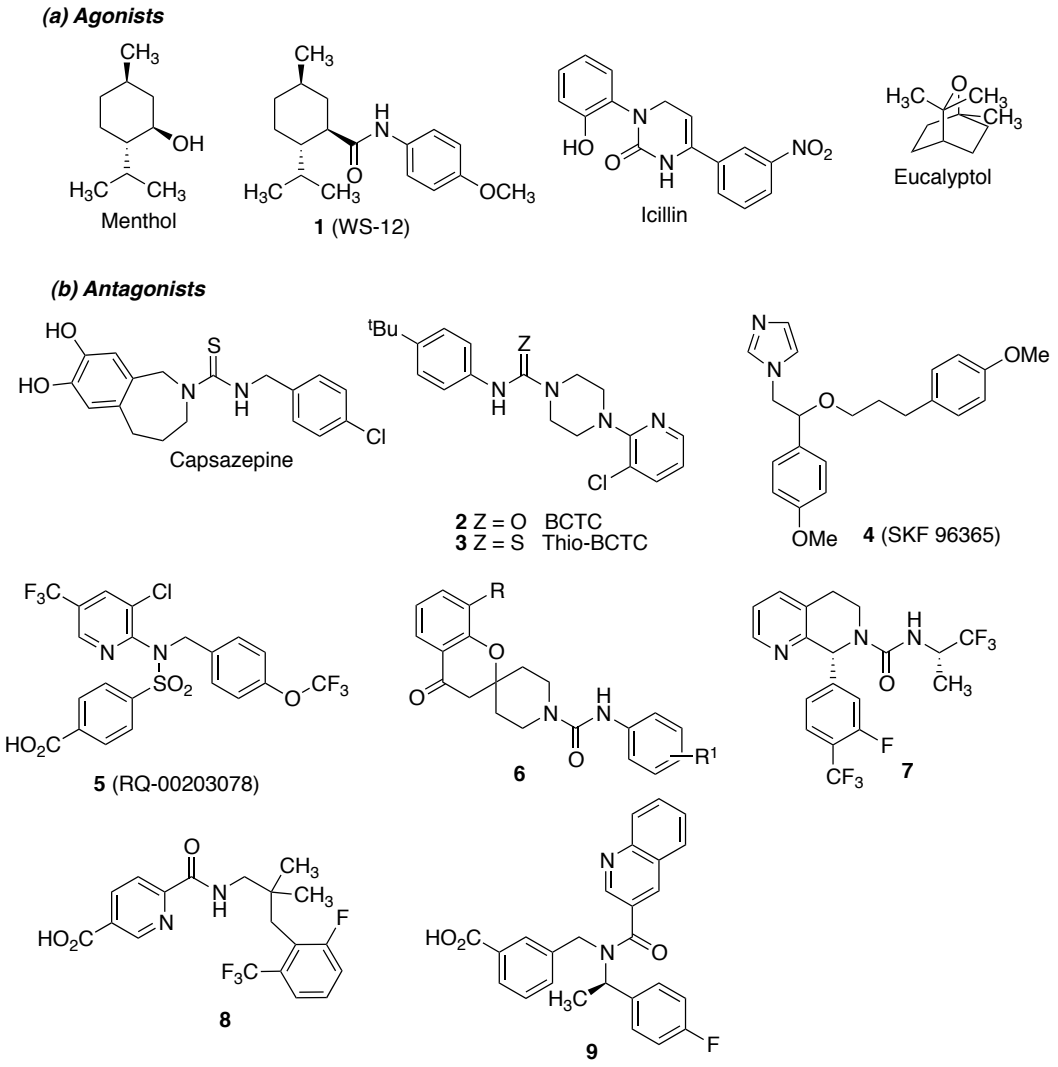

Figure 1. Representative small-molecule TRPM8 agonists (a) and antagonists (b)

The basis for TRPM8 antagonism are not fully understood at the atomic level, but much significant information has been collected over the years. The quaternary structure of human TRPM8 involves a symmetrical arrangement of four subunits, with the TRPM8 putative ligand-binding site encompassing the S1-S4 transmembrane helices and the TRP domain of each subunit. The TRP domain is known to be critical for signal transduction[88] and has been used recently to dock a series of TRPM8 ligands.[89] Mutation studies show that the Tyr745

residue is critical for the inhibition of cold- and voltage-activated TRPM8 currents by menthol and compound **4**. However, the activity of other antagonists, such as compound **2**, is not affected by the mutation. Other antagonists (clotrimazole, econazole, capsazepine), are only partially active in the mutated channel. Taken in the aggregate, these observations suggest the existence in the binding site of several independent pockets able to interact with inhibitors.[63] Molecular docking studies support these conclusions, and show that the known inhibitors interact only partially with the amino acids present at the binding site. For instance, compound **4** interacts at a region close to the icilin site, stabilizing the positions of the S2 and S3 domains by binding to Tyr745 and Asn799.[63] In another example, docking of tryptamine-based derivatives on the rat TRPM8 protein shows electrostatic interactions with Glu-1004, stacking with Tyr754 and several hydrophobic contacts.[89] In such a situation, in which several potential binding sites are in close spatial proximity, the use of bivalent ligands may be of assistance in the discovery of compounds with improved potencies, as often exemplified in the literature on several therapeutic areas.[90,91] We reasoned that the use of symmetrical compounds to probe the full pocket would take advantage of the presence of two arginine residues (Arg842 and Arg1008) at both ends of the cavity. Furthermore, symmetrical molecules have the advantage of allowing for simpler synthetic procedures. Thus, in efforts to identify new types of TRPM8 antagonists and in view of the prevalence of urea and thiourea structural fragments in known TRPM8 antagonists, we planned the synthesis of a library of urea derivatives inspired on the structure of capsazepine but having the symmetrical structures **10** and **11**. We were further attracted to this idea by the fact that the impact of molecular symmetry in the discovery of TRPM8 antagonists has never been examined. For comparison purposes, we planned the preparation of non-symmetrical analogues **12**. We also studied briefly a family of related

compounds derived from a 2,5-diketopiperazine core (compounds **13** and **14**) and finally, again for comparison purposes, we examined the activity of some compounds corresponding only to the tetrahydroisoquinoline moiety of the previously mentioned molecules (**15**) (Figure 2). The 6,7-dimethoxy substitution was inspired on the structure of capsazepine, whose cathecol moiety was modified by methylation in order to achieve a better metabolic stability. Furthermore, subsequent studies (see below) showed that these oxygen functions are crucial for the interaction of our compounds with the Arg residues at both ends of the channel active site.

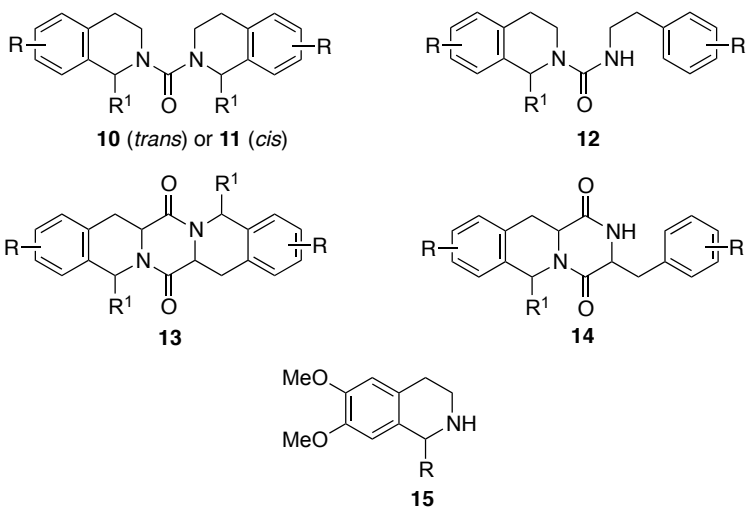

Figure 2. Frameworks of the compounds studied in this article

Results and discussion

Chemistry

While we acknowledged that the fastest approach to our planned symmetrical urea derivatives would involve the use of double Pictet-Spengler reactions from the known[92] urea derivative **16**, this method had the disadvantage that amide-type compounds are challenging Pictet-

Spengler substrates; indeed, ureas have rarely been studied in this regard and usually only for the case of very reactive aldehydes, such as formaldehyde.[93] We found, nevertheless, that our recently developed method based on the generation of α-amidosulfone intermediates[94] provided a general solution to our problem, allowing the preparation of compounds **10** and **11** *via* a pseudo three-component reaction between **16** and two molecules of aliphatic or aromatic aldehydes, in refluxing toluene containing one equivalent of toluenesulfinic acid. Under these conditions, the reaction was fully diastereoselective and afforded exclusively the *trans* isomers **10**, confirming our previous findings[94] (Scheme 1 and Table 1). In some cases, we employed strongly acidic conditions (H_2SO_4, AcOH, 120 °C) as an alternative, which led to the *cis* derivatives **11**, corresponding to the other possible diastereomer of structure **10**. The formation of **10** avoids steric repulsions between the substituent R at the α' position of intermediate **17** and the carbonyl and α-R substituents during the formation of the second isoquinoline ring, thus explaining the observed diastereoselectivity under our usual conditions. This cyclization process is altered under strongly acidic conditions, which may protonate the urea carbonyl, although a precise reason for the formation of the *cis* compounds **11** in these cases remains elusive at present.

The choice of substituents in the design of the urea library was based on the presence of aryl substituents bearing electron-withdrawing groups on most known TRPM8 antagonists (Figure 1). Thus, after preparing the alkyl derivative **10a** for comparison purposes, we obtained a series of α,α'-diaryl derivatives bearing as substituents hydrogen (compound **10b**), halogens at various positions (compounds **10c**, **10e-10g** and **11g**) and nitro at various positions (compounds **10b**, **10h** and **10i**). Because of the high potency of the compound bearing a 4-trifluoromethyl substituent in the tetrahydrothienopyridine family of TRPM8 inhibitors,[79] we

also prepared compound **10j**, which was isolated together with a small amount of its diastereomer **11j**. Some more complex aromatic substituents were also introduced, including (*p*-nitrophenyloxy)phenyl (compounds **10k** and **11k**), 2-naphthyl (compound **10l**) and 6-(3-nitrophenyl)-2-pyridyl (compound **10m**).

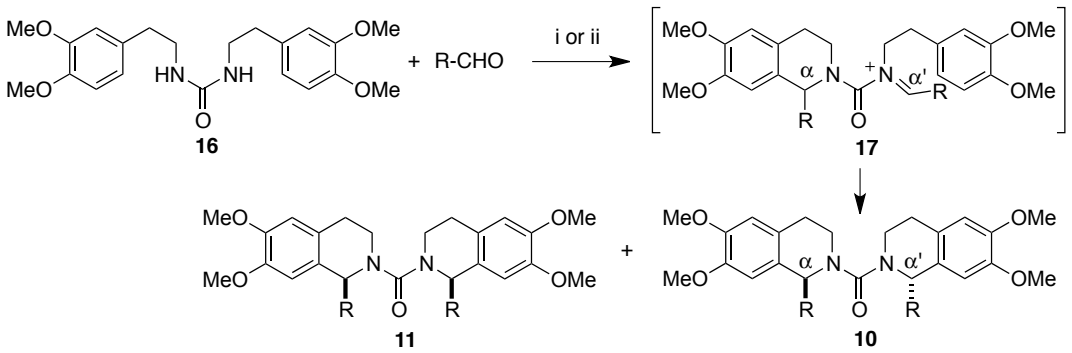

Reagents and conditions: i. $TolSO_2H$, toluene, 120 °C, 12 h; ii. H_2SO_4, AcOH, 65-120 °C, 12 h

Scheme 1. Synthesis of symmetrical urea derivatives

Table 1. Reaction conditions and results obtained in the synthesis of symmetrical urea derivatives

R	Cmpd. [a]	Conditions	*trans*/*cis*	Yield, %
n-Pr	**10a**	$TolSO_2H$, toluene, 120 °C	1/0	60
Ph	**10b**	$TolSO_2H$, toluene, 120 °C	1/0	73
2-ClC_6H_4	**10c**	$TolSO_2H$, toluene, 120 °C	1/0	40 [b]
3-O_2N-C_6H_4	**10d**	$TolSO_2H$, toluene, 120 °C	1/0	82
4-ClC_6H_4	**10e**	$TolSO_2H$, toluene, 120 °C	1/0	37 [c]
4-BrC_6H_4	**10f**	$TolSO_2H$, toluene, 120 °C	1/0	41 [d]

4-FC_6H_4	**10g** **10g** + **11g** **11g**	$TolSO_2H$, toluene, 120 °C H_2SO_4, AcOH, 65 °C H_2SO_4, AcOH, 120 °C	1/0 0.85/0.15 0/1	30 34 37
4-O_2N-C_6H_4	**10h**	$TolSO_2H$, toluene, 120 °C	1/0	50
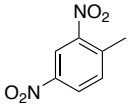	**10i**	H_2SO_4, AcOH, 120 °C $TolSO_2H$, toluene, 120 °C	1/0 ---	20 [e] 16 (**21**)
4-F_3C-C_6H_4	**10j** + **11j**	$TolSO_2H$, toluene, 120 °C	4/1	78
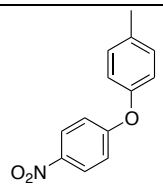	**10k** **11k**	$TolSO_2H$, toluene, 120 °C H_2SO_4, AcOH, 80 °C	1/0 0/1	21 36
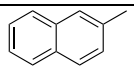	**10l**	$TolSO_2H$, toluene, 120 °C	1/0	40
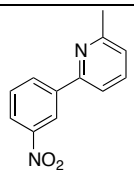	**10m**	H_2SO_4, AcOH, 80 °C H_2SO_4, AcOH, 120 °C	0/1 ---	66 20 (**29**) 30 (**30**)

[a]All compounds have the *trans* structure **10**, except where otherwise noted. [b]Described in reference.94 [c]Together with 37% of compound **27**. [d]Together with 54% of the monocyclic compound **23**. [e]Together with 50% of compound **28**

The known compounds **18-24** (Figure 3) were prepared by treatment of the urea derivative **16** with a variety of aldehydes in the presence of toluenesulfinic acid in refluxing dichloromethane,[94] in order to extend the structure-activity relationship study to non-symmetrical, monocyclic urea derivatives. Compound **25**, which was isolated during the preparation of **19** and arose from the alkylation of the latter compound by the toluenesulfinic

acid-propanal adduct,[94] belongs to the same family of monocyclic ureas and was also studied biologically. In order to further probe the role of molecular symmetry in TRP8 inhibition, we also prepared the known N-acetyl compound **26**,[95] which can be viewed as a "half" of compounds **10** and **11**. Furthermore, side products **27-30**, isolated in small amounts during some of the experiments summarized in Table 1, were considered useful for comparison purposes in connection with the role of a second isoquinoline ring and were also studied biologically.

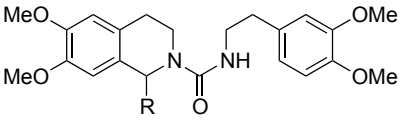

Cmpd.	R
18	Et
19	Pr
20	Ph
21	2-ClC_6H_4

Cmpd.	R
22	3-$NO_2C_6H_4$
23	4-ClC_6H_4
24	4-BrC_6H_4

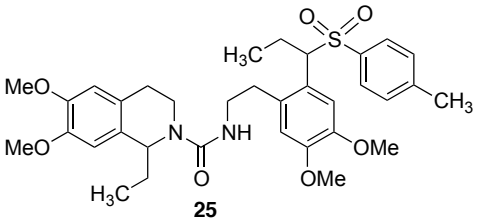

25

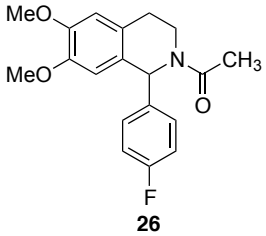

26

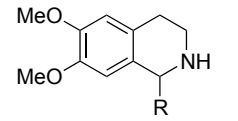

Cmpd.	R
27	4-ClC_6H_4
28	2,4-$(NO_2)_2C_6H_3$

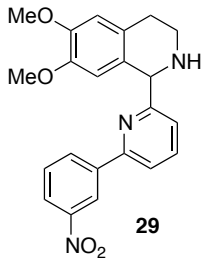

29

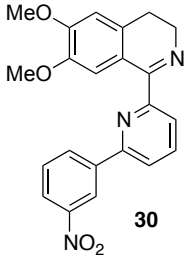

30

Figure 3. Structures of some non-symmetrical, monocyclic urea derivatives studied in this work, together with some additional compounds studied for comparison purposes

We also studied briefly a family of related compounds derived from a 2,5-diketopiperazine core fused to a tetrahydroisoquinoline ring (structures **13** and **14** in the Introduction). Besides some known[94] arylmethylene derivatives of the pyrazino[1,2-*b*]isoquinolin-1-one system (compounds **31-35** in Figure 4), we also examined the activity of their arylmethyl analogues

37 and **38**, which were prepared by Pictet-Spengler cyclization of precursors **36**, either using our α-amidosulfone-mediated protocol (compound **37**) or under more classical acidic conditions (compound **38**). Interestingly, both methods led to different diastereomers, allowing us to explore the influence of this parameter on activity. The related linear pentacyclic compound **39**, arising from a double Pictet-Spengler cyclization, was also studied.

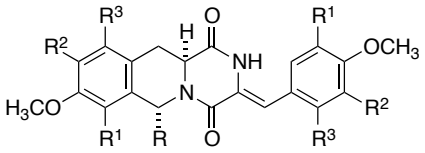

Cmpd.	R	R^1	R^2	R^3
31	Ph	H	OMe	H
32	4-BrC_6H_4	H	OMe	H
33	3-$NO_2C_6H_4$	H	OMe	H
34	2-ClC_6H_4	H	OMe	H
35	Ph	OMe	Me	OMe

Figure 4. 3-Arylmethylenepyrazino[1,2-*b*]isoquinolin-1-one derivatives studied in this work

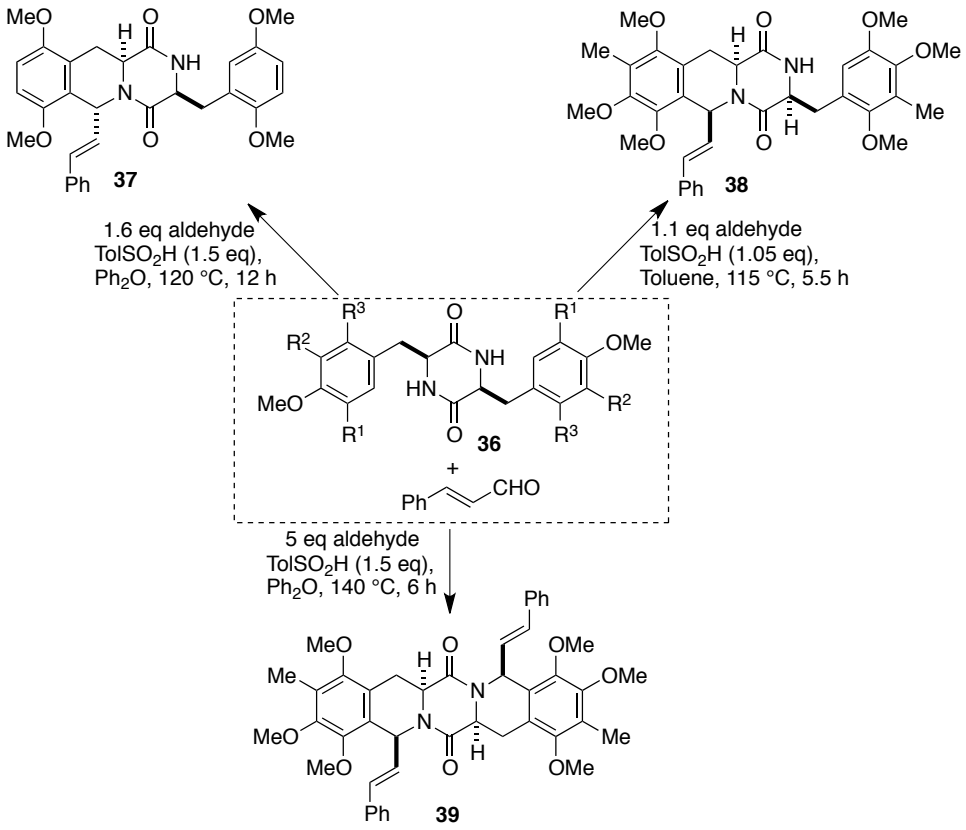

Scheme 2. Synthesis of two 3-arylmethylpyrazino[1,2-*b*]isoquinolin-1-ones **37** and **38** and a pyrazino[1,2-*b*:4,5-*b'*]diisoquinoline-7,15(5*H*,13*H*)-dione **39**

Channel inhibition results and structure-activity relationship (SAR) analysis

The synthesized TRPM8 ligands were evaluated *in vitro* for antagonism, as measured by inhibition of receptor activation by the well-known TRPM8 agonist icilin. The assays were conducted using a fluorometric assay with rat TRPM8 heterologously expressed in human embryonic kidney (HEK-293) cells,[66] and the results obtained are collected in Table 2. The compounds tested did not significantly activate TRPM8-mediated Ca^{2+} elevation in transfected HEK-293 cells (efficacy lower than 10%), with the exception of compounds **10h**, **25**, **31** and **38** but with a very low potency (EC_{50} values higher than 10 μM). On the other hand, preincubation (5 min) of TRPM8-HEK-293 cells with different doses of the tested

compounds, followed by incubation with icilin (0.25 μM), caused an inhibition of the Ca^{2+} elevation due to TRPM8 response to icilin. The IC_{50} values (against icilin at 0.25 μM) are reported in Table 2.

Table 2. TRPM8 activation and inhibition data

Compound	**TRPM8 efficacy** (% ionomycin, 4 μM)	**TRPM8 potency** (EC_{50}, μM)	**IC_{50} inhibition TRPM8, μM** (icilin 0.25 μM)
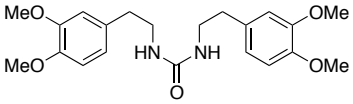 **16**	< 10	NA	> 50
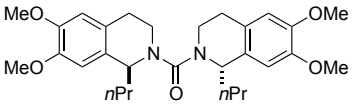 **10a**	< 10	NA	8.5 ± 2.0
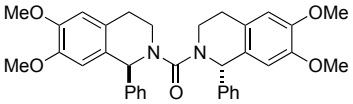 **10b**	< 10	NA	0.50 ± 0.02
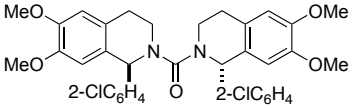 **10c**	< 10	NA	19.8 ± 1.7
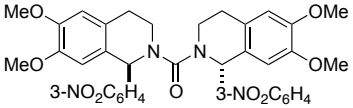 **10d**	< 10	NA	44.4 ± 3.9
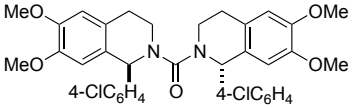 **10e**	< 10	NA	0.43 ± 0.10
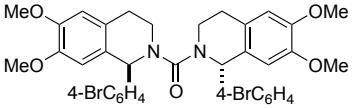 **10f**	< 10	NA	2.2 ± 0.5
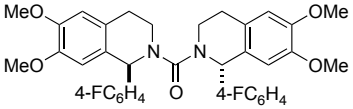 **10g**	< 10	NA	0.072 ± 0.004

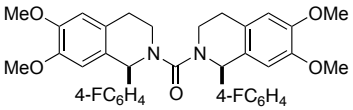 **11g**	< 10	NA	> 50
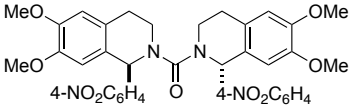 **10h**	22.7 ± 1.7	14.2 ± 4.2	> 50
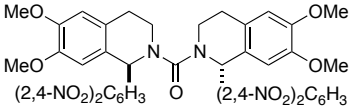 **10i**	< 10	NA	> 50
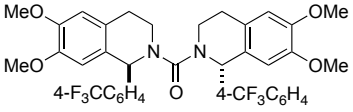 **10j**	< 10	NA	0.18 ± 0.11
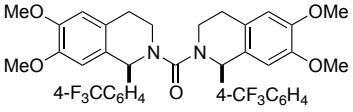 **11j**	< 10	NA	10.6 ± 1.4
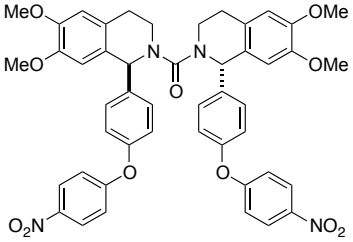 **10k**	< 10	NA	> 50
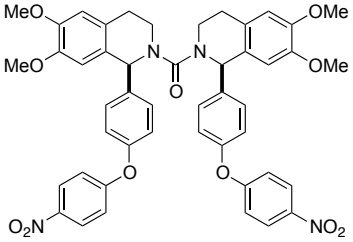 **11k**	< 10	NA	> 50
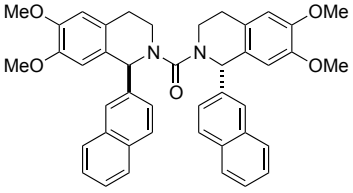 **10l**	< 10	NA	> 50

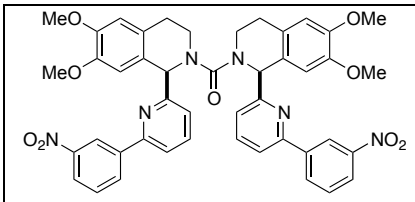 **10m**	< 10	NA	43.7 ± 2.1
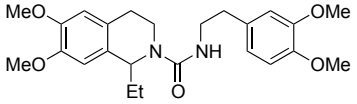 **18**	< 10	NA	> 50
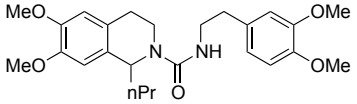 **19**	< 10	NA	> 50
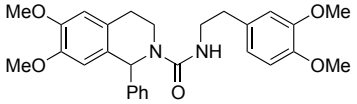 **20**	< 10	NA	1.2 ± 0.3
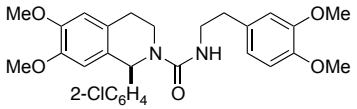 **21**	< 10	NA	46.1 ± 1.5
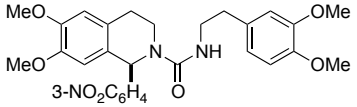 **22**	< 10	NA	> 50
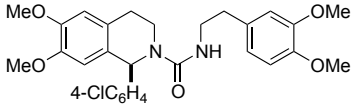 **23**	< 10	NA	31.7 ± 1.3
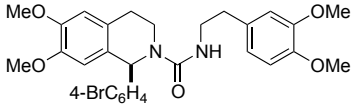 **24**	< 10	NA	48.2 ± 3.0
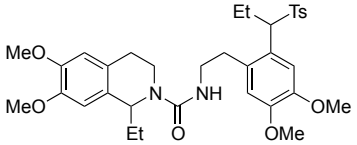 **25**	15.3 ± 0.1	26.1 ± 0.1	> 50
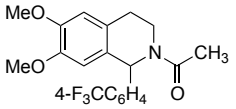 **26**	< 10	NA	> 50
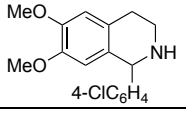	< 10	NA	> 50

27			
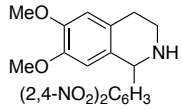 **28**	< 10	NA	> 50
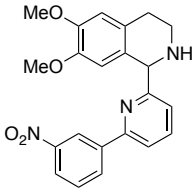 **29**	< 10	NA	> 50
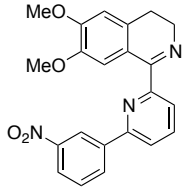 **30**	< 10	NA	22.9 ± 3.2
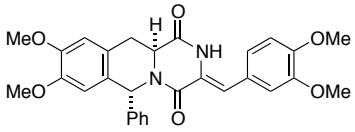 **31**	14.7 ± 0.1	15.9 ± 0.1	12.8 ± 0.3
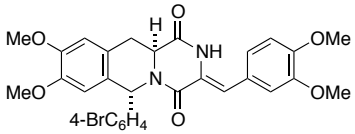 **32**	< 10	NA	42.4 ± 0.4
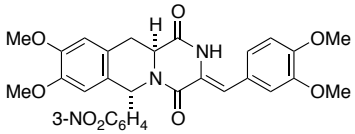 **33**	< 10	NA	35.2 ± 2.3
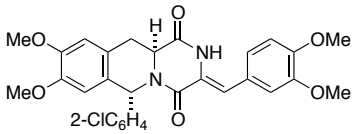 **34**	< 10	NA	39.3 ± 0.3
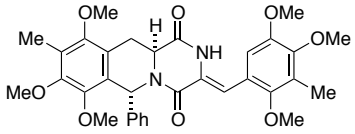 **35**	< 10	NA	0.62 ± 0.06
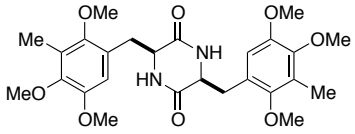 **36**	NA	NA	> 50

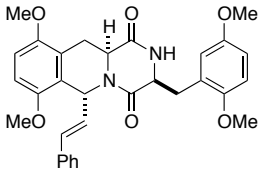 **37**	< 10	NA	30.6 ± 3.7
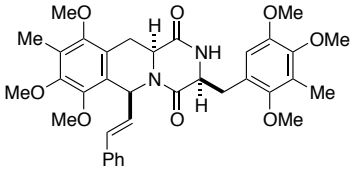 **38**	26.6 ± 0.4	20.8 ± 3.1	3.2 ± 0.1
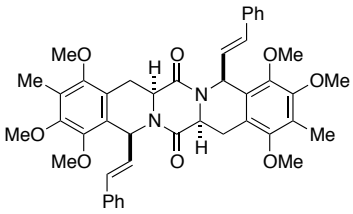 **39**	< 10	NA	8.8 ± 0.7

As shown previously, icilin dose-dependently elevates intracellular Ca^{2+} (EC_{50} of 0.19 ± 0.03 μM) in TRPM8-HEK-293 cells, but not in non-transfected cells.[66] This assay allowed us to profile a number of TRPM8 antagonists. The order of decreasing potency (IC_{50} from lower to higher values) of the most active compounds (*i.e.* those showing IC_{50} < 10 μM against icilin), is as follows:

10g > **10j** > **10e** > **10b** > **35** > **20** > **10f** > **38** > **39** (IC_{50} range from 72 nM to 8.8 μM)

Although some of the compounds have low potency and therefore reliable SAR analysis is difficult in these cases, the data summarized in Table 2 have led to a number of useful conclusions, which are summarized below for the two families of compounds studied.

For urea derivatives:

(a) The urea function is not sufficient for activity and the presence of at least one tetrahydroquinoline ring is required, as shown by the comparison of the activities of compound **16** (no tetrahydroisoquinoline ring) with **20**, **21**, **22** and **23** (one tetrahydroisoquinoline ring).

(b) The isoquinoline ring, on its own, is also insufficient for activity. This is deduced from comparison of the activities of isoquinoline derivatives **27** and **29** with the corresponding bis- tetrahydroisoquinoline compounds generated by linking two isoquinoline units with a carbonyl, leading to an urea moiety (**10e** and **10m**, respectively).

(c) Symmetric systems containing two tetrahydroisoquinoline rings linked by a carbonyl unit are more potent than their analogues bearing a single THQ ring. This conclusion holds true for all cases in which a direct comparison was possible (**10a** > **19**; **10b** > **20**; **10c** > **21**; **10d** > **22**; **10e** > **23**; **10f** > **24**). The N-acetyl derivative **26**, related to **10g** but having a single tetrahydroisoquinoline ring and a carbonyl group on nitrogen, was inactive, giving further support to the above conclusion.

(d) C-1 phenyl substituents lead to higher potency than C-1 alkyl groups, both in the mono-tetrahydroisoquinoline and the bis-tetrahydroisoquinoline series. Thus, **18**, **19** and **25** (ethyl-substituted) were less potent than **20** (phenyl-substituted) and similarly **10a** (*n*-propyl-substituted) was less potent than **10b** (phenyl-substituted).

(e) The nature of substituents on the aromatic ring does not have a clear-cut influence on activity, although a *p*-halogen substituent is generally favourable in the case of bis-tetrahydroisoquinoline derivatives (*cf.* compounds **10e**, **10f** and **10g** *vs*. the unsubstituted

compound **10b**). Fluorinated substituents, which include *p*-fluoro (**10g**) and *p*-trifluoromethyl (**10j**) lead to the highest potencies.

(f) A *cis* arrangement between the C-1 and C-1' substituents in bis-tetrahydroisoquinoline systems seems detrimental to activity, judging by the comparison between compounds **10g**-**11g** and **10j**-**11j**.

For pyrazino[1,2-*b*]isoquinolin-1-one derivatives:

(a) As in the previous case, the presence of an isoquinoline ring is essential for activity. This can be deduced from the comparison of the activities of the open diketopiperazine derivative **36** and compounds **37** and **38**. The presence of a second isoquinoline ring, as in **39**, did not further improve the activity.

(b) A high degree of substitution in the isoquinoline ring increases activity, as shown by the comparison of the activities of compounds **31** and **35**, and also **37** and **38**, although in the latter case there is a stereochemical difference that makes the conclusion less clear-cut.

In order to rationalize our results on the basis of modeling data, the most active compound within our series, i.e. **10g**, was docked into the putative ligand binding site encompassing the S1-S4 transmembrane helices and the TRP domain domain site of the rat TRPM8, built as described in the Experimental section. One of the noteworthy features of this model is the position of both Asn799 and Asp802 residues, lying on S3 and known to affect icilin binding,[3] which are located inside the pocket. The study of **10g** by a docking protocol requires, as a prerequisite, a detailed conformational analysis, since it can assume different, interdependent

conformational states of its two non-aromatic rings. Unfortunately, the implementation of ring conformational flexibility in most docking programs is at best problematic, and thus molecular conformations corresponding to all the energetically-accessible combinations of ring dihedral angles were generated by a conformational search, followed by *ab-initio* optimization, and separately docked for both enantiomers of **10g**. A total of 28 best poses, selected as described in the Experimental Section from docking runs carried out on twelve (*i.e.* six for each enantiomer) conformers, were energy minimized and scored by ligand-protein interaction energy (EI) (see Table S.1 of the Supporting Information). Figure 5 shows the most stable pose for each enantiomer, while Table 3 lists interaction energies and the main polar interactions for these poses, along with those of the other four exhibiting EI below -95 kcal mol^{-1}. The emerging pattern of ligand-protein interactions involves: the arginine residues at both ends of the site, i.e. Arg842, Arg1008, with the dimethoxytetrahydroisoquinoline moieties (H bonds) and, in some cases, with the fluorobenzene groups (ionic-π interactions); Tyr754 and Tyr1005 with either fluorophenyl or tetrahydroisoquinoline groups (aromatic interactions); Arg851 and Asn692 with the urea group (H-bonds). Ligand fluorine atoms also engage in favorable polar interactions with protein backbone carbonyl groups, a kind of interactions frequently occurring in X-ray structures of proteins with fluorinated ligands.[96] The peculiar interactions engaged by the fluorine atoms with both backbone and arginine residues help to rationalize the higher activity of this derivative in comparison with those bearing other halogens (compounds **10e** and **10f**) and/or hydrogen (compound **3**) in place of fluorine. The ability of compound **10g** to engage multiple favorable polar interactions validates our starting assumption that symmetrical molecules containing two

tetrahydroisoquinolines linked by a urea moiety would provide strong interactions with the TRPM8 binding site.

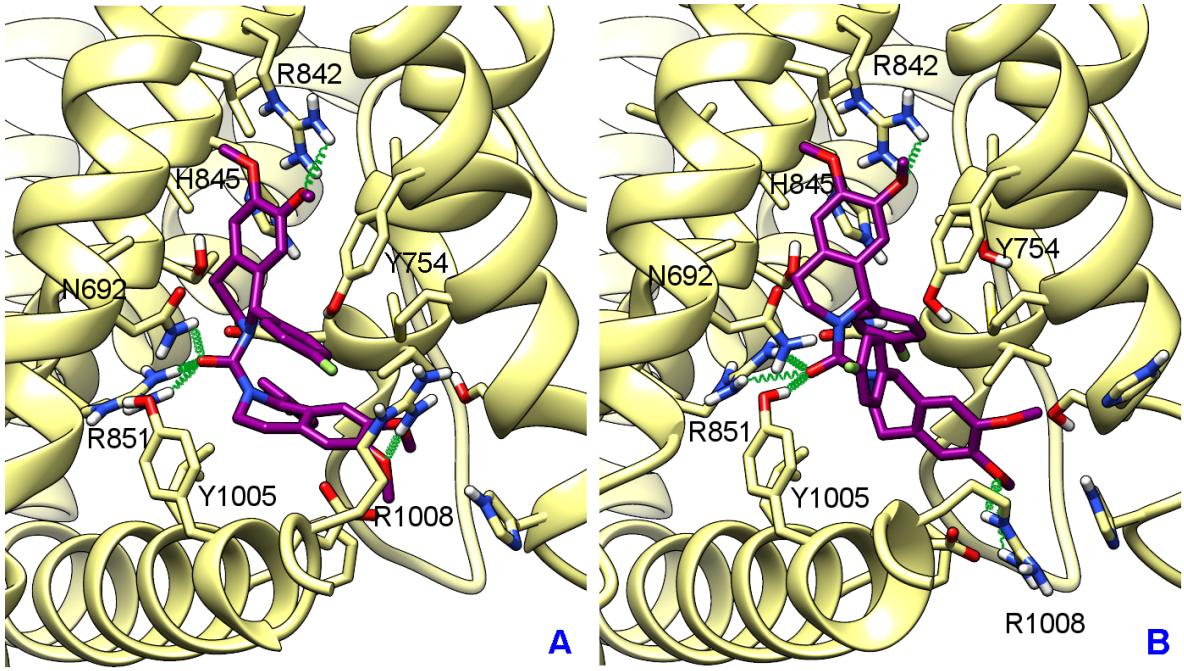

Figure 5. The best docked complexes of rat TRPM8 monomer model with the *RR* (A) and *SS* (B) enantiomers of compound **10g** are shown, using a ribbon representation for the protein backbone and sticks for the ligands and the side chains of protein residues involved in contacts with the ligand, which is colored in dark magenta. Atoms are colored with the following code: O=red, N=blue, H=white, F=green. Ligand-protein H-bonds are depicted with a green spring.

The main contacts and interaction energies associated to docking poses A and B are summarized in Table 3.

Table 3: Interaction energy (EI) and main interactions in the docking binding poses of compound **10g** with EI < 95 kcal mol^{-1}. Poses are numbered with roman numerals by increasing EI and the corresponding ligand chiralities are reported in parenthesis (in **bold** for the stablest pose for both *RR* and *SS* enantiomers, corresponding to panels **A** and **B** in Figure 5, respectively).

Ligand pose (chirality)	Interaction Energy (kcal mol^{-1})	H-Bonds[a]	Polar/aromatic interactions[a]
***I* (*RR*)**	**-121.586**	Urea CO-Asn692(sc)/Arg851(sc) MeO-THIQ1-Arg1008(sc) MeO-THIQ2-Arg842(sc)	FB2-Arg1008(sc)/Tyr754, THIQ2-Arg842(sc)/His845(sc)
II (*RR*)	-108.579	Urea CO-Asn692(sc), MeO-THIQ1-Arg1008(sc)	THIQ2-Arg842(sc)/His845(sc), FB2-His845(sc)/Asn799(bb) FB1-Tyr754(sc)/Asn692(sc)
***III* (*SS*)**	**-107.264**	Urea CO-Tyr1005(sc)/Arg851(sc) MeO-THIQ1-Arg1008(sc) MeO-THIQ2-Arg842(sc)	FB1-Tyr754(sc)/Asn692(sc)/Tyr1005 THIQ2-Arg842(sc)/His845(sc), FB2-Asn799(bb)/His845(sc)
IV (*SS*)	-103.850	Urea CO-Asn692(sc) MeO-THIQ1-Arg1008(sc)	FB2-Arg842(sc) FB1-His845/Asn799(bb) THIQ1-Tyr1005, THIQ2-Tyr754
V (*RR*)	-97.725	Urea CO-Tyr754(sc) MeO-THIQ2-Arg851(sc)	FB1-Tyr1005(sc)/Asn692(sc) FB2-Arg842(sc)
VI (*RR*)	-95.080	Urea CO-Asn692(sc) MeO-THIQ1-Arg851(sc)	FB1-Arg842(sc)/His845(sc), THIQ2-Tyr754

			FB2-Arg851(sc)/Val849(bb),THIQ1-Arg851

[a] THIQ: tetrahydroisoquinoline moiety; FB=Fluorobenzene ring; the 1 and 2 indices refer to symmetric units of molecule (R_1-CO-R_2); sc= side chain; bb=CO backbone

Some of the more active compounds were also tested as potential inhibitors of other thermo TRP channels. The data displayed in Table 4 indicate IC_{50} values higher than 10 μM for all the compounds and for all the receptors tested, showing a good degree of selectivity for TRPM8 for all these compounds, but particularly in the case of compound **10g**.

Table 4. Inhibition of TRPM8 and other thermo TRP channels by compounds **10b**, **10e**, **10g** and **35** (IC_{50} μM). The values in parentheses correspond to the TRPM8/TRPx selectivities

Channel	**10b**	**10e**	**10g**	**35**
TRPM8 (icilin 0.25 μM)	0.50 ± 0.02	0.43 ± 0.10	0.072 ± 0.004	0.62 ± 0.06
TRPA1 (AITC 100 μM)	10.0 ± 2.0 (20:1)	23.9 ± 0.7 (56:1)	16.4 ± 2.1 (228:1)	14.2 ± 0.6 (23:1)
TRPV1 (capsaicin 0.1 μM)	53.0 ± 1.0 (106:1)	49.7 ± 1.7 (116:1)	68.5 ± 2.1 (951:1)	68.9 ± 1.5 (111:1)
TRPV2 (LPC 3 μM)	51.9 ± 8.0 (104:1)	54.9 ± 9.4 (128:1)	94.3 ± 10.0 (1309:1)	12.4 ± 1.4 (20:1)
TRPV3	> 100	> 100	72.9 ± 4.0	34.3 ± 4.0

(thymol 100 μM)	(> 200:1)	(> 233:1)	(1012:1)	(55:1)
TRPV4 (4αPDD 1μM)	82.6 ± 0.1 (194:1)	81.5 ± 0.1 (189:1)	96.2 ± 16.3 (1336:1)	> 100 (> 161:1)

Anti-proliferative activity

TRPM8 mRNA has been detected in malignant cells and this channel has been extensively studied in prostate cancer,[47] Our previous study showed that TRPM8 mRNA is highly expressed in LNCaP epithelial prostate cancer cells.[50] It has been reported that TRPM8 might be a useful marker for prostate cancer, since loss of TRPM8 expression appears to be associated to transition to androgen independence and poor prognosis.[97,98].

Against this backdrop, we have studied the anti-proliferative activity on LNCaP prostate cancer cell lines of a selection of the most active TRPM8 inhibitors, namely compounds **10b**, **10e**, **10g** and **35**. We found that at all these compounds, at 10 μM concentration, exert a marked anti-proliferative activity, inhibiting after three days of treatment the cellular growth from a minimum of 50.4 % (for **10e**) to a maximum of 64.3 % (for **10g**). We employed compound **11g**, a diastereomer of **10g** that does not inhibit TRPM8, as a negative control. As positive control, we used compound **40**, an antagonist of TRPM8 whose effectiveness has been previously tested on LNCaP cells[71] (Figure 6). On the other hand, cell viability was only moderately affected, as evaluated by the viability-dye CBNF (see Figure 6 below). At the concentrations used, we did not observe any cytotoxic effects of the drugs, as measured by trypan blue.

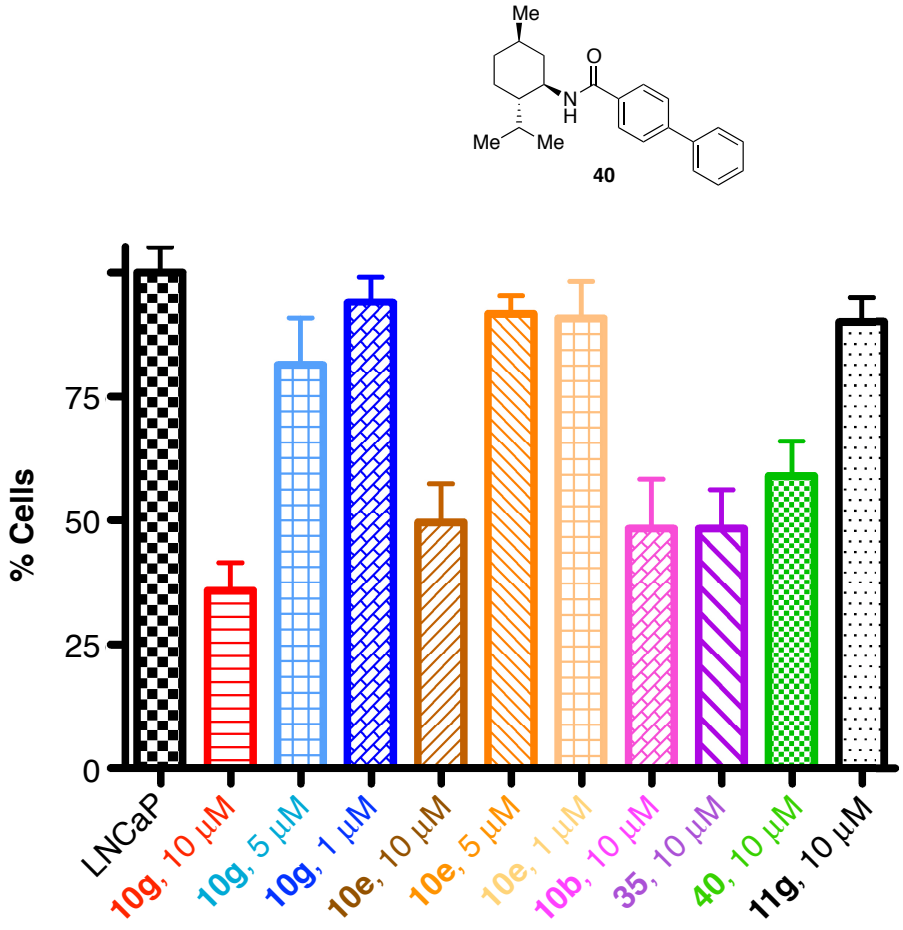

Figure 6. Evaluation of compounds **10b**, **10e**, **10g**, **11g**, **35** and **40** on LNCaP cell growth. LNCaP cells were cultured for 72 hours and treated with the compounds under assay at the indicated concentrations, as described in the Experimental Section. The cell number was evaluated and the statistical analysis performed as described in the Experimental Section ($p < 0.001$ **10g** *vs* LNCaP).

As shown in Figure 7 and in Table 5, the effect of compound **10g** on cell viability of prostatic tumor cell LNCaP and 22RV1 and of human normal prostate epithelium cells PNT1A, was evaluated by the viability dye CBFN. The cells were gated by selecting the threshold of red-fluorescence at ≥ 10 fluorescence units. A different response of the three cell lines was observed. In fact, in the case of LNCaP cells the percent of gated cells was 83.3 % *vs* 54.4 %

and the fluorescence mean value in the gated regions was 215.97 *vs* 176.01 for the vehicle and cells treated with compound **10g**, respectively. These data indicated a different viability degree in LNCaP treated by compound **10g**, thus confirming the slowdown of cell growth. On the contrary, for the 22RV1 and PNT1A cells, both the percent of gated cells and the fluorescence mean values were unaffected by the treatment. In order to evaluate if these effects on the cell growth and viability are mediated by the TRPM8 receptor, the transcriptional TRPM8 levels were evaluated by qRT-PCR in the three prostatic cell lines and in the human kidney embryonic cells HEK-293.

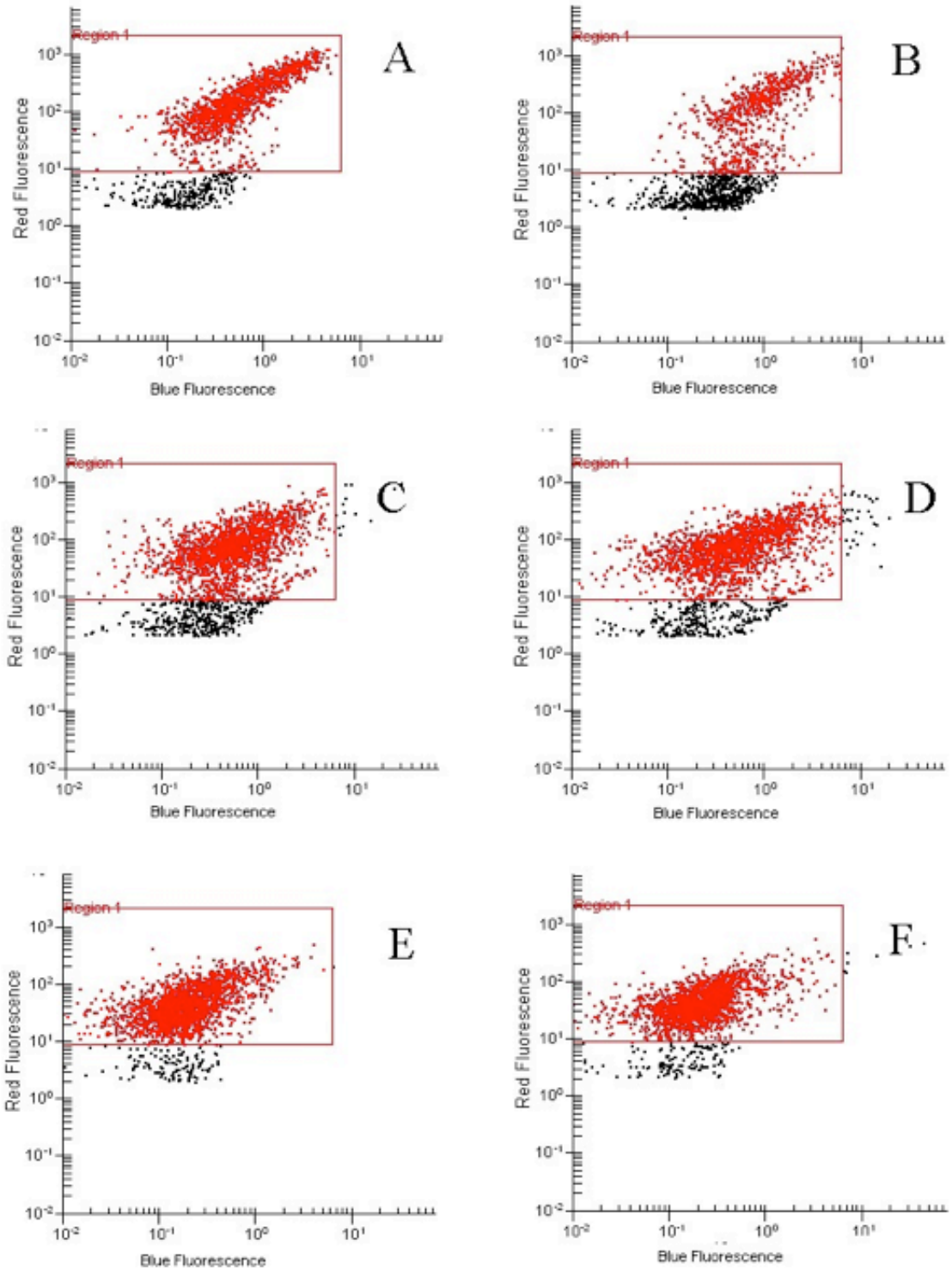

Figure 7. Evaluation of cell viability by CBNF assay. The figure shows a typical experiment of cell viability performed by the vital dye CBFN in a 2100 Bioanalyzer, as described in the Experimental section: Panel A: LNCaP cell treated for 72 h by vehicle; panel B, LNCaP

treated for 72 h by 10 μM compound **10g**; panel C and panel D: comparable treatments performed on 22RV1 cells; panel E and panel F: comparable treatments performed on PNT1A cells.

Table 5. Statistical analysis data. Total events, number of cell analyzed; %Gated region events, % of total cells gated in the region; Gated Red-Fluo. (mean), mean of red-fluorescence (Y) in the gated region; CV%, coefficient of variation %.

Panel	Sample Id.	Total Events	Gated Region Events %	Gated Red-Fluo. (mean)	CV%
A	LNCaP	1547	83.30	215.97	97.44
B	LNCaP + **10g**	1387	54.40	176.01	105.07
C	22RV1	2254	81.30	93.29	95.80
D	22RV1 + **10g**	2173	82.20	93.62	92.47
E	PNT1A	2202	94.10	54.78	86.87
F	PNT1A + **10g**	2108	92.70	49.84	81.65

To confirm that these effects on the cell growth are mediated by the TRPM8 receptor, we compared the behaviour of LNCaP cells to: (a) 22Rv1 prostate cancer cells that do not express TRPM8 channels; (b) non-tumoral (SV40 immortalized) prostate cell line, PNT1A; (c) non-prostate human cells (HEK-293) (Figure 8). These four cell lines were selected on the basis of the different transcriptional TRPM8 levels, as evaluated by qRT-PCR.

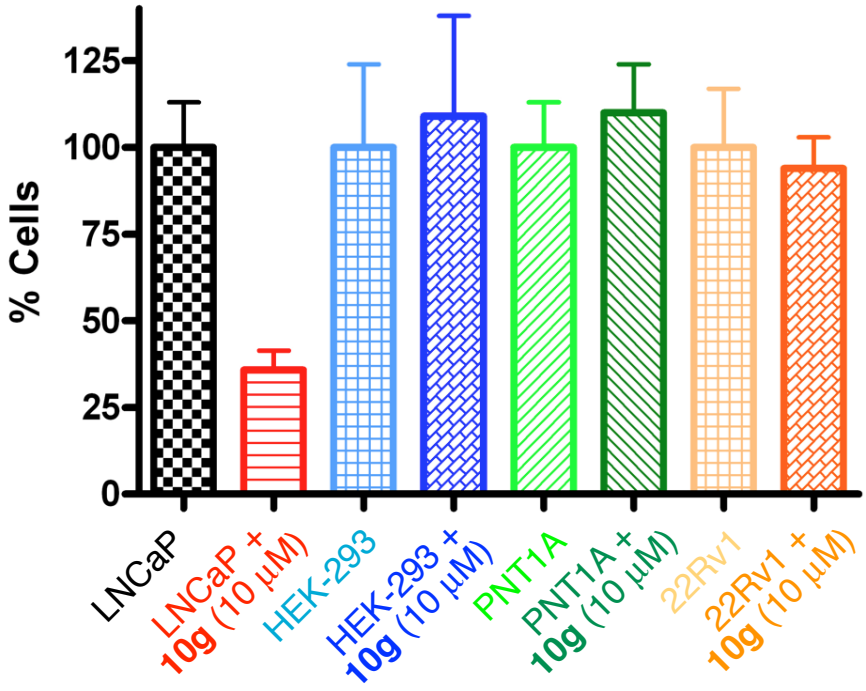

Figure 8. Evaluation of compound **10g** on prostatic tumor cells (LNCaP and 22Rv1, human normal prostate epithelium cells (PNT1A) and human kidney embryonic 293 cells (HEK) cell growth. The cells were cultured for 72 hours and treated with 10 µM compound **10g**, as described in the Experimental section. The cell number was evaluated and the statistical analysis performed as described in the Experimental Section ($p < 0.001$ **10g** vs LNCaP).

As shown in Figure 9, a robust expression of TRPM8 mRNA was observed in LNCaP, while in PNT1A and in 22Rv1 prostate tumor cells, the expression levels were about 6 and more than 15 fold lower, respectively. The expression of the TRPM8 receptor in non-prostate human HEK-293 cells turned out to be very close to background. It is noteworthy that in PNT1A cells it has been described the absence of TRPM8 at protein level, counterweighed by a detectable transcriptional expression.[99] Previous reports had shown that the proliferation of LNCaP cells is reduced by inhibition of TRPM8.[49,100] The inhibition of growth rate seems to reflect the content and/or the role of TRPM8 channels in these cells. In other words,

compound **10g** was able to inhibit significantly only the growth of LNCaP cells in which TRPM8 channels are abundantly expressed at both mRNA and protein levels.

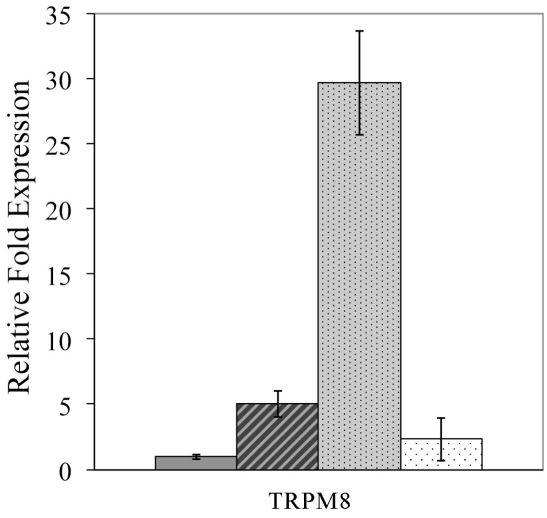

Figure 9. TRPM8 transcriptional expression in prostatic tumor cells, in benign prostatic hypoplasia cells and in human kidney embryonic cells. Relative TRPM8 mRNA levels (TRPM8) were evaluated, by qRT-PCR as described in methods, in prostatic tumor cell LNCaP and 22RV1, in human normal prostate epithelium cells PNT1A and in human kidney embryonic cells HEK-293 by using 20 ng of cDNA for assay (5 replicates). Relative fold expressions values were scaled respect to the lower expression value (HEK-293) put as 1, quantitative cycles (Cq) = 33.73. The higher relative expression was detected in LNCaP cells, Cq = 28.13 (background over 40 Cq). Standard deviations were calculated by the Gene expression module of iQ5 real-time PCR. The relative expression difference LNCaP vs PNT1A (about 6 fold) was significant ($P < 0.001$) as evaluated by REST-2009 software.[101].

Apoptotic activity

To further confirm this behavior, caspase 3/7 was employed to assay the apoptotic levels induced by the above treatments on LNCaP cells. A significant increase of caspase 3/7 activity was observed for compound **10g** (Figure 10A) and the data obtained for all the compounds

tested are summarized in Figure 10B describing an enhancement of caspase 3/7 activity, compared to control cells, of about 200% for all four compounds tested (**10a**, 220±40; **10e**, 190±100; **10g**, 198±21; **35**, 200±20). Taking in account the viability data, this modest increase of apoptosis can probably be ascribed to a G_o/G_1 arrest, instead of a direct pro-apoptotic effect of the compounds.

Further studies will be needed to clarify at molecular level the role of TRPM8 channels in LNCaP cells that are commonly accepted as a cell-model for human prostatic tumour.

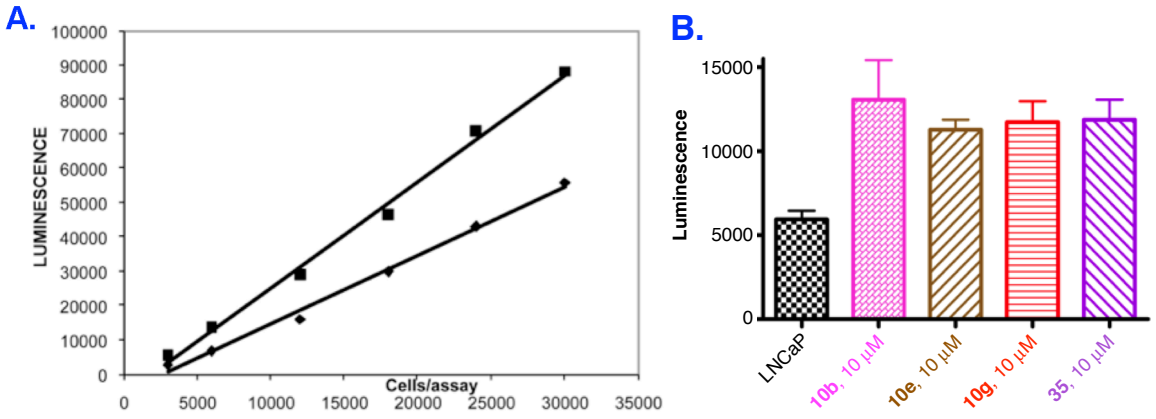

Figure 10. Compounds **10b**, **10e**, **10g** and **35** are able to induce apoptosis as evaluated by Caspase Glo 3/7 assay. **Panel A.** LNCaP were cultured for 72 hours in presence of vehicle or 10 µM of compound **10g**. The panel depicts a typical experiment performed by using different amounts of cell in the assay and shows the linearity of response. **Panel B.** LNCaP were cultured for 72 hours in presence of vehicle (LNCaP) or 10 µM of compounds **10b**, **10e**, **10g** and **35**, as described in the Experimental Section. Apoptosis was evaluated by Caspase Glo 3/7 assay, as described in the Experimental Section, by using 10000 cells/assay in triplicate.

1-Aryl-1,2,3,4-tetrahydroisoquinoline derivatives related to our compounds have been reported as metabolically labile, probably by CYP oxidation at their and their benzylic positions.[79,80] For this reason, we examined the metabolic stability of representative

compounds from our library on mouse liver microsomes, which are very close to the human ones in terms of metabolic reactivity. The *in vitro* clearance data obtained from liver microsomes has been shown to provide a suitable assesment of the *in vivo* situation.[102]

The results of this study are summarized in Table 6, and show a very good stability (better than that of acetaminophen, used as a reference) for the potent *p*-trifluoromethyl derivative **10j**, having a sub-micromolar potency as a TRPM8 antagonist. The *p*-bromo derivative **10f** also showed a good metabolic stability, but other halogenated derivatives (compounds **10c** and **10g**) were less suitable. These stability trends are parallel to the electron-withdrawing effect of the substituents on the aryl substituent, suggesting that the main metabolic pathway is oxidation at the doubly benzylic positions. The phenyl-unsubstituted compound **20**, containing only one tetrahydroisoquinoline ring, was also quite labile. Finally, compound **35**, representing our second family of diketopiperazine-related compounds and having a potency similar to that of **10j**, showed a good metabolic stability.

Table 6. Hepatic microsomal intrinsic clearance data of representative compounds

Compound	CL_{int}, mL/(min.kg)
10c	52.9
10f	19.1
10g	75.2
10j	10.1
20	39.6
35	15.6
Acetaminophen	12.2

Finally, in order to address potential concerns about the drug-likeness of our compounds, we measured experimentally the aqueous solubility of representatives selected among our most potent derivatives, namely **10g**, **10j** and **35**. The results are summarized in Table 7, and show that the urea derivatives **10g** and **10j** have solubilities at least 10 times higher than the fused diketopiperazine **35**. For comparison purposes, the aqueous solubilities of several widely used, orally active drugs are also included in the Table.[103-105] Although a direct comparison is hampered by the fact that the experiment temperature may not be the same in all cases, it can nevertheless be concluded that the urea derivatives have solubilities in the same range as the reference drugs and can thus be regarded as acceptable candidates at this early stage.

Table 7. Aqueous solubility of representative compounds

Compound	log *S* (mol.L^{-1})
10g[a]	- 5.19
10j[a]	- 4.94
35[a]	- 6.17
Raloxifene hydrochloride[b]	- 5.91[103]
Danazol[c]	- 5.51[104]
Megestrol acetate[c]	- 5.35[104]
Tadalafil[a]	- 5.14[105]
Nifedipine[c]	- 4.76[104]

[a]Measured at 37 °C. [b]Measured at 25 °C. [c]Temperature not specified

Conclusions

Two families of tetrahydroisoquinoline derivatives, namely tetrahydroisoquinolines containing an embedded urea function and pyrazino[1,2-*b*]isoquinolin-1-ones, were identified as TRPM8 channel receptor antagonists. All together, we describe here the characterization of 39 compounds, some of which potently inhibited the icilin-induced increase in intracellular calcium in cells expressing rat TRPM8. Several structure activity relationships were discovered for the urea series, including the higher activity of bis(1-aryl-6,7-dimethoxy-1,2,3,4-tetrahydroisoquinolyl)ureas. This suggests a role for molecular symmetry in TRPM8 inhibition, which was rationalized by docking studies. None of the compounds activated TRPM8 at concentrations up to 10 μM, indicating that they do not act as partial agonists. All compounds were tested against a small panel of TRP-receptor agonists (allyl isothiocyanate activated TRPA1, capsaicin activated TRPV1, 2-aminoethoxydiphenyl borate and thymol activated TRPV3, and 4α-phorbol-12,13-didecanoate activated TRPV4) to verify their selectivity for TRPM8 channel receptor, and we found no significant inhibition at concentrations up to 10 μM. The most potent and selective compound was the 4-F derivative (compound **10g**), with IC_{50} in the 10^{-8} M range and *ca.* 1000:1 selectivities for most other TRP receptors. On the other hand, the 4-CF_3 derivative, although slightly less potent, showed an improved metabolic stability towards hepatic microsomes. A selection of compounds demonstrated strong anti-proliferative activity in prostate cancer cells, but not in other cancer cell lines, with the available evidence suggesting that this activity is linked to TRPM8 inhibition.

Experimental Section

General experimental information

All reagents and solvents were of commercial quality and were used as received. Ultrapure water was produced using a Milli-Q Direct 8 water purification system. Reactions were monitored by thin layer chromatography, on aluminium plates coated with silica gel with fluorescent indicator. Separations by flash chromatography were performed on silica gel (40-63 μm). Melting points were measured on a hot stage microscope, and are uncorrected. Infrared spectra were recorded on a FT-IR spectrophotometer, with all compounds examined as thin films on NaCl disks. NMR spectra were obtained on an instrument operating at 250 MHz for ^{1}H and 63 MHz for ^{13}C, using $CDCl_3$ as solvent and residual $CHCl_3$ as the internal standard. All compounds were shown to have higher than 95% purity by combustion microanalysis. Some of them were observed as rotamer mixtures in the NMR spectra. Reverse phase HPLC experiments were performed using a C18 column as stationary phase and 85/15 methanol-water as mobile phase, at a 1mL/min flow rate and employing UV–Vis detection.

Synthesis

General procedures for the Pictet-Spengler reactions of compound 16

Method A: α-Amidosulfone variation of the Pictet-Spengler reaction: To a solution of 1,3-bis(3,4-dimethoxyphenethyl)urea **16**[92,94] (1.0 eq) in toluene (5 mL) was added the suitable aryl or alkyl aldehyde (3 eq), *p*-toluenesulfinic acid (1.1 – 3.0 eq) and the solution was heated at 120 ºC for 12 h. The mixture was poured onto a saturated solution of $NaHCO_3$ (5 mL), which was extracted with DCM (2 x 30 mL). The combined organic layers were concentrated under reduced pressure and the residue was purified by flash column chromatography using mixtures of petroleum ether: diethyl ether to give compounds **10a-m** and **11j**.

Method B: Conventional acid-promoted Pictet-Spengler reactions: To a solution of compound **16** (1.0 eq) in AcOH (5 mL), the corresponding aryl or alkyl aldehyde (3.0 eq) and sulfuric acid (1.8 – 3.0 eq) were added. The solution was heated at 80 – 120 ºC for 12 h, cooled and quenched with a saturated solution of $NaHCO_3$ (10 mL), which was extracted with DCM (2x30 mL). The combined extracts were dried (Na_2SO_4) and concentrated under reduced pressure, and the crude was purified by flash column chromatography using mixtures of ethyl acetate:methanol to give compounds **11g** and **11k**.

(±)-(*R,*R**)-Bis(6,7-dimethoxy-1-(*n*-propyl)-3,4-dihydroisoquinolin-2(1*H*)-yl)methanone (10a)**. Obtained according to the general procedure A from compound **11** (0.20 g, 0.51 mmol), *p*-toluenesulfinic acid (0.24 g, 1.53 mmol, 3 eq), butyraldehyde (0.37 g, 5.1 mmol) and toluene (5.0 mL) as solvent at 120 ºC. Purification by flash column chromatography on silica gel using diethyl ether as eluent afforded the product **10a** as a white solid that appears as a mixture of rotamers in the NMR spectra, yield 0.15 g, 60 %; m.p. 66 – 68 ºC; IR (neat): $\tilde{\nu}$ = 3072, 2910 cm^{-1}; ^1H NMR (250 MHz, $CDCl_3$): δ = 6.40-6.60 (m, 2 H), 5.03 – 4.27 (m, 2 H), 3.92 – 3.70 (m, 14 H), 3.37 (m, 2 H), 2.92 – 2.58 (m, 2 H), 2.34 (m, 2 H), 1.87 – 1.56 (m, 4 H), 1.44 – 1.20 (m, 4 H), 0.89 (t, J = 7.1 Hz, 6 H) ppm. ^{13}C NMR (63 MHz, $CDCl_3$): δ = 164.6, 164.5, 148.1, 147.7, 147.6, 147.4, 147.3, 147.0, 130.7, 130.6, 125.6, 125.5, 111.6, 111.5, 111.3, 110.3, 110.0, 109.9, 56.2, 56.0, 55.9, 55.9, 55.7, 40.1, 39.3, 39.1, 28.2, 27.6, 26.4, 20.1, 20.0, 19.9, 14.2, 14.1, 14.0 ppm. Analysis for $C_{29}H_{40}N_2O_5$ (496.64): Calcd. C 70.13, H 8.12, N 5.64; found, C 70.00, H 8.10, N 5.46.

(±)-(*R,*R**)-Bis-6,7-dimethoxy-1-phenyl-3,4-dihydroisoquinolin-2(1*H*)-yl)methanone (10b)**. Obtained according to the general procedure A from compound **16** (0.20 g, 0.51 mmol),

p-toluenesulfinic acid (0.24 g, 1.53 mmol, 3 eq), benzaldehyde (0.16 g, 1.52 mmol) and toluene (5.0 mL) as solvent at 120 ºC. Purification by flash column chromatography on silica gel using 1:9 petroleum ether: diethyl ether as eluent afforded the product **10b** as a pale yellow solid that appears as a mixture of rotamers in the NMR spectra, yield 0.21 g, 73 %; m.p. 104 - 106 ºC; IR (neat): $\tilde{\nu}$=3060, 2960 cm^{-1}. ^1H NMR (250 MHz, $CDCl_3$): δ = 7.33 – 7.08 (m, 10 H), 6.68 (s, 1 H), 6.67 (s, 1 H), 6.50 (s, 1 H), 6.47 (s, 1 H), 6.14 (s, 2 H), 6.09 (s, 2 H), 3.90 (s, 6 H), 3.79 – 3.71 (m, 6 H), 3.70 – 3.57 (m, 2 H), 3.41 – 3.13 (m, 2 H), 3.11 – 2.79 (m, 2 H), 2.79 – 2.61 (m, 2 H) ppm. ^{13}C NMR (63 MHz, $CDCl_3$): δ = 163.8, 163.4, 148.0, 147.9, 147.4, 147.3, 143.1, 142.5, 128.9, 128.8, 128.2, 128.1, 127.9, 127.3, 127.2, 127.1, 126.7, 126.5, 111.3, 111.2, 111.1, 111.0, 59.3, 58.9, 55.9, 55.9, 41.0, 40.9, 28.6, 27.8 ppm. Analysis for $C_{35}H_{36}N_2O_5$ (564.67): Calcd. C 74.45, H 6.43, N 4.96; found C 74.25, H 6.51, N 5.00.

(±)-(*R*R)-Bis[1-(2-chlorophenyl)-6,7-dimethoxy-3,4-dihydroisoquinolin-2(1*H*)-yl]methanone (10c)**. Obtained according to the general procedure A from compound **16** (0.20 g, 0.51 mmol), *p*-toluenesulfinic acid (0.24 g, 1.53 mmol, 3 eq), 4-chlorobezanzaldehyde (0.22 g, 1.52 mmol) and toluene (5.0 mL) as solvent at 120 ºC. Purification by flash column chromatography on silica gel using 1:1 petroleum ether:diethyl ether eluent afforded the product **10c** as a white solid, yield 0.28 g, 56 %; m.p. 225 – 226 ºC; IR (neat): $\tilde{\nu}$ = 3070, 2940 cm^{-1}; ^1H NMR (250 MHz, $CDCl_3$): δ = 7.40 (dd, J = 7.8, 1.3 Hz, 2 H), 7.19 (td, J = 7.6, 1.8 Hz, 2 H), 7.09 (td, J = 7.5, 1.4 Hz, 1 H), 6.81 (dd, J = 7.6, 1.7 Hz, 1 H), 6.61 (s, 2 H), 6.54 (s, 1 H), 6.40 (s, 2 H), 3.87 (s, 6 H), 3.70 (s, 6 H), 3.59 – 3.47 (m, 2 H), 3.29 – 3.13 (m, 2 H), 3.06 – 2.92 (m, 1 H), 2.71 – 2.50 (m, 2 H) ppm. ^{13}C NMR (63 MHz, $CDCl_3$): δ = 163.5, 148.1, 147.7, 141.2, 134.7, 131.4, 129.9, 128.6, 127.0, 126.9, 126.3, 111.1, 110.9, 56.0, 55.9,

55.2, 42.5, 28.2 ppm. Analysis for $C_{35}H_{34}Cl_2N_2O_5$ (633.56): Calcd. C 66.3, H 5.41, N 4.42; found C 66.20, H 5.30, N 4.46.

(±)-(*R*R)-Bis-(6,7-dimethoxy-1-(3-nitrophenyl)-3,4-dihydroisoquinolin-2(1*H*)-yl)methanone (10d)**. Obtained according to the general procedure A from compound **16** (0.20 g, 0.51 mmol), *p*-toluenesulfinic acid (0.24 g, 1.53 mmol, 3 eq), 3-nitrobenzaldehyde (0.23 g, 1.52 mmol) and toluene (5 mL) as solvent at 120 ºC. Purification by flash column chromatography on silica gel using 1:9 petroleum ether: diethyl ether as eluent afforded the product **10d** as a pale yellow solid, yield 0.28 g, 82 %; m.p. 94 - 96 ºC; IR (neat): $\tilde{\nu}$ = 3080, 2960, 1584, 1339 cm^{-1}. ^1H NMR (250 MHz, $CDCl_3$): δ = 8.15 – 8.04 (m, 2 H), 8.04 – 7.98 (m, 2 H), 7.61 – 7.51 (m, 2 H), 7.50 – 7.32 (m, 2 H), 6.68 (s, 1 H), 6.67 (s, 1 H), 6.40 (s, 1 H), 6.36 (s, 1 H), 6.18 (s, 1 H), 6.07 (s, 1 H), 3.88 (s, 6 H), 3.74 – 3.57 (m, 8 H), 3.21 (m, 2 H), 3.12 – 2.73 (m, 4 H) ppm. ^{13}C NMR (63 MHz, $CDCl_3$): δ = 163.5, 163.3, 148.5, 148.4, 148.2, 147.9, 147.8, 145.4, 144.7, 135.2, 134.9, 129.4, 129.1, 126.6, 126.4, 126.3, 125.6, 123.6, 123.2, 122.6, 122.5, 111.5, 110.8, 58.7, 58.4, 56.0, 55.9, 41.9, 41.8, 28.5, 28.0 ppm. Analysis for $C_{35}H_{34}N_4O_9$ (654.67): calcd. C 64.21, H 5.23, N 8.56; found C 64.10, H 5.06, N 8.52.

(±)-(*R*R)-Bis-1-(4-chlorophenyl)-6,7-dimethoxy-3,4-dihydroisoquinolin-2(1*H*)-yl)methanone (10e)**. Obtained according to the general procedure A from compound **16** (0.20 g, 0.51 mmol), *p*-toluenesulfinic acid (0.24 g, 1.53 mmol, 3 eq), 4-chlorobenzaldehyde (0.21 g, 1.52 mmol) and toluene (5.0 mL) as solvent at 120 ºC. Purification by flash column chromatography on silica gel using diethyl ether as eluent afforded the product **10e** (0.12 g, 0.19 mmol) as a pale orange solid that appears as a mixture of rotamers in the NMR spectra, yield 37 %; m.p. 103 - 105 ºC; IR (neat): $\tilde{\nu}$ = 3065, 2964 cm^{-1} ^1H NMR (250 MHz, $CDCl_3$): δ = 7.33 7.17 (m, 4 H), 7.17 – 7.04 (m, 4 H), 6.70 (s, 1 H), 6.69 (s, 1 H), 6.47 (s, 1 H), 6.43 (s, 1

H), 6.12 (s, 1 H), 6.02 (s, 1 H), 3.93 (s, 6 H), 3.80, 3.76 (s, 6 H), 3.71 – 3.55 (m, 2 H), 3.43 – 2.96 (m, 2 H), 2.96 – 2.62 (m, 4 H) ppm. ^{13}C NMR (63 MHz, $CDCl_3$): δ = 163.6, 163.3, 148.2, 148.1, 147.6, 147.5, 141.8, 141.0, 133.3, 133.2, 130.4, 130.1, 128.5, 128.3, 127.4, 126.8, 126.6, 126.4, 111.3, 111.2, 110.9, 58.7, 58.2, 56.0, 55.9, 41.3, 41.2, 28.6, 27.9 ppm. Analysis for $C_{35}H_{34}Cl_2N_2O_5$ (633.56): calcd. C 66.35, H 5.41, N 4.42; found: C 66.40, H 5.30, N 4.25.

(±)-(*R*R)-Bis-1-(4-bromophenyl)-6,7-dimethoxy-3,4-dihydroisoquinolin-2(1*H*)-yl)methanone (10f)**. Obtained according to the general procedure A from compound **16** (0.20 g, 0.51 mmol), *p*-toluenesulfinic acid (0.24 g, 1.53 mmol, 3 eq), 4-bromobenzaldehyde (0.28 g, 1.52 mmol) and toluene (5.0 mL) as solvent at 120 ºC. Purification by flash column chromatography on silica gel using 1:9 petroleum ether: diethyl ether as eluent afforded the product **10f** as a pale orange solid that appeared as a mixture of rotamers in the NMR experiments, yield 0.15 g, 41 %; m.p. 90 - 92 ºC; IR (neat): $\tilde{\nu}$ = 3065, 2964 cm^{-1}. ^{1}H NMR (250 MHz, $CDCl_3$): δ = 7.42 – 7.29 (m, 4 H), 7.05 – 6.90 (m, 4 H), 6.65 (s, 1 H), 6.63 (s, 1 H), 6.41 (s, 1 H), 6.38 (s, 1 H), 6.05 (s, 1 H), 5.94 (s, 1 H), 3.87 – 3.71 (m, 12 H), 3.67 – 3.53 (m, 2 H), 3.15 (m, 2 H), 2.77 (s, 4 H, H^4) ppm. ^{13}C NMR (63 MHz, $CDCl_3$): δ = 163.6, 163.3, 148.2, 148.1, 147.7, 147.6, 142.3, 141.6, 131.4, 131.2, 130.8, 130.5, 127.3, 126.7, 126.6, 126.4, 121.5, 121.4, 111.3, 111.2, 110.9, 58.7, 58.2, 56.0, 55.9, 55.9, 41.4, 41.3, 28.6, 28.5 ppm. Analysis for $C_{35}H_{34}Br_2N_2O_5$ (722.46): calcd. C 58.19, H 4.74, N 3.88; found C 58.40, H 4.90, N 4.00.

(±)-(*R*R)-Bis-(1-(4-fluorophenyl)-6,7-dimethoxy-3,4-dihydroisoquinolin-2(1*H*)-yl)methanone (10g)**. Obtained according to the general procedure A from **16** (0.20 g, 0.51 mmol), *p*-toluenesulfinic acid (0.24 g, 1.53 mmol, 3 eq), 4-fluorobenzaldehyde (0.19 g, 1.52

mmol) and toluene (5.0 mL) as solvent at 120 ºC. Purification by flash column chromatography on silica gel using 1:9 petroleum ether: diethyl ether as eluent afforded the product **10g** as a pale yellow solid, yield 0.081 g, 30 %, m.p. 177 - 179 ºC; IR (neat): $\tilde{\nu}$ = 3076, 2930, 1228 cm^{-1}; ^1H NMR (300 MHz, $CDCl_3$): δ = 7.24 – 7.15 (m, 4 H), 6.99 – 6.91 (m, 2 H), 6.66 (s, 2 H), 6.56 (s, 1 H), 6.37 (s, 1 H), 3.87 (s, 6 H), 3.78 (s, 6 H), 3.59 – 3.53 (m, 2 H), 3.45 – 3.33 (m, 2 H), 2.90 (m, 2 H), 2.69 (dt, J = 15.8, 4.8 Hz, 2 H) ppm. ^{13}C NMR (75 MHz, $CDCl_3$): δ = 162.2 (d, J = 244.5 Hz), 158.1, 148.3, 147.7, 138.5, 138.4, 129.8, 129.7, 127.5, 126.9, 115.4, 115.1, 111.3, 111.1, 56.2, 56.1, 56.0, 39.9, 27.9 ppm. Analysis for $C_{35}H_{34}F_2N_2O_5$ (600.65): calcd. C 69.99, H 5.71, N 4.66; found C 69.80, H 5.76, N 4.66.

(±)-(*R*S**)-Bis-1-(4-fluorophenyl)-6,7-dimethoxy-3,4-dihydroisoquinolin-2(1*H*)-yl)methanone (11g)**. Obtained according to the general procedure B from compound **16** (0.20 g, 0.51 mmol), 98% sulfuric acid (0.092 g, 0.94 mmol, 1.8 eq), 4-fluorobenzaldehyde (0.19 g, 1.52 mmol) and AcOH (2.0 mL) as solvent at 120 ºC. Purification by flash column chromatography on silica gel using 9:1 ethyl acetate: methanol as eluent afforded the product **11g** as a pale orange solid that appears as a mixture of rotamers in the NMR spectra, yield 0.12 g, 37 %; m.p. 105 - 107 ºC; IR (neat): $\tilde{\nu}$ = 3076, 2930, 1220 cm^{-1}; ^1H NMR (250 MHz, $CDCl_3$): δ = 7.16 – 7.03 (m, 4 H), 6.98 – 6.89 (m, 4 H), 6.65 (s, 1 H), 6.64 (s, 1 H), 6.41 (s, 1 H), 6.39 (s, 1 H), 6.08 (s, 1 H), 5.98 (s, 1 H), 3.87 (s, 6 H), 3.71 (s, 3 H), 3.74 (s, 3 H), 3.67 – 3.53 (m, 2 H), 3.33 – 2.99 (m, 2 H), 2.91 – 2.60 (m, 4 H, H^4) ppm. ^{13}C NMR (63 MHz, $CDCl_3$): δ = 162.5 (d, J= 270.0 *Hz*), 161.8 (d, J= 270.0 *Hz*), 163.3, 164.0, 148.2, 148.1, 147.7, 147.5, 139.1, 139.0, 138.4, 138.3, 130.8, 130.6, 130.5, 130.4, 127.8, 127.1, 126.6, 126.4, 115.3, 115.1, 114.9, 114.7, 111.3, 111.2, 111.1, 111.0, 58.6, 58.2, 56.0, 55.9, 41.2, 41.1, 28.7, 28.0 ppm. Analysis for $C_{35}F_2H_{34}N_2O_5$ (600.65): calcd. 69.99, H 5.71, N 4.66; found: C, 69.65;

H, 5.67; N, 4.50; LRMS (ES): m/z: (rel. intensity %) 623 ($[M+Na]^+$, 100; HRMS (ES^+): Calcd. for $C_{35}F_2H_{34}N_2NaO_5^+$ $[M+Na]^+$ m/z: 623.2333, found m/z: 623.2331.

(±)-(*R*R)-Bis-6,7-dimethoxy-1-(4-nitrophenyl)-3,4-dihydroisoquinolin-2(1*H*)-yl)methanone (10h)**. Obtained according to the general procedure A from compound **16** (0.20 g, 0.51 mmol), *p*-toluenesulfinic acid (0.24 g, 1.53 mmol, 3 eq), 2-naphthaldehyde (0.24 g, 1.52 mmol) and toluene (5 mL) as solvent at 120 ºC. Purification by flash column chromatography on silica gel using diethyl ether as eluent afforded the product **10h** as a pale yellow solid that appeared as a mixture of rotamers in $CDCl_3$, yield 0.13 g, 40 %, m.p. 130 – 132 ºC; IR (neat): $\tilde{\nu}$ = 3076, 2930, 1519, 1347, cm^{-1}; ^1H NMR (300 MHz, $CDCl_3$): δ = 8.09 (d, *J* = 8.7 Hz, 2H), 8.01 (d, *J* = 8.8 Hz, 2H), 7.35 (d, *J* = 8.4 Hz, 2 H), 7.33 (d, *J* = 8.7 Hz, 2H), 6.67 (s, 1H), 6.64 (s, 1H), 6.41 (s, 1H), 6.34 (s, 1H), 6.17 (s, 1H), 6.06 (s, 1H), 3.85 (s, 6H), 3.72 (s, 2H), 3.67 (s, 4H), 3.65 – 3.49 (m, 2H), 3.37 – 3.13(m, 2H), 3.10 – 2.70 (m, 4H) ppm. ^{13}C NMR (75 MHz, $CDCl_3$): δ = 163.3, 163.2, 150.6, 149.7, 148.5, 148.4, 147.8, 147.7, 147.1, 147.0, 129.8, 129.4, 126.3, 126.2, 125.7, 123.5, 123.2, 111.4, 111.3, 110.7 (two signals), 58.6, 58.0, 55.9, 55.9, 55.8, 42.1, 41.7, 28.6, 27.8 ppm. Analysis for $C_{35}H_{34}N_4O_9$ (654.66): calcd. C 64.21, H 5.23 N, 8.56; found: C 64.20, H 5.10, N 8.46.

(±)-(*R*R)-Bis-(1-(2,4-dinitrophenyl)-6,7-dimethoxy-3,4-dihydroisoquinolin-2(1*H*)-yl)methanone (10i)**. Obtained according to the general procedure A from compound **16** (0.20 g, 0.51 mmol), *p*-toluenesulfinic acid (0.24 g, 1.53 mmol, 3 eq), 2,4-dinitrobenzaldehyde (0.3 g, 1.52 mmol) and toluene (5 mL) as solvent at 120 ºC. Purification by flash column chromatography on silica gel using 9:1 ethyl acetate:methanol as eluent afforded the product **10i** as a pale brown solid, yield 0.083 g, 22 %; m.p. 128 - 129 ºC; IR (neat): $\tilde{\nu}$ = 3076, 2930, 1567, 1347 cm^{-1}. ^1H NMR (300 MHz, $CDCl_3$): δ = 7.19 (dd, *J* = 8.1, 5.6 Hz, 2H), 6.98 – 6.88

(m, 4H), 6.66 (s, 2H), 6.56 (s, 2H), 6.36 (s, 2H), 3.87 (s, 6H), 3.77 (s, 6H), 3.44 – 3.20 (m, 4H), 2.94 – 2.63 (m, 4H) ppm. ^{13}C NMR (75 MHz, $CDCl_3$): δ = 163.7, 160.5, 158.2, 158.1, 148.3, 147.7, 138.5, 138.4, 129.8, 129.7, 127.6, 126.9, 115.4, 115.1, 111.3, 111.1, 56.6, 56.1, 56.0, 39.8, 27.9 ppm. Analysis for $C_{35}H_{32}N_6O_{13}$ (744.66): calcd. C 56.45, H 4.33, N 11.29 found: C 56.20, H 4.44, N 11.50.

(±)-(*R*R) and (*R*S**)-Bis-(1-(4-trifluoromethylphenyl)-6,7-dimethoxy-3,4-dihydroisoquinolin-2(1*H*)-yl)methanone (10j** and **11j)**. Obtained according to the general procedure A from **16** (0.20 g, 0.51 mmol), *p*-toluenesulfinic acid (0.24 g, 1.53 mmol, 3 eq), 4-(trifluoromethyl)benzaldehyde (0.26 g, 1.52 mmol) and toluene (5.0 mL) as solvent at 120 ºC. Purification by flash column chromatography on silica gel using 1:1 petroleum ether: diethyl ether as eluent afforded compounds **10j** (0.223 g, 62 %) and **11j** (0.058 g, 16 %) as white solids.

Compound 10j: m.p. 196-198 ºC; IR (neat): $\tilde{\nu}$ = 3028, 2931, 1648, 1516, 1324, 1107 cm^{-1}; ^{1}H NMR (250 MHz, $CDCl_3$): δ = 7.55 (d, J = 8 Hz, 4 H), 7.25 (d, J = 8 Hz, 4 H), 6.68 (s, 2 H), 6.41 (s, 2 H), 6.18 (s, 2 H), 3.91 (s, 6 H), 3.75 (s, 6 H), 3.66 – 3.58 (m, 2 H), 3.24 - 3.18 (m, 2 H), 2.9 – 2.7 (m, 4 H) ppm. ^{13}C NMR (63 MHz, $CDCl_3$): δ = 163.7, 148.6, 148.1, 147.5, 130.0 (q, $^2J_{CF}$ = 32,5 Hz), 129.4, 126.9, 126.6, 125.6 (q, $^3J_{CF}$ = 3,7 Hz), 124.1 (q, $^1J_{CF}$ = 272,5 Hz), 111.6, 111.2, 58.7, 56.4, 56.3, 41.9, 29.0 ppm. Analysis for $C_{37}H_{34}F_6N_2O_5$ (600.24): calcd. C, 63.42; H, 4.89; N, 4.00; found C, 63.17; H, 4.63; N, 4.14.

Compound 11j: m.p. 197-199 ºC; IR (neat): $\tilde{\nu}$ = 3014, 2935, 1633, 1516, 1324, 1108 cm^{-1}; ^{1}H NMR (250 MHz, $CDCl_3$): δ = 7.49 (d, J = 7,8 Hz, 4 H), 7.30 (d, J = 7 Hz, 4 H), 6.70 (s, 2 H), 6.45 (s, 2 H), 6.07 (s, 2 H), 3.92 (s, 6 H), 3.78 (s, 6 H), 3.78 – 3.67 (m, 2 H), 3.31 - 3.26 (m, 2 H), 3.12 – 3.04 (m, 2 H), 2.84 – 2.78 (m, 2 H) ppm. ^{13}C NMR (63 MHz, $CDCl_3$): δ = 163.9,

148.7, 148.0, 146.9, 130.2 (q, $^{2}J_{CF}$ = 32.5 Hz), 129.7, 127.4, 126.7, 125.5 (q, $^{3}J_{CF}$ = 3.7 Hz), 124.2 (q, $^{1}J_{CF}$ = 272.5 Hz), 111.7, 111.2, 59.2, 56.4, 56.3, 42.0, 28.3 ppm. Analysis for $C_{37}H_{34}F_6N_2O_5$ (600.24): calcd. C, 63.42; H, 4.89; N, 4.00; found C, 63.33; H, 4.74; N, 4.08.

(±)-(*R*R)-Bis-6,7-dimethoxy-1-[4-(4-nitrophenoxy)phenyl]-3,4-dihydroisoquinolin-2(1*H*)-yl)methanone (10k)**. Obtained according to the general procedure from compound **16** (0.20 g, 0.51 mmol) as starting material, *p*-toluenesulfinic acid (0.24 g, 1.53 mmol, 3 eq), 4-(4-nitrophenoxy)benzaldehyde (0.37 g, 1.52 mmol) and toluene (5.0 mL) as solvent at 120 ºC. Purification by flash column chromatography on silica gel using diethyl ether as eluent afforded the product **10k** as a pale yellow solid yield 0.09 g, 21 %; m.p. 114 - 116 ºC; IR (neat): $\tilde{\nu}$ = 3050, 2940, 1580, 1340 cm^{-1}; ^{1}H NMR (300 MHz, $CDCl_3$): δ = 8.10 (d, J = 7.5 Hz, 4H), 7.26 (d, J = 7.5 Hz, 4H), 6.94 (d, J = 7.5 Hz, 4H), 6.93 (d, J = 7.5 Hz, 4H), 6.64 (s, 2H), 6.59 (s, 2H), 6.40 (s, 2H), 3.83 (s, 6H), 3.75 (s, 6H), 3.64 – 3.53 (m, 2H), 3.44 – 3.34 (m, 2H), 2.93 – 2.81 (m, 2H), 2.67-2.62 (m, 2H) ppm. ^{13}C NMR (75 MHz, $CDCl_3$): δ = 163.1, 158.3, 153.7, 148.2, 147.5, 142.5, 139.8, 129.8, 127.4, 126.9, 125.8, 120.1, 117.0, 111.2, 111.0, 56.0, 55.9, 55.8, 39.8, 27.7 ppm. Analysis for $C_{47}H_{42}N_4O_{11}$ (838.86): calcd. C 67.29, H 5.05, N 6.68; found C 67.10, H 5.06, N 6.69.

(±)-(*R*S)-Bis(6,7-dimethoxy-1-(4-(4-nitrophenoxy)phenyl)-3,4-dihydroisoquinolin-2(1*H*)-yl]methanone (11k)**. Obtained according to the general procedure B from compound **16** (0.20 g, 0.51 mmol), sulfuric acid 98% (0.092 g, 0.94 mmol, 1.8 eq), 4-(4-nitrophenoxy)benzaldehyde (0.37 g, 1.52 mmol) and AcOH (2.0 mL) as solvent at 80 ºC. Purification by flash column chromatography on silica gel using ethyl acetate as eluent afforded the product **11k** as a pale orange solid that appeared as a mixture of rotamers in the NMR spectra, yield 0.16 g, 37 %; m.p. 114 - 116 ºC; IR (neat): $\tilde{\nu}$ = 3050, 2940, 1580, 1340

cm^{-1}. 8.16 (d, J = 7.5 Hz, 4H); 7.24 and 7.21 (2 d, J = 7.5 Hz, 4H); 6.98 (d, J = 7.5 Hz, 4H), 6.97 (d, J = 7.5 Hz, 4H), 6.68 and 6.64 (s, 2H), 6.48 and 6.45 (s, 2H), 6.13 and 6.05 (2 s, 2H), 3.87 (s, 6H), 3.74 and 3.71 (2 s, 6H), 3.70-3.60 and 3.50 – 2.62 (m, 8H) ppm. ^{13}C NMR (75 MHz, $CDCl_3$): δ = 163.6, 163.3, 163.1 and 163.0, 153.9 and 153.8, 148.2, 147.7, 142.7, 140.3 and 139.7, 130.9 and 130.7, 127.6, 126.9, 126.6 and 126.4, 126.0, 120.1 and 120.0, 117.3 and 117.2, 111.3 and 111.2, 111.0, 58.7 and 58.5, 56.0, 55.9, 41.3 and 41.1, 28.6 and 28.0 ppm. Analysis for $C_{47}H_{42}N_4O_{11}$ (838.86): calcd. C 67.29, H 5.05, N 6.68; found C 67.02, H 4.98, N 6.43.

(±)-(*R*R**)-Bis-6,7-dimethoxy-1-(naphthalen-2-yl)-3,4-dihydroisoquinolin-2(1*H*)-yl)methanone (10l)**. Obtained according to the general procedure A from compound **16** (0.20 g, 0.51 mmol), *p*-toluenesulfinic acid (0.24 g, 1.53 mmol, 3 eq), 2-naphthaldehyde (0.24 g, 1.52 mmol) and toluene (5.0 mL) as solvent at 120 ºC. Purification by flash column chromatography on silica gel using diethyl ether as eluent afforded the product **10l** as a pale yellow solid that appears as a mixture of rotamers in the NMR spectra, yield 0.13 g, 40 %; m.p. 118 – 120 ºC; IR (neat): $\tilde{\nu}$ = 3060, 2961 cm^{-1}. ^{1}H NMR (250 MHz, $CDCl_3$): δ = 7.63 – 7.37 (m, 6H), 7.30 – 7.04 (m, 8H), 6.51 (s, 1H), 6.50 (s, 1H), 6.33 (s, 2H), 6.15 (s, 1H), 6.02 (s, 1H), 3.71 (s, 6H), 3.53 (s, 3H), 3,50 (s, 3H, OCH_3), 3.60 – 3.40 (m, 2H), 3.25 – 2.99 (m, 2H), 2.99 – 2.40 (m, 4H) ppm. ^{13}C NMR (63 MHz, $CDCl_3$): δ = 163.9, 163.4, 148.0, 147.5, 147.3, 140.7, 140.0, 133.0, 132.9, 132.7, 132.6, 128.1, 127.9, 127.8, 127.7, 127.7, 127.5, 127.5, 127.1, 126.8, 126.8, 126.7, 126.6, 126.1, 126.0, 125.9, 111.3, 111.2, 111.1, 59.5, 58.8, 55.9, 41.3, 41.1, 28.7, 27.9 ppm. $C_{43}H_{40}N_2O_5$ (664.79): calcd. C 77.69, H 6.06, N 4.21; found C 77.50, H 6.10, N 4.25.

(±)-(*R*R)-Bis-6,7-dimethoxy-1-(6-(3-nitrophenyl)pyridin-2-yl)-3,4-dihydroisoquinolin-2(1*H*)-yl)methanone (10m)**. Obtained according to the general procedure A from compound **16** (0.20 g, 0.51 mmol) as starting material, *p*-toluenesulfinic acid (0.24 g, 1.53 mmol, 3 eq), 6-(3-nitrophenyl)picolinaldehyde (0.35 g, 1.52 mmol) and toluene (5 mL) as solvent at 80 ºC. Purification by flash column chromatography on silica gel using diethyl ether as eluent afforded the product **10m** as a pale orange solid that appeared as a mixture of rotamers in NMR spectra, yield 0.27 g, 66 %; m.p. 139 – 140 ºC. IR (neat): $\tilde{\nu}$ = 3070, 2940, 1347, 1519 cm^{-1}. ^1H NMR (250 MHz, $CDCl_3$): δ = 8.81 (t, 1.8 Hz, 1H), 8.77 (t, 1.8 Hz, 1H), 8.28 – 8.13 (m, 4H), 7.74 – 7.57 (m, 4H), 7.54 – 7.44 (m, 2H), 7.27 – 7.10 (m, 2H), 6.77 (s, 1H), 6.70 (m, 3H), 6.25 (s, 1H, H^1), 6.21 (s, 1H), 4.11 (dd, J = 13.0, 4.9 Hz), 3.85 (s, 2H), 3.85 (s, 3H), 3.85 (s, 3H), 3.85 (s, 6H), 3.67 – 3.50 (m, 2H), 3.31 – 3.11 (m, 2H), 2.83 (m, 2H) ppm. ^{13}C NMR (63 MHz, $CDCl_3$): δ = 164.2, 164.0, 162.2, 162.2, 153.8, 153.7, 148.7, 148.6, 148.2, 148.1, 147.2, 147.1, 140.8, 140.7, 137.6, 137.5, 137.4, 132.5, 132.4, 129.5, 127.2, 127.1, 126.5, 126.4, 123.5, 123.4, 122.0, 121.8, 121.6, 118.6, 111.4, 111.2, 111.0, 61.9, 61.6, 55.9, 55.8, 55.8, 41.5, 41.4, 28.0, 27.9 ppm. $C_{45}H_{40}N_6O_9$ (808.83): calcd. C 66.82, H 4.98, N 10.39; found C 66.70, H 4.86, N 10.19.

When the same reaction was carried out at 120 °C, it afforded decomposition products **29** and **30** (see below).

(±)-1-(2-Chlorophenyl)-6,7-dimethoxy-*N*'-(3,4-dimethoxyphenethyl)-1,2,3,4-tetrahydroisoquinoline-2-carboxamide (21). To a solution of compound **16** (0.20 g, 0.51 mmol), *p*-toluenesulfinic acid (0.24 g, 1.53 mmol, 3 equiv), 2-chlorobenzaldehyde (0.22 g, 1.57 mmol) in AcOEt (5.0 mL) as solvent was stirred at 80 ºC for 12 h. The mixture was quenched with a saturated solution of $NaHCO_3$ (10 mL), which was extracted with DCM (2 x

30 mL). The combined organic layers were dried (Na_2SO_4) and concentrated under reduced pressure. Purification by flash column chromatography on silica gel using 8:2 diethyl ether:ethyl acetate as eluent afforded the product **21** as a pale yellow solid, yield 0.14 g, 54 %; m.p. 72 – 74ºC. IR (neat): $\tilde{\nu}$ = 3300, 2980, 1535 cm^{-1}. ^1H NMR (250 MHz, $CDCl_3$): δ = 7.32 (dd, J = 7.3, 2.0 Hz, 1 H), 7.20 – 7.06 (m, 2 H), 6.99 (dd, J = 7.5, 2.0 Hz, 1 H), 6.76 – 6.67 (m, 1 H), 6.66 – 6.58 (m, 3 H), 6.42 (s, 1 H), 6.22 (s, 1 H), 4.86 (t, J = 5.5 Hz, 1 H), 3.98 (ddd, J = 13.2, 5.0, 3.1 Hz, 1 H), 3.83 (s, 3 H), 3.82 (s, 3 H), 3.76 (s, 3 H), 3.67 (s, 3 H), 3.52 – 3.39 (m, 2 H), 3.30 (ddd, J = 13.7, 10.9, 4.1 Hz, 1 H), 2.92 (ddd, J = 16.1, 10.8, 5.4 Hz, 1 H), 2.75 – 2.62 (m, 3 H) ppm. ^{13}C NMR (63 MHz, $CDCl_3$): δ = 157.7, 148.8, 148.0, 147.6, 147.4, 140.7, 133.0, 131.7, 130.4, 129.7, 128.9, 127.2, 127.1, 126.8, 120.5, 111.8, 111.3, 111.2, 110.3, 55.9, 55.8, 55.7, 55.2, 42.1, 38.9, 35.6, 27.6 ppm. $C_{28}H_{31}ClN_2O_5$ (511.01): calcd. C 65.81. H 6.11. N 5.48; found C 65.75, H 6.16, N 5.44.

The related **18-20** and **22-25** are known compounds.[94]

General procedure to obtain 6,7-dimethoxy-1,2,3,4-tetrahydroisoquinolines 27-30

To a solution of compound **16** (1.0 eq) in AcOH or toluene (5.0 mL) was added the suitable aldehyde (3 eq) and the suitable catalyst (1.8 – 3.0 eq) and the reaction mixture was heated at 80-120 ºC for 12 h. The mixture was quenched with a saturated solution of $NaHCO_3$ (10 mL), which was extracted with DCM (2 x 30 mL). The combined organic layers were dried (Na_2SO_4) and concentrated under reduced pressure. The crude was purified by flash column chromatography using ethyl acetate: methanol mixtures to give the target compounds.

The related compound **26** was prepared using a literature method.[95]

(±)-1-(4-Chlorophenyl)-6,7-dimethoxy-1,2,3,4-tetrahydroisoquinoline (27). Obtained according to the general procedure from compound **16** (0.20 g, 0.51 mmol), *p*-toluenesulfinic

acid (0.24 g, 1.53 mmol, 3 eq), 4-chlorobenzaldehyde (0.22 g, 1.53 mmol, 3 eq) and toluene (5.0 mL) as solvent at 120 ºC. Purification by flash column chromatography on silica gel using ethyl acetate eluent afforded the product **27** as a brown solid, yield 0.049 g, 32 %. Spectral data were identical to those found in the literature.[106]

(±)-1-(2,4-Dinitrophenyl)-6,7-dimethoxy-1,2,3,4-tetrahydroisoquinoline (28). Obtained according to the general procedure from compound **16** (0.20 g, 0.51 mmol), *p*-toluenesulfinic acid (0.24 g, 1.53 mmol, 3 eq), 2,4-dinitrobenzaldehyde (0.30 g, 1.50 mmol) and toluene (5.0 mL) as solvent at 120 ºC. Purification by flash column chromatography on silica gel using 9:1 ethyl acetate: methanol as eluent afforded the product **28** as a pale brown oil, yield 0.03 g, 16 %; IR (neat): $\tilde{\nu}$ = 3106, 1940, 1340, 1519 cm^{-1}. ^1H NMR (250 MHz, $CDCl_3$): δ = 8.67 (d, J = 2.3 Hz, 1 H), 8.25 (dd, J = 8.6, 2.3 Hz, 1 H), 7.34 (d, J = 8.6 Hz, 1 H), 6.67 (s, 1 H), 6.19 (s, 1 H), 5.66 (s, 1 H), 3.88 (s, 3 H), 3.87 – 3.81 (m, 1 H), 3.68 (s, 3 H), 3.07 – 2.96 (m, 2 H), 2.82 (dd, J = 11.2, 5.6 Hz, 2 H) ppm. ^{13}C NMR (63 MHz, $CDCl_3$): δ = 150.1, 148.6, 147.7, 146.8, 145.9, 133.5, 128.5, 126.3, 126.1, 119.8, 111.9, 110.6, 56.1, 56.0, 55.0, 40.4, 28.9 ppm. $C_{17}H_{17}N_3O_6$ (359.33): calcd. C 56.82, H 4.77, N 10.69; found C 57.96, H 4.66, N 10.69.

(±)-6,7-Dimethoxy-1-(6-(3-nitrophenyl)pyridin-2-yl)-1,2,3,4-tetrahydroisoquinoline (29) and (±)-6,7-Dimethoxy-1-(6-(3-nitrophenyl)pyridin-2-yl)-3,4-dihydroisoquinoline (30). Obtained as decomposition products in the reaction carried according to the general procedure from compound **16** (0.20 g, 0.51 mmol), 98% sulfuric acid (0.092 g, 0.94 mmol, 1.8 eq), 6-(3-nitrophenyl)picolinaldehyde (0.35 g, 1.52 mmol) and AcOH (2.0 mL) as solvent at 120 ºC. Purification by flash column chromatography on silica gel using diethyl ether as eluent afforded the product **29** (0.01 mmol) as a brown solid, yield 0.039 g, 38 % and **30** as a pale orange solid, yield 0.075 g, 20 %

Data for **29**: m.p. 98 – 100 ºC; IR (neat): $\tilde{\nu}$ = 3156, 1972, 1519 cm^{-1}. ^1H NMR (250 MHz, $CDCl_3$): δ = 8.88 (t, 1 H), 8.39 (dd, J = 7.8, 0.9 Hz, 1 H), 8.27 – 8.17 (m, 1 H), 7.79 – 7.68 (m, 2 H), 7.60 (d, J = 8.1 Hz, 1 H), 7.16 (dd, J = 6.9, 1.6 Hz, 1 H), 6.66 (s, 1 H), 6.45 (s, 1 H), 5.30 (s, 1 H), 3.86 (s, 3 H), 3.68 (s, 3 H), 3.28 – 3.01 (m, 2 H), 3.01 – 2.77 (m, 2 H) ppm. ^{13}C NMR (63 MHz, $CDCl_3$): δ = 163.8, 154.1, 148.8, 148.0, 147.2, 140.9, 137.7, 132.8, 129.8, 127.7, 127.5, 123.6, 122.6, 121.9, 119.2, 111.7, 110.9, 61.9, 56.0, 55.9, 41.0, 29.0 ppm. Analysis for $C_{22}H_{21}N_3O_4$ (391.42): calcd. C 67.51, H 5.41, N 10.74; found: C 67.53, H 5.42, N 10.60.

Data for **30**: m.p. 139 – 140 ºC; IR (neat): $\tilde{\nu}$ = 3076, 1945, 1340, 1519 cm^{-1}. ^1H NMR (250 MHz, $CDCl_3$): δ = 8.87 (t, J = 1.9 Hz, 1 H), 8.51 – 8.34 (m, 1 H), 8.23 (ddd, J = 8.2, 2.2, 1.0 Hz, 1 H), 7.99 – 7.85 (m, 3 H,), 7.61 (t, J = 8.0 Hz, 1 H), 7.33 (s, 1 H), 6.79 (s, 1 H), 3.95 (s, 3 H), 3.94 – 3.85 (m, 2 H), 3.74 (s, 3 H), 2.85 – 2.72 (m, 2 H) ppm. ^{13}C NMR (63 MHz, $CDCl_3$): δ = 164.6, 157.7, 153.0, 151.2, 148.9, 147.1, 140.8, 138.2, 132.8, 132.6, 129.9, 123.8, 123.6, 121.6, 120.8, 120.6, 112.2, 110.2, 56.2, 56.1, 48.0, 26.0 ppm. Analysis for $C_{22}H_{19}N_3O_4$ (389.40): calcd. C 67.86, H 4.92, N 10.79; found C 67.76, H 4.86, N 10.89.

(±)-3,6-Bis(2,4,5-trimethoxy-3-methylbenzyl)piperazine-2,5-dione (36)

A solution of (3*Z*,6*Z*)-3,6-bis(2,4,5-trimethoxy-3-methylbenzyl)piperazine-2,5-dione[107] (2.00 g, 4.0 mmol) in EtOH (110 mL) was hydrogenated at 45 psi and 60 ºC for 12 h in the presence of 10% Pd/C (1 g). The reaction mixture was filtered through celite to remove the C/Pd and the celite layer was washed with DCM (3 x 30 mL). The filtrates were washed with saturated aqueous $NaHCO_3$ (2 x 30 mL), which were back-extracted with DCM (2 x 10 mL). The combined organic layers were dried over anhydrous Na_2SO_4 and concentrated *in vacuo* to furnish compound **36** as a white solid, yield 2.05 g, 99%; m.p. 194–195 ºC. IR (neat): $\tilde{\nu}$ =

2938, 2360 cm^{-1}. ^1H NMR (250 MHz, $CDCl_3$): δ = 6.57 (s, 2 H), 6.54 (br. s, 2 H), 4.16 (dd, *J* = 9.0 and 3.3 Hz, 2 H), 3.81 (s, 6 H), 3.77 (s, 6 H), 3.67 (s, 6 H), 3.30 (dd, *J* = 14.0, 3.4 Hz, 2 H), 2.73 (dd, *J* = 14.0, 9.2 Hz, 2 H), 2.20 (s, 6 H) ppm. ^{13}C NMR (63 MHz, $CDCl_3$): δ = 168.3, 150.9, 149.7, 147.4, 126.1, 124.0, 111.8, 60.7, 60.3, 56.1, 55.8, 32.9, 9.8 ppm. Analysis for $C_{26}H_{34}N_2O_8$ (502.56): calcd. C 62.14, H 6.82, N 5.57. Found C 62.10, H 6.76, N 5.41.

General procedure to obtain 3-benzyl-2,3,11,11a-tetrahydro-6*H*-pyrazino[1,2-*b*]isoquinoline-1,4-diones 37 – 39.

To a solution of **36** (1.00 eq) in dry toluene, acetic acid or diphenyl ether (5 mL), *p*-toluenesulfinic acid (1.00 – 1.10 eq) and the corresponding aryl aldehyde (1.00 – 1.05 eq) were added and the reaction was stirred at 120–140 ºC for 3–12 h. The reaction mixture was quenched with a saturated solution of $NaHCO_3$ (10 mL) extracted with DCM (2x 20 mL), and the organic layer was dried over anhydrous Na_2SO_4 and filtered. The solution was concentrated under reduced pressure and purified by flash column chromatography using a mixture of diethyl ether:ethyl acetate as eluent to obtain **37 – 39**.

(±)-(3*S,6*R**,11a*S**,*E*)-3-(2,5-dimethoxybenzyl)-7,10-dimethoxy-6-styryl-2,3,11,11a-tetrahydro-6*H*-pyrazino[1,2-*b*]isoquinoline-1,4-dione (37):**

Obtained according to the general procedure using compound **36** (0.20 g, 0.47 mmol) as starting material, *p*-toluenesulfinic acid (0.11 g, 0.71 mmol), cinnamaldehyde (0.1 mL, 0.79 mmol) and $(Ph)_2O$ (1.60 mL) as solvent at 120 ºC for 12 h. Purification by flash column chromatography on silica gel using 5:5 diethyl ether: ethyl acetate as eluent afforded product **37** as a brown solid, yield 0.17 g, 65%; m.p. 104–105 ºC. IR (neat): $\tilde{\nu}$ = 3100, 2920, 1613, 1600 cm^{-1}. ^1H NMR (250 MHz, $CDCl_3$): δ = 7.38 – 7.27 (m, 5 H), 6.82 – 6.67 (m, 5 H), 6.66

(d, *J* = 3.9 Hz, 1 H), 6.54 (s, 1 H), 6.33 (dd, *J* = 16.5, 3.6 Hz, 1 H), 6.19 (d, *J* = 16.1 Hz, 1 H), 4.51 (t, *J* = 4.7 Hz, 1 H), 4.29 (dd, *J* = 12.0, 4.5 Hz, 1 H), 3.85 – 3.68 (m, 9 H), 3.41 (dd, *J* = 13.3, 4.3 Hz, 1 H), 3.29 (s, 3 H), 3.21 – 2.99 (m, 2 H), 1.41 (dd, *J* = 18.3, 13.5 Hz, 1 H) ppm. ^{13}C NMR (63 MHz, $CDCl_3$): δ = 167.7, 163.6, 153.4, 152.1, 151.1, 150.1, 136.4, 132.7, 128.5, 127.8, 126.6, 126.5, 124.1, 123.1, 116.0, 114.4, 111.8, 108.6, 108.0, 56.4, 55.8, 55.6, 55.5, 55.1, 50.5, 49.2, 35.0, 28.1 ppm. Analysis for $C_{31}H_{32}N_2O_6$ (528.59): calcd. C 70.44, H 6.10, N 5.30. found C 70.49, H 6.11, N 5.20.

(±)-(3*S,6*S**,11a*S**,*E*)-7,8,10-trimethoxy-9-methyl-3-(2,4,5-trimethoxy-3-methylbenzyl)-6-styryl-2,3,11,11a-tetrahydro-6*H*-pyrazino[1,2-*b*]isoquinoline-1,4-dione (38):**

Obtained according to the general procedure using compound **36** (0.60 g, 1.20 mmol) as starting material, *p*-toluenesulfinic acid (0.21 g, 1.32 mmol), cinnamaldehyde (0.17 g, 1.26 mmol) and toluene (6.0 mL) as solvent at 115 ºC for 5.5 h. Purification by flash column chromatography on silica gel using 5:5 diethyl ether:ethyl acetate as eluent afforded product **38** as a brown solid, yield 0.30 g, 40%; m.p. 107–109ºC. IR (neat): $\tilde{\nu}$ = 2981, 2838, 2360, 1594 cm^{-1}. ^{1}H NMR (250 MHz, $CDCl_3$): δ = 7.29- 7.21 (m, 5 H), 6.61 (br d, *J* = 4.9 Hz, 1 H), 6.44 (s, 1 H), 6.41 (d, *J* = 1.5 Hz, 1 H), 6.32 (dd, *J* = 15.9, 5.0 Hz, 1 H), 6.20 (d, *J* = 16.0 Hz, 1 H), 4.44 (b.t, *J* = 4.0 Hz, 1 H), 4.24 (dd, *J* = 11.8, 4.7 Hz, 1 H), 3.79 (s, 3 H), 3.78 (s, 3 H), 3.69 (s, 3 H), 3.64 (s, 3 H), 3.62 (s, 3 H), 3.44 (s, 3 H), 3.24 (dd, *J* = 13.7, 4.4 Hz, 1 H), 3.19 (dd, *J* = 16.9, 4.8 Hz, 1 H), 3.04 (dd, *J* = 13.7, 6.2 Hz, 3 H), 2.19 (s, 3 H), 2.17 (s, 3 H), 1.91 (dd, *J* = 16.9, 11.9 Hz, 1 H) ppm. ^{13}C NMR (63 MHz, $CDCl_3$): δ = 167.1, 163.8, 152.3, 151.5, 150.3, 149.4, 147.4, 146.1, 136.1, 133.4, 128.6, 128.1, 127.0, 126.7, 126.0, 125.1, 124.9, 123.1, 121.7, 111.2, 60.7, 60.3, 60.3, 60.2, 60.0, 56.5, 55.5, 51.1, 49.6, 35.1, 28.0, 9.9, 9.5 ppm. $C_{35}H_{40}N_2O_8$ (616.70): calcd. C 68.17, H 6.54, N 4.54. found C 68.09, H 6.44, N 4.59.

(±)-(5R*,13*S*,1'E,1''E*)-1,3,4,9,11,12-hexamethoxy-2,10-dimethyl-5,13-distyryl-7a,8,15a,16-tetrahydropyrazino[1,2-*b*:4,5-*b'*]diisoquinoline-7,15(5*H*,13*H*)-dione (39)

Obtained according to the general procedure using compound **36** (0.10 g, 0.193 mmol) as starting material, *p*-toluenesulfinic acid (0.045 g, 0.29 mmol), cinnamaldehyde (0.128 g, 0.96 mmol) and $(Ph)_2O$ (1.40 g) as solvent at 140 ºC for 6 h. Purification by flash column chromatography on silica gel using diethyl ether as eluent afforded product **39** as a brown solid yield0.14 g, 99%; m.p. 105–107ºC. IR (neat): $\tilde{\nu}$ = 2938, 2359 cm^{-1}. ^1H NMR (250 MHz, $CDCl_3$): δ = 7.36 – 7.23 (m, 10 H), 6.61 (d, J = 5.1 Hz, 2 H), 6.40 (dd, J = 15.9, 5.1 Hz, 2 H), 6.27 (d, J = 16.0 Hz, 2 H), 4.48 (dd, J = 12.5, 4.3 Hz, 2 H), 3.81 (s, 6 H), 3.80 (s, 6 H), 3.68 (s, 6 H), 3.54 (m, J = 16.9, 4.3 Hz, 2 H), 2.72 (dd, J = 16.9, 12.6 Hz, 2 H), 2.22 (s, 6 H) ppm. ^{13}C NMR (63 MHz, $CDCl_3$): δ = 163.9, 152.3, 150.6, 146.5, 136.2, 133.9, 128.7, 128.2, 127.0, 126.8, 125.2, 121.8, 60.3, 60.2, 60.1, 51.65, 49.8, 9.6 ppm. $C_{44}H_{46}N_2O_8$ (730.84): calcd. C 72.31, H 6.34, N 3.83; found C 72.30, H 6.32, N 3.86.

Cell cultures

Human prostate carcinoma epithelial 22RV1 and LNCaP cells were purchased from Deutsche Sammlung von Mikroorganismen und Zellkulturen GmbH (DSMZ, Braunschweig, Berlin, Germany). Cells were cultivated according to the information provided by the supplier. LNCaP cells were cultivated in RPMI-1640 medium supplemented with 10% foetal bovine serum (FBS), 100 $U \cdot mL^{-1}$ penicillin and 0.1 $mg \cdot mL^{-1}$ streptomycin; 22Rv1 cells were cultivated in 40% RPMI-1640 and 40% DMEM medium supplemented with 20% FBS, 100 $U \cdot mL^{-1}$ penicillin and 0.1 $mg \cdot mL^{-1}$ streptomycin; HEK-293 (human embryonic kidney) were grown as monolayers in EMEM supplemented with nonessential amino acids, 10% FBS, and

2 mM glutamine; PNT1A (human normal prostate epithelium) cells were purchased from Sigma-Aldrich. Cells were grown in Dulbecco's modified Eagle's medium (DMEM) containing 10% foetal bovine serum, 2 mM L-glutamine, 100 U mL^{-1} penicillin and 0.1 mg mL^{-1} streptomycin. All the cellular lines were maintained at 37°C in a humidified atmosphere containing 5% CO_2. All media were from Lonza.

The cells were chronically treated by a daily dose (from 1 to 10 μM) of the compounds to test, monitored during the treatment and after 72 hours collected and counted by a Burker-chamber. For the LNCaP cells, due to tendency to form clusters, the cell number was also calculated by evaluating the amount of genomic DNA in cell suspension by Quant-iT dsDNA Assay Kit (Invitrogen) after sonication of the cell suspension by a Branson sonifier. To calculate the cell number from the amount of genomic DNA, an empirically determined conversion factor of 4 pg of DNA/cell was utilized. The maximum discrepancy within the two approaches was less than 15%.

Dead cells were evaluated by Trypan Blue 0.4% solution treatment (Sigma- Aldrich). LNCaP viability was also estimated by using the cell dye carboxynaphtofluorescein (CBNF) (Molecular Probes) as follow: cells were washed and resuspended in Hank's Balanced Salt Solution (HBSS) with Pluronic F-127 (Sigma, Aldrich) 0,05%. After 5 minutes cells were pelleted and resuspended in HBSS with the live cell dye CBNF (Molecular Probe) 1 μM. Cells were incubated in the dark at room temperature on moderate agitation for 15 minutes. Cell samples were run in a 2100 Bioanalyzer equipped with 2100 Expert Software (Agilent Technologies, Palo Alto, CA) with the Cell Chips kit (Agilent technologies, Palo Alto, CA). Statistical analysis was performed by analysis of variance at each point using ANOVA followed by Bonferroni's test.

Intracellular calcium assay

HEK-293 cells were grown as described above. HEK-293 cells stably over-expressing recombinant rat TRPM8, human TRPV1, rat TRPV2, rat TRPV3, rat TRPV4 or rat TRPA1, were grown as monolayers on 100-mm diameter Petri dishes. The effect of the compounds under assay on intracellular Ca^{2+} concentration ($[Ca^{2+}]_i$) was determined by using Fluo-4-AM, a selective intracellular fluorescent probe for Ca^{2+}. On the day of the experiment, cells were loaded for 1 h at 25°C with the methyl ester Fluo-4-AM (4 μM containing 0.02% Pluronic F-127; Invitrogen) in EMEM without foetal bovine serum, then were washed twice in Tyrode's buffer (145 mM NaCl, 2.5 mM KCl, 1.5 mM $CaCl_2$, 1.2 mM $MgCl_2$, 10mM D-glucose and 10 mM HEPES, pH 7.4), re-suspended in Tyrode's buffer, and transferred to the quartz cuvette of the spectrofluorimeter (Perkin-Elmer LS50B equipped with PTP-1 Fluorescence Peltier System; PerkinElmer Life and Analytical Sciences, Waltham, MA) under continuous stirring. $[Ca^{2+}]_i$ was determined before and after the addition of various concentrations of test compounds by measuring cell fluorescence (λ_{ex} = 488 nm, λ_{em} = 516 nm). Potency was expressed as the concentration of test substances exerting a half-maximal agonist effect (i.e. half-maximal increases in $[Ca^{2+}]_i$) (EC_{50}). The efficacy of agonists was first determined by normalizing their effect to the maximum Ca^{2+} influx effect on $[Ca^{2+}]_i$ observed with application of 4 μM ionomycin (Alexis). The effects of TRPA1 agonists are expressed as a percentage of the effect obtained with 100 μM allyl isothiocyanate (AITC). The values of the effect on $[Ca^{2+}]_i$ in wild type HEK-293 were taken as baselines and subtracted from the values obtained from HEK-293 transfected cells. Curve fitting (sigmoidal dose-response variable slope) and parameter estimation were performed with GraphPad Prism® (GraphPad Software Inc., San Diego, CA). Antagonist/desensitizing behavior was evaluated against icilin (0.25

μM) for TRPM8; capsaicin (0.1 μM) for TRPV1, lysophosphatidylcholine (LPC) (3 μM) for TRPV2, in the case of TRPV3, TRPV3-expressing HEK-293 cells were first sensitized with 2-aminoethoxydiphenyl borate (100 μM) and then thymol (100 μM) for TRPV3; 4-α-phorbol 12,13-didecanoate (4-α -PDD) (1 μM) for TRPV4; allyl isothiocyanate (AITC) (100 μM) for TRPA1; by adding the test compounds in the quartz cuvette 5 min before stimulation of cells with agonists. The effect on $[Ca^{2+}]_i$ exerted by agonist alone was taken as 100%. Data are expressed as the concentration exerting a half-maximal inhibition of agonist effect (IC_{50}). Determinations were performed at least in triplicate. Statistical analysis of the data was performed by analysis of variance at each point using ANOVA followed by Bonferroni's test.

Measurement of caspase 3/7 activity

Apoptosis was evaluated by means of the Caspase-Glo® 3/7 Chemioluminescent Assay Kit (Promega Corporation, Madison, WI, USA). Human prostate carcinoma LNCaP cells were cultured in the presence of drugs for 72 h. After incubation, cells were washed with PBS and processed. The assay was performed in 96-well white-walled plates, adding 100 μL of Caspase-Glo® 3/7 reagent to each well containing 1 x 10^4 and 2 x 10^4 cells in 100 μL of culture medium. After 1 h incubation in the dark at room temperature, luminescence was measured by a VersaDoc MP System equipped by the Quantity One® version 4.6 software (Bio-Rad). Luminescence values from the blank reaction (vehicle-treated cells) were subtracted from experimental values. In order to evaluate the commitment to apoptosis of PCCs, cells grown in presence of vehicle were treated for 24 h with 0.1 $\mu g \cdot mL^{-1}$ *S*-(+)-camptothecin (Sigma-Aldrich) plus 0.2 $\mu g \cdot mL^{-1}$ anti-Fas antibody (Exbio, Praha, CZ), two compounds known to potently induce apoptosis. All samples were assayed at least in

triplicate. Statistical analysis was performed by analysis of variance at each point using ANOVA followed by Bonferroni's test.

Quantitative RT-PCR analyses

Total RNA was extracted from cell pellets in 1.0 mL of Trizol® (Invitrogen) following the manufacturer's instructions, dissolved in RNA storage solution (Ambion, Life Technologies, Grand Island, NY, USA), UV-quantified by a Bio-Photometer® (Eppendorf, Hamburg, Germany) and stored at -80°C until use. RNA aliquots (5 µg) were digested by RNAse-free DNAse I (Ambion DNA-free™ kit) in a 20 µL final volume reaction mixture to remove residual contaminating genomic DNA. After DNAse digestion, concentration and purity of RNA samples were evaluated by the RNA-6000-Nano® microchip assay using a 2100 Bioanalyzer® equipped with a 2100 Expert Software® (Agilent, Santa Clara, CA, USA) following the manufacturer's instructions. 1 µg of total RNA, as evaluated by the 2100 Bioanalyzer, was reverse-transcribed in cDNA and analysed as previously described.[108] Optimized primers for SYBR green analysis and optimum annealing temperatures were designed by the Allele-Id software version 7.0 (PREMIER Biosoft International, Palo Alto, CA, USA) and were synthesized (HPLC purification grade) by Eurofins MWG, Ebersberg, Germany. In the presence of splicing variants, all the sequences were aligned and the primers were designed in the homologous regions. Primer sequences for transient receptor potential cation channel, subfamily M, member 8 [Homo sapiens NM_024080.4] (TRPM8) were forward primer: ATGTGTTCTTCTTCCTGTTCCTC, reverse primer: CGCTGCTCATTCTGCCTAAG. Relative gene expression calculation, corrected for PCR

efficiency and normalized with respect to the reference gene (RNA polymerase II subunit, Acc Z27113), was performed by the IQ5 software, as previously described.[101]

Intrinsic clearance (CL_{int}) determination in microsomes

Microsomal protein extracts from six pooled C57BL/6 mouse livers were prepared using standard ultracentrifugation techniques.[109] Microsomal pellets were resuspended in 0.1 M potassium phosphate buffer pH 7.4 containing 20% glicerol and stored at -80 ºC until use. Total protein concentration was determined by the Bradford protein assay using BSA as a standard.

Liver microsomal stability was measured at 37 ºC in phosphate buffer (0.1 M, pH 7.4). Compounds (3 μM) were incubated with 0.25 mg/mL of microsomal protein and NADPH (1 mM) for different periods of time (15, 30, 45, 60 min). Control incubations with no cofactor and/or no compound were performed concurrently to validate the assay. The reactions were initiated by the addition of microsomal protein and terminated by the addition of acetonitrile. After stopping the metabolic reaction, the tubes were centrifuged at 10,000g for 5 min. An aliquot of the supernatant was analyzed by HPLC for measuring the unchanged compound concentration.

Intrinsic clearance was calculated based on substrate disappearance rate, assuming first-order elimination of the compound over the 60 min incubation period.[102,110]

Aqueous solubility studies

Six tubes containing a stirring bar and increasing amounts of the compound under assay suspended in purified water (*e.g.* 0.1 mg/mL, 0.13 mg/mL, 0.33 mg/mL, 1 mg/mL, 2 mg/mL

and 4 mg/mL and for the case of compound **10j**) were placed in a bath thermostated at 37 ± 0.5 °C. The suspensions or solutions were stirred for 48 h and filtered through regenerated cellulose membrane filters with a pore size 22 μm, previously heated to 37 °C, to separate the solutions from the solid compound. The filtered solutions were diluted with methanol so that the final methanol/water ratio was 85/15, and the concentrations of dissolved compound were determined by HPLC, using a calibration curve obtained from standard solutions in the mobile phase that were prepared from a stock solution in the same solvent. All measurements were carried out at least in triplicate sets, and correlation coefficients were at least 0.999.

Computational methods

TRPM8 homology modeling

The sequence of rat TRPM8 was retrieved from the publicly available sequence database www.uniprot.org (UNIPROT: Q8R455). Phyre2[111] was used to identify the best template (TRPV1, PDB entry 3J5P) and to obtain a structural alignment that was locally manually modified to be consistent with the UNIPROT topology assignment and with the secondary structure prediction of PredictProtein server.[112] Fifty homology models were built with MODELLER[113,114] version 9.14 and the best model in terms of both Modeller Objective Function and Dope Score was selected for the subsequent energy minimization and docking calculations.

Compound 10g model building

To carry out docking calculations, the starting ligand geometries of compound **10g** were built with Ghemical 2.99.2[115] and energy minimized at molecular mechanics level first, using Tripos 5.2 force field parametrization[116] and then at AM1 semi-empirical level.

Compound 10g conformational analysis

The first step in the conformational analysis of compound **10g** was the exploration and minimization at the DFT level of the representative conformational states of the tetrahydroisoquinoline ring. This analysis was performed on a simplified model system, namely (1*S*)-1-(4-fluorophenyl)-6,7-dimethoxy-N,N-dimethyl-1,2,3,4-tetrahydroisoquinoline-2-carboxamide. Candidate structures of compound **10g** were generated by properly overlapping the ureide region of all possible pairs of structures of the model compound, removing the redundant N,N-dimethylamido group of one unit and N,N-dimethylamino moiety of the other and, in case of bumps, rotating the dihedrals corresponding to the central amide bonds. This procedure generated all the physically reasonable conformations of the *SS* diastereomer of compound **10g** which were then submitted to DFT energy minimization, thus providing the main stable conformers of this compound, selected with an energetic cutoff of 6 kcal mol^{-1} from the stablest conformer of each diastereomer. The *RR* isomer was obtained by mirroring the corresponding *SS* enantiomers.

Geometry optimization was performed with ORCA 3.0.3[117] at the DFT level, using BP86 functionals,[118–120] Def2-TZV basis set,[121,122] Def2-TZV/J auxiliary basis set, DFT-D3 empirical dispersion correction with Becke-Johnson damping,[123,124] COSMO chloroform solvent model[125] and the RI-J approximation to speed-up the calculation of Coulomb energy.[126] Simultaneous convergence tolerances of $5.0 \cdot 10^{-6}$ Eh for the energy change between subsequent steps, $3.0 \cdot 10^{-4}$ Eh $bohr^{-1}$ for the maximum gradient, $1.0 \cdot 10^{-4}$ Eh $bohr^{-1}$ for the

RMS gradient, $4.0 \cdot 10^{-3}$ bohr for the maximum atomic displacement, and $2.0 \cdot 10^{-3}$ bohr for the RMS atomic displacement between subsequent steps, were applied.

AMBER force field parametrization of compound 10g

Since the structure of **10g** is characterized by different conformations due to puckering, nitrogen geometry etc, nine representative conformations from conformational analysis were independently optimized using GAMESS program[127] at the Hartree-Fock level with the STO-3G basis set, followed by a single-point HF energy evaluation at the 6-31G* level to derive the partial atomic charges for the ligand by the RESP procedure.[128]

Docking of compound 10g in TRPM8

Docking studies were performed with AutoDock 4.2.[129] The TRPM8 monomer model and the selected conformations for compounds **10g** from conformational analysis, for a total of twelve conformations (six each for *RR*/*SS* enantiomer pair) were processed with AutoDock Tools (ADT) package version 1.5.6rc1[129] to merge non polar hydrogens, calculate Gasteiger charges and select rotatable sidechain bonds. Grid dimensions of 22.5 x 22.5 x 22.5 Å, centered in the putative binding pocket, were used for docking evaluation, generated with the program AutoGrid 4.2 included in Autodock 4.2 distribution, with a spacing of 0.375 Å. Docking runs were carried out by allowing the rotation of Arg851, Tyr1005, Asn692, Arg1008 and Glu1004. 100 molecular AutoDock docking runs for each docking calculation were performed adopting a Lamarckian Genetic Algorithm (LGA) and the following associated parameters: 100 individuals in a population with a maximum of 15 million energy evaluations and a maximum of 37000 generations, followed by 300 iterations of Solis and Wets local search. Flexibility was used for all rotatable bonds of both docked ligands. For each docking run, the

poses endowed with the best 10 poses in term of binding free energy were subjected to visual inspection and those forming productive interactions involving at least one fluorine atom with the residues of binding site were selected for the subsequent energy minimization with Amber12 package using ff12SB version of AMBER force field[130] for the protein and gaff[131] parameters for the ligands. Ligand-protein interaction energy was calculated with the NAMD 2.10 program.[132]

Visual inspection and graphical analysis were performed with VMD 1.9.2[133] and UCSF Chimera 1.10.1;[134] the latter program was also used to draw the figures.

Corresponding Author Information: Luciano De Petrocellis. Phone: +390818675173. E-mail: luciano.depetrocellis@icb.cnr.it J. Carlos Menéndez: Phone (+34)-913941840. E-mail: josecm@farm.ucm.es

Author Contributions: L.DP., P.L.-A., F.J.A. and J.C.M. conceived the research and designed the experiments. F.J.A., P.O., A.S., C.R., P.L.A., G.B., M.A.M. and A.S.M. carried out the synthetic, pharmacological, biochemical and analytical experimental work. L.DP., P.L.-A. and J.C.M. supervised the experimental work. R.M.V. and P.A. conceived and performed the modeling studies. L.DP., P.L.-A. and J.C.M. wrote the paper, with assistance from the other authors.

Acknowledgments. Financial support from MINECO (grants CTQ-2012-33272-BQU and CTQ2015-68380-R) is gratefully acknowledged.

Supporting Information Available: Copies of ^{1}H- and ^{13}C-NMR spectra of all new compounds and additional details of the docking studies.

Abbreviations: BSA: Bovine serum albumin. CBFN: Carboxynaphtofluorescein. CCI: Chronic constriction injury. CMR-1: Cold menthol receptor-1. HEK 293: Human Embryonic Kidney 293. LNCaP: Lymph node metastasis in Caucasian male prostate. PNT1A: Normal prostate epithelium imortalized with SV40 qRT-PCR: quantitative real-time RT-PCR TRP: Transient receptor potential. TRPM8: Transient receptor potential melastatin 8.

References

(1) Peier, A. M.; Moqrich, A.; Hergarden, A. C.; Reeve, A. J.; Andersson, A. D.; Story, G. M.; Earley, T. J.; Dragoni, I.; McIntyre, P.; Bevan, S.; Patapoutian, A. A TRP channel that senses cold stimuli and menthol. *Cell* **2002**, *108*, 705-715.

(2) McKemy, D. D.; Neuhausser, W. M.; Julius, D. Identification of a cold receptor reveals a general role for TRP channels in thermosensation. *Nature* **2002**, *416*, 52-58.

(3) Behrendt, H. J.; Germann, T.; Gillen, C.; Hatt, H.; Jostock, R. Characterization of the mouse cold-menthol receptor TRPM8 and vanilloid receptor type-1 VR1 using a fluorometric imaging plate reader (FLIPR) assay. *Br. J. Pharmacol*. **2004**, *141*, 737-745.

(4) Kühn, F. J.; Kühn, C.; Luckhoff, A. Inhibition of TRPM8 by icilin distinct from desensitization induced by menthol and menthol derivatives. *J. Biol. Chem*. **2009**, *284*, 4102–4111.

(5) Patapoutian, A.; Peier, A. M.; Story, G. M.; Viswanath, V. ThermoTRP channels and beyond: mechanisms of temperature sensation. *Nat. Rev. Neurosci*. **2003**, *4*, 529-539.

(6) Caterina, M. J.; Leffler, A.; Malmberg, A. B.; Martin, W. J.; Trafton, J.; Petersen-Zeitz, K. R.; Koltzenburg, M.; Basbaum, A. I.; Julius, D. Impaired nociception and pain sensation in mice lacking the capsaicin receptor. *Science* **2000**, *288*, 306-313.

(7) Moqrich, A.; Hwang, S. W.; Earley, T. J.; Petrus, M. J.; Murray, A. N.; Spencer, K. S.; Andahazy, M.; Story, G. M.; Patapoutian, A. Impaired thermosensation in mice lacking TRPV3, a heat and camphor sensor in the skin. *Science* **2005**, *307*, 1468-1472.

(8) Lee, H.; Iida, T.; Mizuno, A.; Suzuki, M.; Caterina, M. J. Altered thermal selection behavior in mice lacking transient receptor potential vanilloid 4. *J. Neurosci*. **2005**, *25*, 1304-1310.

(9) Story, G. M.; Peier, A. M.; Reeve, A. J.; Eid, S. R.; Mosbacher, J.; Hricik, T. R.; Earley, T. J.; Hergarden, A. C.; Andersson, D. A.; Hwang, S. W.; McIntyre, P.; Jegla, T.; Bevan, S.; Patapoutian, A. ANKTM1, a TRP-like channel expressed in nociceptive neurons, is activated by cold temperatures. *Cell* **2003**, *112*, 819–829.

(10) Klionsky, L.; Tamir, R.; Gao, B.; Wang, W.; Immke, D.C.; Nishimura, N.; Gavva, N. R. Species-specific pharmacology of trichloro(sulfanyl)ethyl benzamides as transient receptor potential ankyrin 1 (TRPA1) antagonists. *Mol. Pain* **2007**, *3*, 39.

(11) Karashima, Y.; Talavera, K.; Everaerts, W.; Janssens, A.; Kwan, K. Y.; Vennekens, R.; Nilius, B.; Voets, T. TRPA1 acts as a cold sensor in vitro and in vivo. *Proc. Natl. Acad. Sci. USA* **2009**, *106*, 1273–1278.

(12) Bautista, D. M.; Simens, J.; Glazer, J. M.; Tsuruda, P. R.; Basbaum, A. I.; Stucky, C. L.; Jordt, S. E.; Julius, D. The menthol receptor TRPM8 is the principal detector of environmental cold. *Nature* **2007**, *448*, 204-208.

(13) Colburn, R. W.; Lubin, M. L.; Stone Jr., D. J.; Wang, Y.; Lawrence, D.; D'Andrea, M. R.; Brandt, M. R.; Liu Y.; Flores, C. M.; Qin, N. Attenuated cold sensitivity in TRPM8 null mice. *Neuron* **2007**, *54*, 379-386.

(14) Dhaka, A.; Murray, A. N.; Mathur, J.; Earley, T. J.; Petrus, M. J.; Patapoutian, A. TRPM8 is required for cold sensation in mice. *Neuron* **2007**, *54*, 371-378.

(15) Knowlton, W. M.; Bifolck-Fisher, A.; Bautista, D. M.; McKemy, D. D. TRPM8, but not TRPA1, is required for neural and behavioral responses to acute noxious cold temperatures and cold-mimetics in vivo. *Pain* **2010**, *150*, 340–350.

(16) McCoy, D. D.; Knowlton, W. M.; McKemy, D. D. Scraping through the ice: uncovering the role of TRPM8 in cold transduction. *Am. J. Physiol. Regul. Integr. Comp. Physiol*. **2011**, *300*, R1278-R1287.

(17) Gavva, N. R.; Davis, C.; Lehto, S. G.; Rao, S.; Wang, W.; Zhu, D.X. Transient receptor potential melastatin 8 (TRPM8) channels are involved in body temperature regulation. *Mol. Pain* **2012**, *8*, 36.

(18) Ruskin, D. N.; Anand, R.; LaHoste, G. J. Menthol and nicotine oppositely modulate body temperature in the rat. *Eur. J. Pharmacol*. **2007**, *559*, 161–164.

(19) Ding, Z.; Gomez, T.; Werkheiser, J. L.; Cowan, A.; Rawls, S. M. Icilin induces a hyperthermia in rats that is dependent on nitric oxide production and NMDA receptor activation. *Eur. J. Pharmacol*. **2008**, *578*, 201–208.

(20) Wei, E. T. Chemical stimulants of shaking behaviour. *J. Pharm. Pharmacol*. **1976**, *28*, 722–724.

(21) Tajino, K.; Matsumura, K.; Kosada, K.; Shibakusa, T.; Inoue, K.; Fushiki, T.; Hosokawa, H.; Kobayashi, S. Application of menthol to the skin of whole trunk in mice induces autonomic and behavioral heat-gain responses. *Am. J. Physiol. Regul. Integr. Comp*. *Physiol*. **2007**, *298*, R2128-R2135.

(22) Tajino, K.; Hosokawa, H.; Maegawa, S.; Matsumura, K.; Dhaka, A.; Kobayashi, S. Cooling-sensitive TRPM8 is thermostat of skin temperature against cooling. *PLoS One* **2011**, *6*, e17504.

(23) Knowlton, W. M.; Daniels, R. L.; Palkar, R.; McCoy, D. D.; McKemy, D. D. Pharmacological blockade of TRPM8 ion channels alters cold and cold pain responses in mice. *PLoS One* **2011**, *6*, e25894.

(24) Almeida, M. C.; Hew-Butler, T.; Soriano, R. N.; Rao, S.; Wang, W.; Wang, J.; Tamayo, N.; Oliveira, D. L.; Nucci, T. B.; Aryal, P.; Garami, A.; Bautista, D.; Gavva, N. R.; Romanovsky, A. A. Pharmacological blockade of the cold receptor TRPM8 attenuates autonomic and behavioral cold defenses and decreases deep body temperature. *J. Neurosci*. **2012**, *32*, 2086-2099.

(25) Li, M.; Yu, Y.; Yang, J. Structural biology of TRP channels. *Adv. Exp. Med. Biol*. **2011**, *704*, 1–23.

(26) Bandell, M.; Dubin, A. E.; Petrus, M. J.; Orth, A.; Mathur, J.; Hwang, S. W. Patapoutian, A. High-throughput random mutagenesis screen reveals TRPM8 residues specifically required for activation by menthol A. *Nat. Neurosci*. **2006**, *9*, 493–500.

(27) Chuang, H. H.; Neuhausser, W. M.; Julius, D. The super-cooling agent icilin reveals a mechanism of coincidence detection by a temperature-sensitive TRP channel. *Neuron* **2004**, *43*, 859–869.

(28) Kühn, F. J.; Knop, G.; Lückhoff, A. The transmembrane segment S6 determines cation versus anion selectivity of TRPM2 and TRPM8. *J. Biol. Chem*. **2007**, *282*, 27598–27609.

(29) Voets, T.; Owsianik, G.; Janssens, A.; Talavera, K.; Nilius, B. TRPM8 voltage sensor mutants reveal a mechanism for integrating thermal and chemical stimuli. *Nat. Chem. Biol*. **2007**, *3*, 174–182.

(30) Thut, P. D.; Wrigley, D.; Gold, M. S. Cold transduction in rat trigeminal ganglia neurons in vitro. *Neuroscience* **2003**, *119*, 1071–1083.

(31) Nealen, M. L.; Godl, M. S.; Thut, P. D.; Caterina, M. J. TRPM8 mRNA is expressed in a subset of cold-responsive trigeminal neurons from rat. *J. Neurophysiol*. **2003**, *90*, 515-520.

(32) Kobayashi, K.; Fukuoka, T.; Obata, K.; Yamanaka, H.; Dai, Y.; Tokunaga, A.; Noguchi, K. Distinct expression of TRPM8, TRPA1, and TRPV1 mRNAs in rat primary afferent neurons with adelta/c-fibers and colocalization with trk receptors. *J. Comb. Neurol*. **2005**, *493*, 596-606.

(33) Dhaka, A.; Earley, T. J.; Watson, J.; Patapoutian, A. Visualizing cold spots: TRPM8-expressing sensory neurons and their projections. *J. Neurosci*. **2008**, *28*, 566-575.

(34) Takashima, Y.; Daniels, R. L.; Knowlton, W.; Teng, J.; Liman, E. R.; McKemy, D. D. Diversity in the neural circuitry of cold sensing revealed by genetic axonal labeling of transient receptor potential melastatin 8 neurons. *J. Neurosci*. **2007**, *27*, 14147-14157.

(35) Fonfria, E.; Murdock, P. R.; Cusdin, F. S.; Benham, C. D.; Kelsell, R. E.; McNulty, S. Tissue distribution profiles of the human TRPM cation channel family. *J. Recept. Signal Tr. R*. **2006**, *26*, 159–178.

(36) Proudfoot, C. J.; Garry, E. M.; Cottrell, D. F.; Rosie, R.; Anderson, H.; Robertson, D. C.; Fleetwood-Walker, S. M.; Mitchell, R. Analgesia mediated by the TRPM8 cold receptor in chronic neuropathic pain. *Curr. Biol*. **2006**, *16*, 1591–1605.

(37) Chung, M. -K.; Caterina, M. J. TRP channel knockout mice lose their cool. *Neuron* **2007**, *54*, 345-347.

(38) Xing, H.; Chen, M.; Ling, J.; Tan, W.; Gu, J. G. TRPM8 mechanism of cold allodynia after chronic nerve injury. *J. Neurosci*. **2007**, *27*, 13680-13690.

(39) Caspani, O.; Zurborg, S.; Labuz, D.; Heppenstall, P. A. The contribution of TRPM8 and TRPA1 channels to cold allodynia and neuropathic pain. *PLoS One* **2009**, *4*, e7383.

(40) Rossi, H. L.; Jenkins, A. C.; Kaufman, J.; Bhattacharyya, I.; Caudle, R. M.; Neubert, J. K. Characterization of bilateral trigeminal constriction injury using an operant facial pain assay. *Neuroscience* **2012**, *224*, 294-306.

(41) Brignell, J. L.; Chapman, V.; Kendall, D. A. Comparison of icilin- and cold-evoked responses of spinal neurones, and their modulation of mechanical activity, in a model of neuropathic pain. *Brain Res*. **2008**, *1215*, 87–96.

(42) Harrington, A. M.; Hughes, P. A.; Martin, C. M.; Yang, J.; Castro, J.; Isaacs, N. J.; Blackshaw, L. A.; Brierley, S. M. A novel role for TRPM8 in visceral afferent function. *Pain* **2011**, *152*, 1459–1468.

(43) Patel, R.; Gonçalves, L.; Newman, R.; Jiang, F. L.; Goldby, A.; Reeve, J.; Hendrick, A.; Teall, M.; Hannah, D.; Almond, S.; Brice, N.; Dickenson, A. H. Novel TRPM8 antagonist attenuates cold hypersensitivity after peripheral nerve injury in rats. *J. Pharmacol. Exp. Ther*. **2014**, *349*, 47-55.

(44) Broad, L. M.; Mogg, A. J.; Beattie, R. E.; Ogden, A. M.; Blanco, M. J.; Bleakman, D. TRP channels as emerging targets for pain therapeutics. *Expert Opin. Ther. Targets* **2009**, *13*, 69-81.

(45) Stucky, C. L.; Dubin, A. E.; Jeske, N. A.; Malin, S. A.; McKemy, D. D.; Story, G. M. Roles of transient receptor potential channels in pain. *Brain Res. Rev*. **2009**, *60*, 2-23.

(46) Winchester, W.; Gore, K.; Glatt, S.; Petit, W.; Gardiner, J. C.; Conlon, K.; Postlethwaite, M.; Saintot, P. P.; Roberts, S.; Gosset, J. R.; Matsuura, T; Andrews, M. D.; Glossop, P. A.; Palmer, M. J.; Clear, N.; Collins, S.; Beaumont, K.; Reynolds, D. S. Inhibition of TRPM8 channels reduces pain in the cold pressor test in humans. *J. Pharmacol. Exp. Ther*. **2014**, *351*, 259-269.

(47) Tsavaler, L.; Shapero, M. H.; Morkowski, S.; Laus, R. Trp-p8, a novel prostate-specific gene, is up-regulated in prostate cancer and other malignancies and shares high homology with transient receptor potential calcium channel proteins. *Cancer Res*. **2001**, *61*, 3760-3769.

(48) Yamamura, H.; Ugawa, S.; Ueda, T.; Morita, A.; Shimada, S. TRPM8 activation suppresses cellular viability in human melanoma. *Am. J. Physiol. Cell Physiol*. **2008**, *295*, 296–301.

(49) Zhang, L.; Barritt, G. J. Evidence that TRPM8 is an androgen-dependent Ca^{2+} channel required for the survival of prostate cancer cells. *Cancer Res*. **2004**, *64*, 8365-8373.

(50) De Petrocellis, L.; Ligresti, A.; Schiano Moriello, A.; Iappelli, M.; Verde, R.; Stott, C. G.; Cristino, L.; Orlando, P.; Di Marzo, V. Non-THC cannabinoids inhibit prostate carcinoma growth *in vitro* and *in vivo*: pro-apoptotic effects and underlying mechanisms. *Br. J. Pharmacol*. **2013**, *168*, 79-102.

(51) Borrelli, F.; Pagano, E.; Romano, B.; Panzera, S.; Maiello, F.; Coppola, D.; De Petrocellis, L.; Buono, L.; Orlando, P.; Izzo, A. A. Colon carcinogenesis is inhibited by the TRPM8 antagonist cannabigerol, a Cannabis-derived non-psychotropic cannabinoid. *Carcinogenesis* **2014**, *35*, 2787-2797.

(52) Mukerji, G.; Yiangou, Y.; Corcoran, S. L.; Selmer, I. S.; Smith, G. D.; Benham, C. D.; Bountra, C.; Agarwal, S. K.; Anand, P. Cool and menthol receptor TRPM8 in human urinary bladder disorders and clinical correlations. *BMC Urol*. **2006**, *6*, 6.

(53) Lashinger, E. S.; Steiginga, M. S.; Hieble, J. P.; Leon, L. A.; Gardner, S. D.; Nagilla, R.; Davenport, E. A.; Hoffman, B. E.; Laping, N. J.; Su, X. AMTB, a TRPM8 channel blocker: evidence in rats for activity in overactive bladder and painful bladder syndrome. *Am. J. Physiol. Renal. Physiol*. **2008**, *295*, F803-F810.

(54) Sherkheli, M. A.; Vogt-Eisele, A. K.; Bura, D.; Beltrán Márques, L. R.; Gisselmann, G.; Hatt, H. Characterization of selective TRPM8 ligands and their structure activity response (S.A.R) relationship. *J. Pharm. Pharm. Sci*. **2010**, *13*, 242-253.

(55) Gentry, C.; Stoakley, N.; Andersson, D. A.; Bevan, S. The roles of iPLA2, TRPM8 and TRPA1 in chemically induced cold hypersensitivity. *Mol. Pain* **2010**, *6*, 4.

(56) Bharate, S. S.; Bharate, S. B. Modulation of thermoreceptor TRPM8 by cooling compounds. *ACS Chem. Neurosci.* **2012**, 3, 248-267.

(57) Weil, A.; Moore, S. E.; Waite, N. J.; Randall, A.; Gunthorpe, M. J. Conservation of functional and pharmacological properties in the distantly related temperature sensors TRPV1 and TRPM8. *Mol. Pharmacol*. **2005**, *68*, 518-527.

(58) Walpole, C. S.; Bevan, S.; Bovermann, G.; Boelsterli, J. J.; Breckenridge, R.; Davies, J. W.; Hughes, G. A.; James, I.; Oberer, L.; Winter, J.; Wrigglesworth, R. The discovery of capsazepine, the first competitive antagonist of the sensory neuron excitants capsaicin and resiniferatoxin. *J. Med. Chem*. **1994**, *37*, 1942–1954.

(59) Docherty, R. J.; Yeats, J. C.; Piper, A. S. Capsazepine block of voltage-activated calcium channels in adult rat dorsal root ganglion neurones in culture. *Br. J. Pharmacol*. **1997**, *121*, 1461–1467.

(60) Liu, L.; Simon, S. A. Capsazepine, a vanilloid receptor antagonist, inhibits nicotinic acetylcholine receptors in rat trigeminal ganglia. *Neurosci Lett*. **1997**, *228*, 29–32.

(61) Madrid, R.; Donovan-Rodríguez, T.; Meseguer, V.; Acosta, M. C.; Belmonte, C.; Viana, F. Contribution of TRPM8 channels to cold transduction in primary sensory neurons and peripheral nerve terminals. *J. Neurosci*. **2006**, *26*, 12512–12525.

(62) Meseguer, V.; Karashima, Y.; Talavera, K.; D'Hoedt, D.; Donovan-Rodriguez, T.; Viana, F.; Nilius, B.; Voets, T. Transient receptor potential channels in sensory neurons are targets of the antimycotic agent clotrimazole. *J. Neurosci*. **2008**, *28*, 576-586.

(63) Malkia, A.; Pertusa, M.; Fernández-Ballester, G.; Ferrer-Montiel, A.; Viana, F. Differential role of the menthol-binding residue Y745 in the antagonism of thermally gated TRPM8 channels. *Mol. Pain* **2009**, *5*, 62.

(64) Merritt, J. E.; Armstrong, W. P.; Benham, C. D.; Hallam, T. J.; Jacob, R.; Jaxa-Chamiec, A.; Leigh, B. K.; McCarthy, S. A.; Moores, K. E.; Rink, T. J. SK&F 96365, a novel inhibitor of receptor-mediated calcium entry. *Biochem. J*. **1990**, *271*, 515–522.

(65) Schwarz, G.; Droogmans, G.; Nilius, B. Multiple effects of SK&F 96365 on ionic currents and intracellular calcium in human endothelial cells. *Cell Calcium* **1994**, *15*, 45–54.

(66) Mälkiä, A.; Madrid, R.; Meseguer, V.; de la Peña, E.; Valero, M.; Belmonte, C.; Viana, F. Bidirectional shifts of TRPM8 channel gating by temperature and chemical agents modulate the cold sensitivity of mammalian thermoreceptors. *J. Physiol*. **2007**, *581*, 155-174.

(67) De Petrocellis, L.; Starowicz, K.; Schiano Moriello, A.; Vivese, M.; Orlando, P.; Di Marzo, V. Regulation of transient receptor potential channels of melastatin type 8 (TRPM8): effect of cAMP, cannabinoid CB(1) receptors and endovanilloids. *Exp. Cell Res*. **2007**, *313*, 1911-1920.

(68) De Petrocellis, L.; Vellani, V.; Schiano-Moriello, A.; Marini, P.; Magherini, P. C.; Orlando, P.; Di Marzo, V. Plant-derived cannabinoids modulate the activity of transient receptor potential channels of ankyrin type-1 and melastatin type-8. *J. Pharmacol. Exp. Ther*. **2008**, *325*, 1007-1015.

(69) De Petrocellis, L.; Ligresti, A.; Schiano Moriello, A.; Allarà, M.; Bisogno, T.; Petrosino, S.; Stott, C. G.; Di Marzo, V. Effects of cannabinoids and cannabinoid-enriched Cannabis extracts on TRP channels and endocannabinoid metabolic enzymes. *Br. J. Pharmacol*. **2011**, *163*, 1479-1494.

(70) Ohmi, M.; Shishido, Y.; Inoue, T.; Ando, K.; Fujiuchi, A.; Yamada, A.; Watanabe, S.; Kawamura, K. Identification of a novel 2-pyridyl-benzensulfonamide derivative, RQ-00203078, as a selective and orally active TRPM8 antagonist. *Bioorg. Med. Chem. Lett*. **2014**, *24*, 5364-5368.

(71) Ortar, G.; De Petrocellis, L.; Morera, L.; Schiano Moriello, A.; Orlando, P.; Morera, E.; Nalli, M.; Di Marzo, V. (-)-Menthylamine derivatives as potent and selective antagonists of transient receptor potential melastatin type-8 (TRPM8) channels. *Bioorg. Med. Chem. Lett*. **2010**, *20*, 2729-2732.

(72) DeFalco, J.; Steiger, D.; Dourado, M.; Emerling, D.; Duncton, M. A. 5-benzyloxytryptamine as an antagonist of TRPM8. *Bioorg. Med. Chem. Lett*. **2010**, *20*, 7076-7079.

(73) Brown, A.; Ellis, D.; Favor, D. A.; Kirkup, T.; Klute, W.; MacKenny, M.; McMurray, G.; Stennett, A. Serendipity in drug-discovery: A new series of 2-(benzyloxy)benzamides as TRPM8 antagonists. *Bioorg. Med. Chem. Lett*. **2013**, *23*, 6118-6122.

(74) De Petrocellis, L.; Ortar, G.; Schiano Moriello, A.; Serum, E. M.; Rusterholz, D. B. Structure–activity relationships of the prototypical TRPM8 agonist icilin. *Bioorg. Med. Chem. Lett.* **2015**, *25*, 2285–2290.

(75) Parks, D. J.; Parsons, W. H.; Colburn, R. W.; Meegalla, S. K.; Ballentine, S. K.; Illig, C. R.; Qin, N.; Liu, Y.; Hutchinson, T. L.; Lubin, M. L.; Stone, D. J.; Baker, J. F.; Shneider, C. R.; Ma, J.; Damiano, B. P.; Flores, C. M.; Player, M. R. Design and optimization of benzimidazole-containing transient receptor potential melastatin 8 (TRPM8) antagonists. *J. Med. Chem*. **2011**, *54*, 233-247.

(76) Calvo, R. R.; Meegalla, S. K.; Parks, D. J.; Parsons, W. H.; Ballentine, S. K.; Lubin, M. L.; Schneider, C.; Colburn, R. W.; Flores, C. M.; Player, M. R. Discovery of vinylcycloalkyl-substituted benzimidazole TRPM8 antagonists effective in the treatment of cold allodynia. *Bioorg. Med. Chem. Lett*. **2012**, *22*, 1903-1907.

(77) (a) Matthews, J. M.; Qin, N.; Colburn, R. W.; Dax, S. L.; Hawkins, M.; McNally, J.; Reany, L.; Youngman, M.; Baker, J.; Hutchinson, T.; Liu, Y.; Lubin, M. L.; Neeper, M.; Brandt, M. R.; Stone, D. J.; Flores, C. M. The design and synthesis of novel, phosphonate-containing transient receptor potential melastatin 8 (TRPM8) antagonists. *Bioorg. Med. Chem. Lett*. **2012**, *22*, 2922-2926.

(78) Colburn, R. W.; Dax, S. L.; Flores, C. M.; Matthews, J. M. Cold menthol receptor antagonists. US0053347, **2012**.

(79) N. A.; Bo, Y.; Gore, V.; Ma, V.; Nishimura, N.; Tang, P.; Deng, H.; Klionsky, L.; Lehto, S. G.; Wang, W.; Youngblood, B.; Chen, J.; Correll, T. L.; Bartberger, M. D.; Gavva, N. R.; Norman, M. H. Fused piperidines as a novel class of potent and orally available transient receptor potential melastatin type 8 (TRPM8) antagonists. *J. Med. Chem*. **2012**, *55*, 1593-1611.

(80) Horne, D. B.; Tamayo, N. A.; Bartberger, M. D.; Bo, Y.; Nikimura, N.; Nguyen, T. T.; Tang, P.; Wang, W.; Youngblood, B. D.; Zhang, M.; Gavva, N. R.; Monenschein, H.; Norman, M. H. Optimization of potency and pharmacokinetic properties of tetrahydroisoquinoline transient receptor potential melastatin 8 (TRPM8) antagonists. *J. Med. Chem*. **2014**, *57*, 2989−3004.

(81) Irlaplati, N. R.; Thomas, A.; Kurhe, D. K.; Shelke, S. K.; Khairatkar, J. N.; Viswanadha, S.; Mukhopadhyay, I. Fused oxazole and thiazole derivatives as TRPM8 modulators. Patent WO 2010010435 (July 19 2009).

(82) Zhu, B.; Xia, M.; Xu, X.; Ludovici, D. W.; Tennakoon, M.; Youngman, M. A.; Matthews, J. M.; Dax, S. L.; Colburn, R. W.; Qin, N.; Hutchinson, T. L.; Lubin, M. L.; Brandt, M. R.; Stone, D. J.; Flores, C. M.; Macielag, M. J. Arylglycine derivatives as potent transient receptor potential melastatin 8 (TRPM8) antagonists. *Bioorg. Med. Chem. Lett*. **2013**, *23*, 2234-2237.

(83) Ohmi, M.; Shishido, Y.; Inoue, T.; Ando, K.; Fujiuchi, A.; Yamada, A.; Watanabe, S.; Kawamura, K. Identification of a novel 2-pyridyl-benzensulfonamide derivative, RQ-00203078, as a selective and orally active TRPM8 antagonist. *Bioorg. Med. Chem. Lett*. **2014**, *24*, 5364-5368.

(84) Terada, Y.; Kitajima, M.; Taguchi, F.; Takayama, H.; Horie, S.; Watanabe, T. Identification of indole alkaloid structural units important for stimulus-selective TRPM8 inhibition: SAR study of naturally occurring *Iboga* derivatives. *J. Nat. Prod*. **2014**, *77,* 1831–1838.

(85) DeFalco, J.; Duncton, M. A.; Emerling, D. TRPM8 biology and medicinal chemistry. *Curr. Top Med. Chem*. **2011**, *11*, 2237-2252.

(86) Ferrer-Montiel, A.; Fernández-Carvajal, A.; Planells-Cases, R.; Fernández-Ballester, G.; González-Ros, J. M.; Messeguer, A.; González-Muñiz, R. Advances in modulating thermosensory TRP channels. *Expert Opin. Ther. Pat*. **2012**, 22, 999-1017.

(87) Brederson, J. D.; Kym, P. R.; Szallasi, A. Targeting TRP channels for pain relief. *Eur. J. Pharmacol.* **2013**, *716*, 61–76.

(88) Taberner, F. J.; López-Córdoba, A.; Fernández-Ballester, G.; Korchev, Y.; Ferrer-Montiel, A. The region adjacent to the C-end of the inner gate in transient receptor potential melastatin 8 (TRPM8) channels plays a central role in allosteric channel activation. *J. Biol. Chem*. **2014**, *289*, 28579–28594.

(89) Bertamino, A.; Ostacolo, C.; Ambrosino, P.; Musella, S.; Di Sarno, V.; Ciaglia, T.; Soldovieri, M. V.; Iraci, N.; Fernández Carvajal, A.; de la Torre-Martínez, R.; Ferrer-Montiel, A.; González Muniz, R.; Novellino, E.; Taglialatela, M.; Campiglia, P.; Gómez-Monterrey, I. Tryptamine-based derivatives as transient receptor potential melastatin type 8 (TRPM8) channel modulators. *J. Med. Chem*. **2016**, *59*, 2179-2191.

(90) Contreras, J.-M.; Sippl, W. Homo and heterodimer ligands: The twin drug approach, in Wermuth, C. G. (ed.), The practice of Medicinal Chemistry, 3rd Ed. Elsevier, 2008.

(91) Staderini, M.; Legname, G.; Bolognesi, M. L.; Menéndez, J. C. Modulation of prions by small molecules: from monovalent to bivalent ligands. *Curr. Top. Med. Chem.* **2013**, *13*, 2491-2503

(92) Jagtap, S. R.; Patil, Y. P.; Panda, A. G.; Bhanage, B. M. Synthesis of 1,3-disubstituted symmetrical/unsymmetrical ureas via Cs_2CO_3-catalyzed transamination of ethylene carbonate and primary amines. *Synth. Commun*. **2009**, *39*, 2093–2100.

(93) Ivanov, I.; Venkov, A. Application of hexamethylenetetramine in a Pictet-Spengler type reaction for synthesis of isoquinoline derivatives. *Heterocycles* **2001**, *55*, 1569-1572.

(94) Arroyo, F. J.; López-Alvarado, P.; Ganesan, A.; Menéndez, J. C. One-pot α-amidosulfone-mediated variation of the Pictet–Spengler tetrahydroisoquinoline synthesis, suitable for amide-type substrates. *Eur. J. Org. Chem*. **2014**, *26*, 5720–5727.

(95) Gitto, R.; Barreca, M. L.; De Luca, L.; De Sarro, G.; Ferreri, G.; Quartarone, S.; Russo, E.; Constanti, A.; Chimirri, A. Discovery of a novel and highly potent noncompetitive AMPA receptor antagonist. *J. Med. Chem.* **2003**, *46*, 197-200.

(96) Muller, K.; Faeh, C.; Diederich, F. Fluorine in Pharmaceuticals: Looking Beyond Intuition. *Science* **2007**, *317*, 1881–1886.

(97) Bidaux, G.; Roudbaraki, M.; Merle, C.; Crépin, A.; Delcourt, P.; Slomianny, C.; Thebault, S.; Bonnal, J. L.; Benahmed, M.; Cabon, F.; Mauroy, B.; Prevarskaya, N. Evidence for specific TRPM8 expression in human prostate secretory epithelial cells: functional androgen receptor requirement. *Endocr. Relat. Cancer* **2005**, *12*, 367-382.

(98) Bidaux, G.; Flourakis, M.; Thebault, S.; Zholos, A.; Beck, B.; Gkika, D.; Roudbaraki, M.; Bonnal, J. L.; Mauroy, B.; Shuba, Y.; Skryma, R.; Prevarskaya, N. Prostate cell differentiation status determines transient receptor potential melastatin member 8 channel subcellular localization and function. *J. Clin. Invest*. **2007**, *117*, 1647-1657.

(99) Valero, M.; Morenilla-Palao, C.; Belmonte, C.; Viana, F. Pharmacological and functional properties of TRPM8 channels in prostate tumor cells. *Pflugers Arch*. **2011**, *461*, 99-114.

(100) Valero, M. L.; Mello de Queiroz, F.; Stühmer, W.; Viana, F.; Pardo, L. A. TRPM8 ion channels differentially modulate proliferation and cell cycle distribution of normal and cancer prostate cells. *PLoS One* **2012**, *7*, e51825.

(101) Pfaffl, M. W. The ongoing evolution of qPCR. *Methods* **2010**, *50*, 215-216.

(102) Obach, R. S. Prediction of human clearance of twenty-nine drugs from hepatic microsomal intrinsic clearance data: An examination of in vitro half-life approach and nonspecific binding to microsomes. *Drug Metab*. *Dispos*. **1999**, *27*, 1350-1359.

(103) Teeter, J. S.; Meyerhoff, R. Environmental fate and chemistry of raloxifene hydrochloride. *Environ. Toxicol. Chem*. **2002**, *21*, 729–736.

(104) Ran, Y.; He, Y.; Yang, G.; Johnson, J. L. H.; Yalkowsky, S. H. Estimation of aqueous solubility of organic compounds by using the general solubility equation. *Chemosphere* **2002**, *48*, 487–509.

(105) Wlodarski, K.; Sawicki, W.; Paluch, K. J.; Tajber, L.; Grembecka, M.; Hawelek, L.; Wojnarowska, Z.; Grzybowska, K.; Talik, E.; Paluch, M. The influence of amorphization methods on the apparent solubility and dissolution rate of tadalafil. *Eur. J. Pharm. Sci.* **2014**, *62*, 132–140.

(106) Coskun, N.; Tuncman, S. Synthesis of stable azomethine ylides by the rearrangement of 1,3-dipolar cycloadducts of 3,4-dihydroisoquinoline-2-oxides with DMAD. *Tetrahedron* **2006**, *62*, 1345-1350.

(107) Shawe, T. T.; Liebeskind, L. S. Saframycin synthetic studies. *Tetrahedron* **1991**, *47*, 5643-5666.

(108) Grimaldi, P.; Orlando, P.; Di Siena, S.; Lolicato, F.; Petrosino, S.; Bisogno, T.; Geremia, R.; De Petrocellis, L.; Di Marzo, V. The endocannabinoid system and pivotal role of the CB2 receptor in mouse spermatogenesis. *Proc. Natl. Acad. Sci. USA* **2009**, *106*, 11131-11136.

(109) Perloff, M. D.; von Moltke, L. L.; Court, M. H.; Kotegawa, T.; Shader, R. I.; Greenblatt, D. J. Midazolam and triazolam biotransformation in mouse and human liver microsomes: Relative contribution of CYP3A and CYP2C isoforms. *J. Pharmacol. Exp. Ther.* **2000**, *292*, 618-628.

(110) Obach, R. S. Nonspecific binding to microsomes: Impact on scale-up of *in vitro* intrinsicclearance to hepatic clearance as assessed through examination of warfarin, imipramine, and propranolol. *Drug Metab Dispos* **1997**, *25*, 1359–1369.

(111) Kelley, L. A.; Mezulis, S.; Yates, C. M.; Wass, M. N.; Sternberg, M. J. E. The Phyre2 Web portal for protein modeling, prediction and analysis. *Nat. Protoc*. **2015**, *10*, 845–858.

(112) Yachdav, G.; Kloppmann, E.; Kajan, L.; Hecht, M.; Goldberg, T.; Hamp, T.; Honigschmid, P.; Schafferhans, A.; Roos, M.; Bernhofer, M.; Richter, L.; Ashkenazy, H.; Punta, M.; Schlessinger, A.; Bromberg, Y.; Schneider, R.; Vriend, G.; Sander, C.; Ben-Tal, N.; Rost, B. PredictProtein-an open resource for online prediction of protein structural and functional features. *Nucleic Acids Res*. **2014**, *42*, W337–W343.

(113) Sali, A.; Blundell, T. L. Comparative protein modelling by satisfaction of spatial restraints. *J. Mol. Biol.* **1993**, *234*, 779–815.

(114) Eswar, N.; Webb, B.; Marti-Renom, M. A.; Madhusudhan, M. S.; Eramian, D.; Shen, M.-Y.; Pieper, U.; Sali, A. Comparative protein structure modeling using Modeller, in Current Protocols in Bioinformatics; John Wiley & Sons, Inc.: Hoboken, NJ, USA, **2006**; Vol. Chapter 5, pp 5.6.1–5.6.30.

(115) Acton, A.; Banck, M.; Bréfort, J.; Cruz, M.; Curtis, D.; Hassinen, T.; Heikkilä, V.; Hutchison, G.; Huuskonen, J.; Jensen, J.; Liboska, R.; Rowley, C. GHEMICAL, http://www.bioinformatics.org/ghemical/ghemical/index.html.

(116) Clark, M.; Cramer, R. D.; Van Opdenbosch, N. Validation of the general purpose Tripos 5.2 force field. *J. Comput. Chem*. **1989**, *10*, 982–1012.

(117) Neese, F. The ORCA program system. *Wiley Interdisciplinary Rev. Comput. Mol. Sci*. **2012**, *2*, 73–78.

(118) Becke, A. D. Density-Functional exchange-energy approximation with correct asymptotic *Behavior. Phys. Rev. A* **1988**, *38*, 3098–3100.

(119) Perdew, J. P.; Zunger, A. Self-interaction correction to Density-Functional approximations for many-electron systems. *Phys. Rev. B* **1981**, *23*, 5048–5079.

(120) Perdew, J. P. Density-Functional approximation for the correlation energy of the inhomogeneous electron gas. *Phys. Rev. B* **1986**, *33*, 8822–8824.

(121) Schäfer, A.; Horn, H.; Ahlrichs, R. Fully optimized contracted Gaussian basis sets for atoms Li to Kr. *J. Chem. Phys*. **1992**, *97*, 2571.

(122) Weigend, F.; Ahlrichs, R. Balanced basis sets of split valence, triple zeta valence and quadruple zeta valence quality for H to Rn: Design and assessment of accuracy. *Phys. Chem. Chem. Phys.* **2005**, *7*, 3297–3305.

(123) Grimme, S. Density Functional theory with London dispersion corrections. *Wiley Interdisciplinary Rev. Comput. Mol. Sci.* **2011**, *1*, 211–228.

(124) Grimme, S.; Antony, J.; Ehrlich, S.; Krieg, H. A consistent and accurate *Ab Initio* parametrization of Density Functional Dispersion correction (DFT-D) for the 94 elements H-Pu. *J. Chem. Phys*. **2010**, *132*, 154104.

(125) Sinnecker, S.; Rajendran, A.; Klamt, A.; Diedenhofen, M.; Neese, F. Calculation of solvent shifts on electronic G-tensors with the conductor-like screening model (COSMO) and its self-consistent generalization to real solvents (direct COSMO-RS). *J. Phys. Chem*. A **2006**, *110*, 2235–2245.

(126) Eichkorn, K.; Treutler, O.; Öhm, H.; Häser, M.; Ahlrichs, R. Auxiliary basis sets to approximate Coulomb potentials. *Chem. Phys. Lett*. **1995**, *240*, 283–290.

(127) Schmidt, M. W.; Baldridge, K. K.; Boatz, J. A.; Elbert, S. T.; Gordon, M. S.; Jensen, J. H.; Koseki, S.; Matsunaga, N.; Nguyen, K. A.; Su, S.; Windus, T. L.; Dupuis, M.; Montgomery, J. A. General atomic and molecular electronic structure system. *J. Comput. Chem*. **1993**, *14*, 1347–1363.

(128) Fox, T.; Kollman, P. A. Application of the RESP methodology in the parametrization of organic solvents. *J. Phys. Chem. B* **1998**, *102*, 8070–8079.

(129) Morris, G. M.; Huey, R.; Lindstrom, W.; Sanner, M. F.; Belew, R. K.; Goodsell, D. S.; Olson, A. J. AutoDock4 and AutoDock Tools 4: Automated docking with selective receptor flexibility. *J. Comput. Chem.* **2009**, *30*, 2785–2791.

(130) Case, D. A.; Darden, T. A.; Cheatham III, T. E.; Simmerling, C. L.; Wang, J.; Duke, R. E.; Luo, R.; Walker, R. C.; Zhang, W.; Merz, K. M.; Roberts, B.; Hayik, S.; Roitberg, A.; Seabra, G.; Swails, J.; Goetz, A. W.; Kolossváry, I.; Wong, K. F.; Paesani, F.; Vanicek, J.; Wolf, R. M.; Liu, J.; Wu, X.; Brozell, S. R.; Steinbrecher, T.; Gohlke, H.; Cai, Q.; Ye, X.; Hsieh, M. J.; Cui, G.; Roe, D. R.; Mathews, D. H.; Seetin, M. G.; Salomon-Ferrer, R.; Sagui, C.; Babin, V.; Luchko, T.; Gusarov, S.; Kovalenko, A.; Kollman, P. A. AMBER 12, University of California, San Francisco. University of California: San Francisco **2012**.

(131) Wang, J.; Wolf, R. M.; Caldwell, J. W.; Kollman, P. A.; Case, D. A. Development and testing of a general Amber force field. *J. Comput. Chem*. **2004**, *25*, 1157–1174.

(132) Phillips, J. C.; Braun, R.; Wang, W.; Gumbart, J.; Tajkhorshid, E.; Villa, E.; Chipot, C.; Skeel, R. D.; Kalé, L.; Schulten, K. Scalable molecular dynamics with NAMD. *J. Comput. Chem*. **2005**, 26 (16), 1781–1802.

(133) Humphrey, W.; Dalke, A.; Schulten, K. VMD: Visual Molecular Dynamics. *J. Mol. Graph*. **1996**, *14*, 33–38.

(134) Pettersen, E. F.; Goddard, T. D.; Huang, C. C.; Couch, G. S.; Greenblatt, D. M.; Meng, E. C.; Ferrin, T. E. UCSF Chimera - A visualization system for exploratory research and analysis. *J. Comput. Chem.* **2004**, *25*, 1605–1612.

Tetrahydroisoquinoline-derived urea and 2,5-diketopiperazine derivatives as selective antagonists of the transient receptor potential melastatin 8 (TRPM8) channel receptor and anti-prostate cancer agents

Luciano De Petrocellis[a,*], Francisco J. Arroyo,[b] Pierangelo Orlando,[c] Aniello Schiano Moriello,[a] Rosa Maria Vitale,[a] Pietro Amodeo,[a] Aránzazu Sánchez,[d] Cesáreo Roncero,[d] Giulia Bianchini,[b] M. Antonia Martín,[e] Pilar López-Alvarado[b], J. Carlos Menéndez[b,*]

Table of content graphic

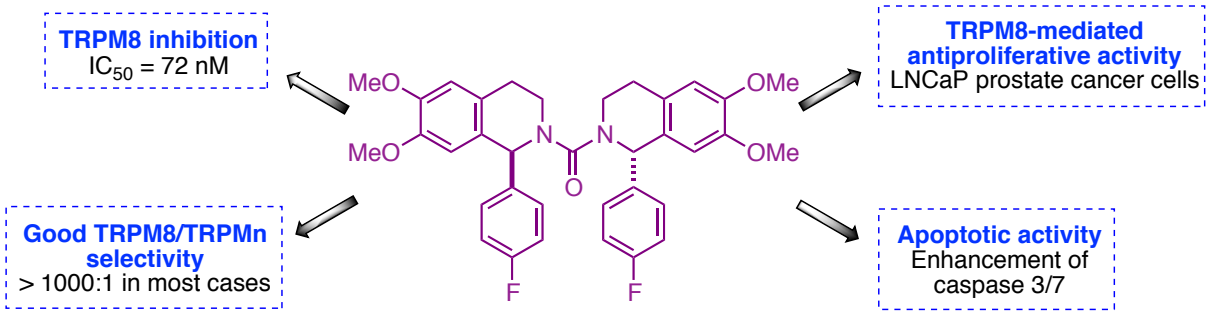

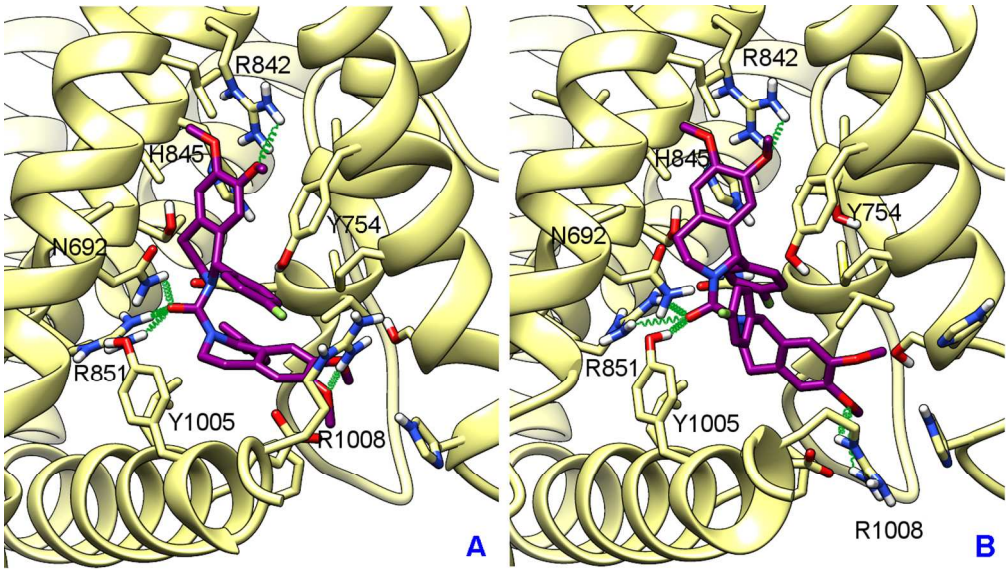

The best docked complexes of rat TRPM8 monomer model with the RR (A) and SS (B) enantiomers of compound 10g are shown, using a ribbon representation for the protein backbone and sticks for the ligands and the side chains of protein residues involved in contacts with the ligand, which is colored in dark magenta. Atoms are colored with the following code: O=red, N=blue, H=white, F=green. Ligand-protein H-bonds are depicted with a green spring.
117x66mm (300 x 300 DPI)

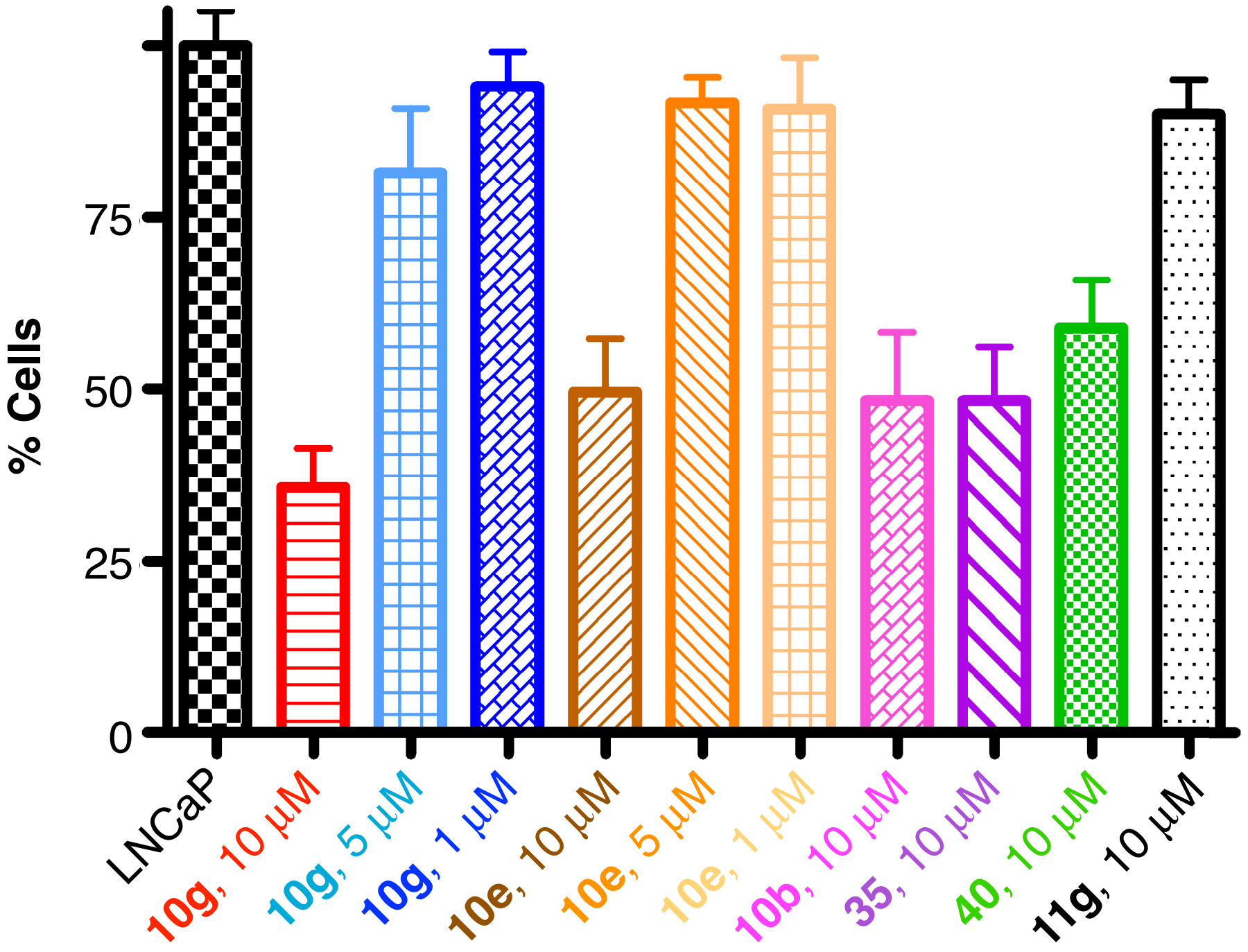
% Cells
0
25
50
75
LNCaP
10g, 10 μM
10g, 5 μM
10g, 1 μM
10e, 10 μM
10e, 5 μM
10e, 1 μM
10b, 10 μM
35, 10 μM
40, 10 μM
11g, 10 μM

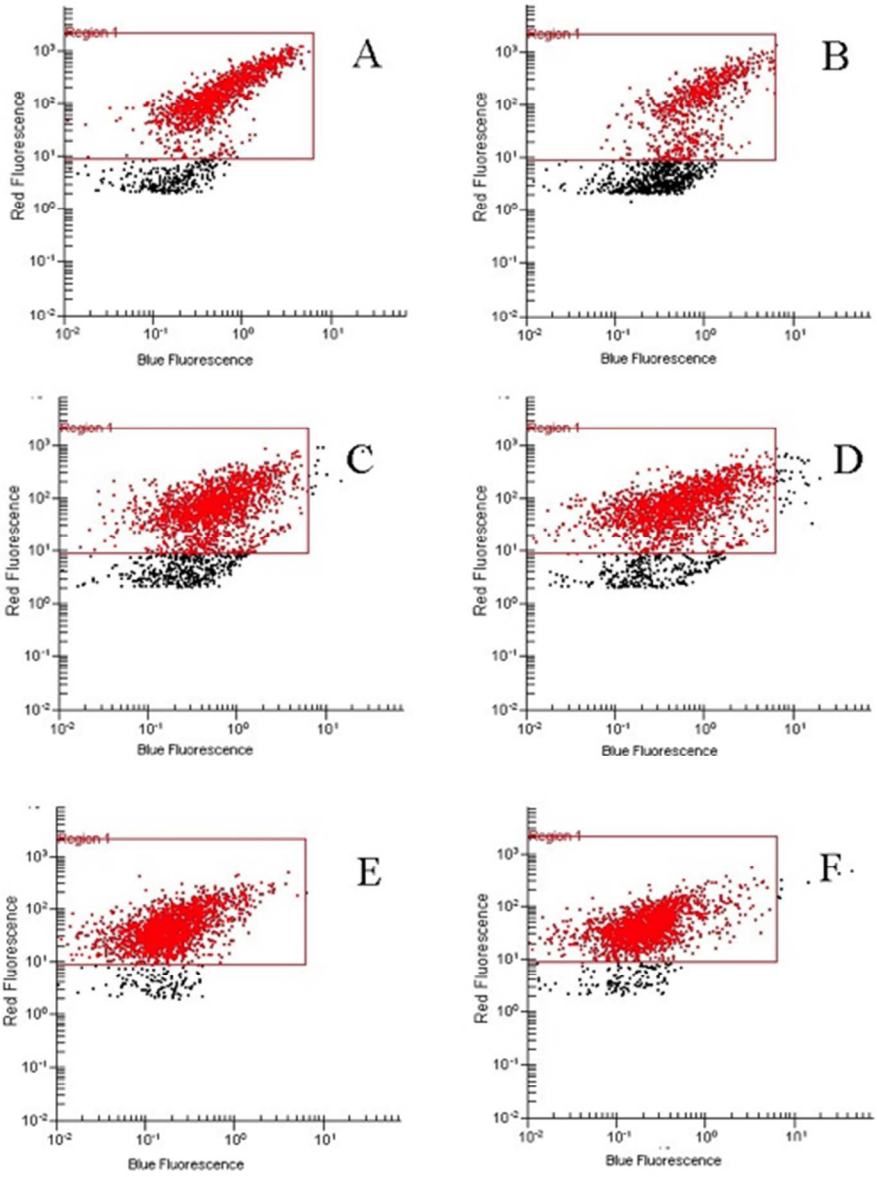

Evaluation of cell viability by CBNF assay. The figure shows a typical experiment of cell viability performed by the vital dye CBFN in a 2100 Bioanalyzer, as described in the Experimental section: Panel A: LNCaP cell treated for 72 h by vehicle; panel B, LNCaP treated for 72 h by 10 μM compound 10g; panel C and panel D: comparable treatments performed on 22RV1 cells; panel E and panel F: comparable treatments performed on PNT1A cells.
192x250mm (72 x 72 DPI)

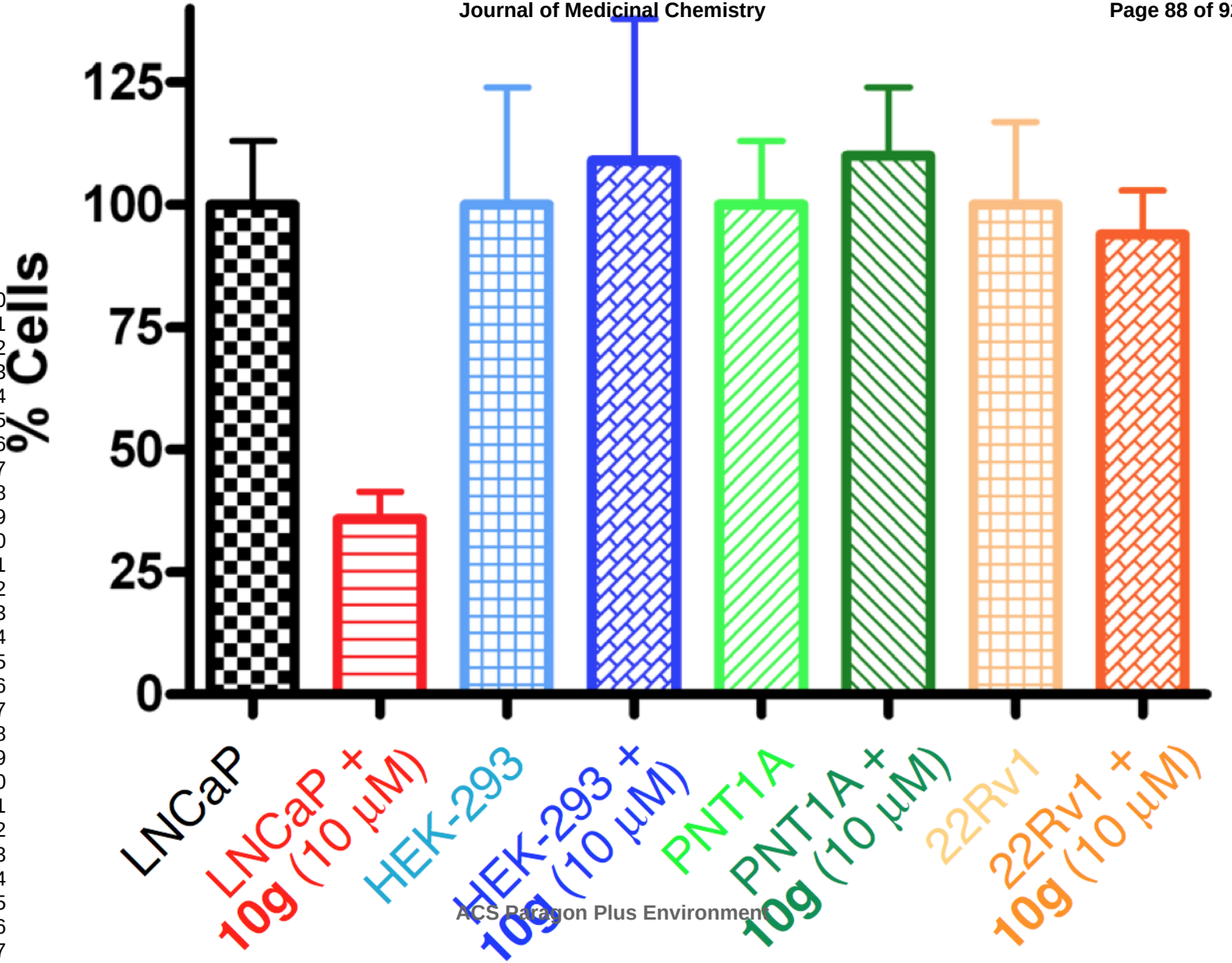
% Cells
125
100
75
50
25
0
LNCaP
LNCaP + 10g (10 μM)
HEK-293
HEK-293 + 10g (10 μM)
PNT1A
PNT1A + 10g (10 μM)
22Rv1
22Rv1 + 10g (10 μM)

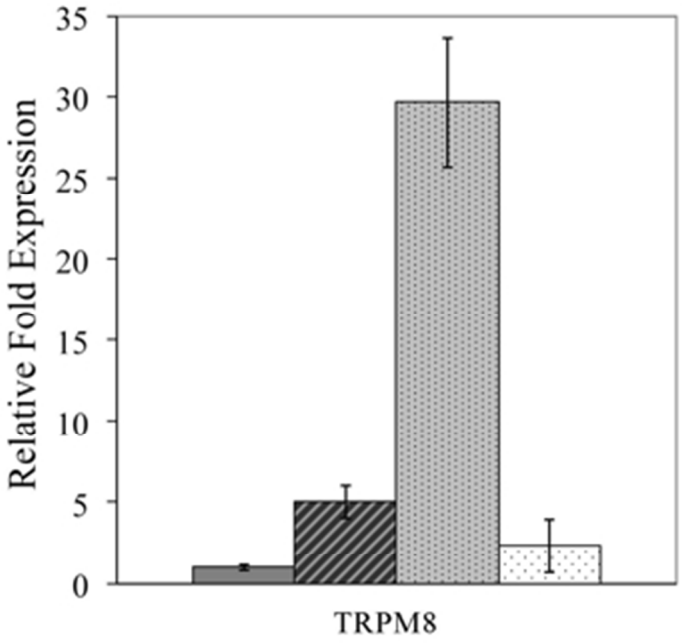

TRPM8 transcriptional expression in prostatic tumor cells, in benign prostatic hypoplasia cells and in human kidney embryonic cells. Relative TRPM8 mRNA levels (TRPM8) were evaluated, by qRT-PCR as described in methods, in prostatic tumor cell LNCaP and 22RV1 , in human normal prostate epithelium cells PNT1A and in human kidney embryonic cells HEK-293 by using 20 ng of cDNA for assay (5 replicates). Relative fold expressions values were scaled respect to the lower expression value (HEK-293) put as 1, quantitative cycles (Cq) = 33.73. The higher relative expression was detected in LNCaP cells, Cq = 28.13 (background over 40 Cq). Standard deviations were calculated by the Gene expression module of iQ5 real-time PCR. The relative expression difference LNCaP vs PNT1A (about 6 fold) was significant ($P < 0.001$) as evaluated by REST-2009 software.101

135x126mm (72 x 72 DPI)

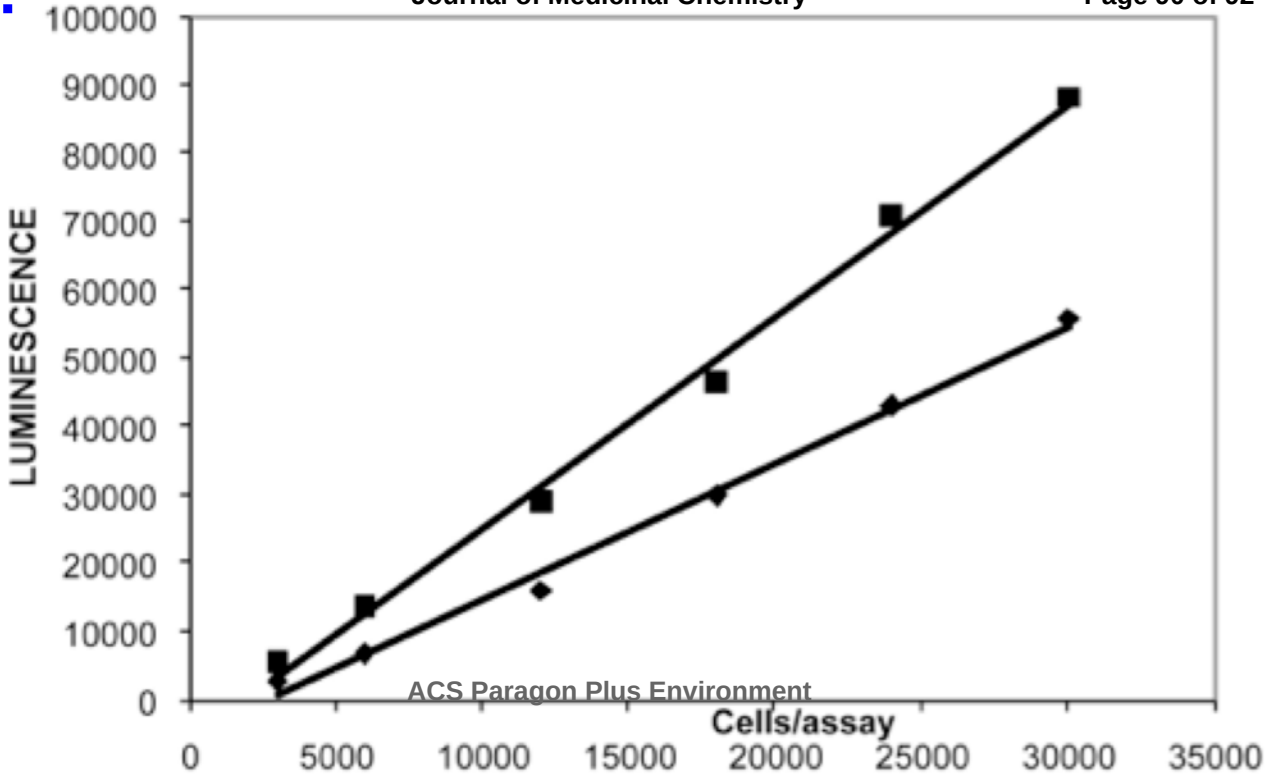

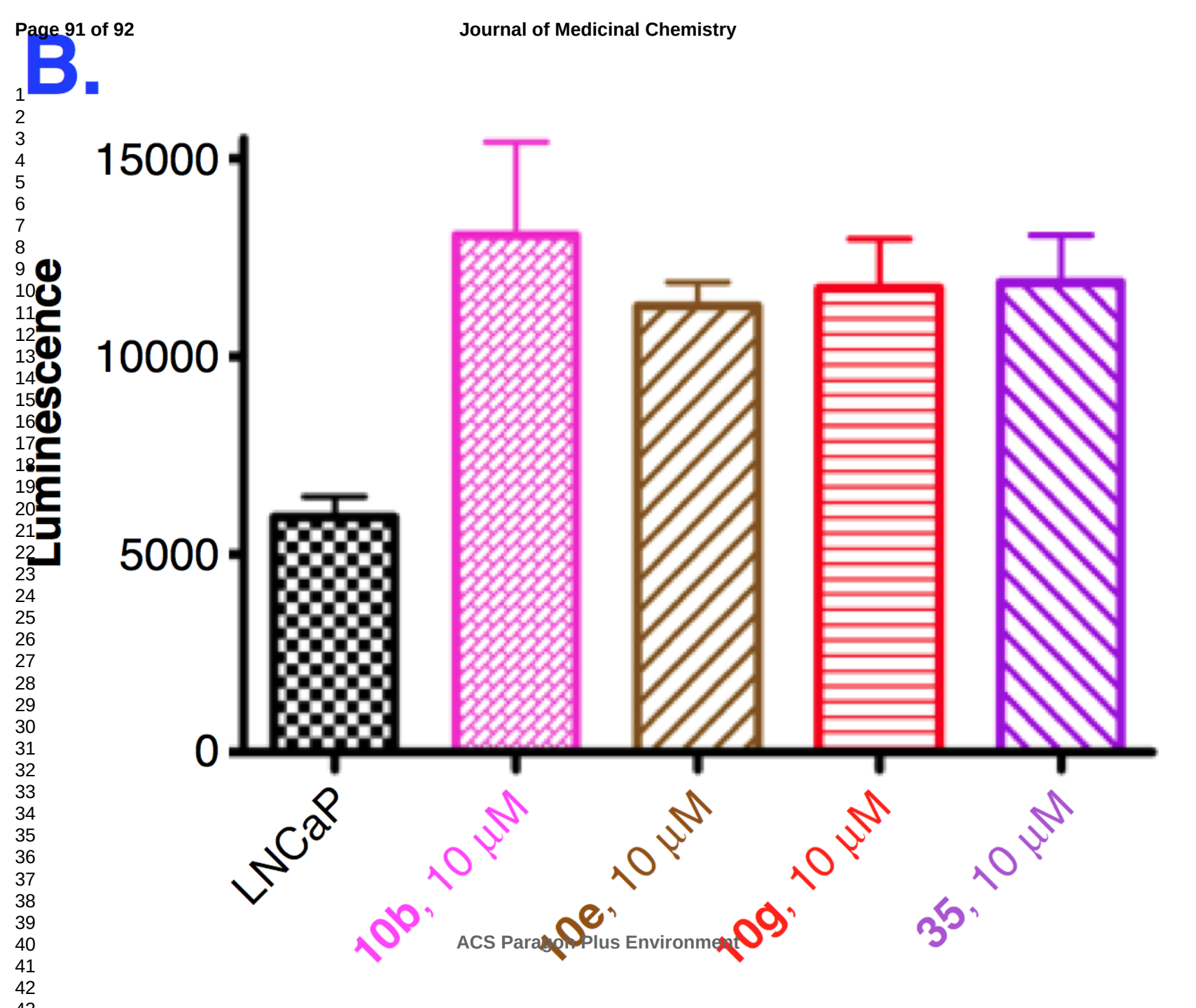
B.
Luminescence
15000
10000
5000
0
LNCaP
10b, 10 μM
10e, 10 μM
10g, 10 μM
35, 10 μM

TRPM8 inhibition
IC_{50} = 72 nM

TRPM8-mediated antiproliferative activity
LNCaP prostate cancer cells

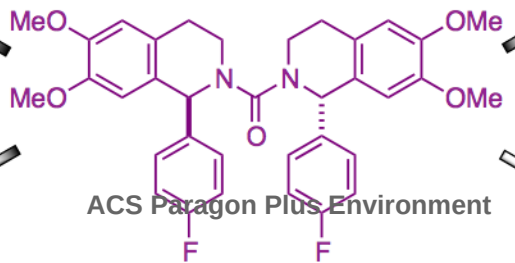

Good TRPM8/TRPMn selectivity
> 1000:1 in most cases

Apoptotic activity
Enhancement of caspase 3/7